INITIATION OF DELAYED HYDRIDE CRACKING IN Zr-2.5Nb

by

DOUGLAS KEITH RODGERS

A Thesis presented to the University of Ottawa
in partial fulfillment of the requirements
for the degree of

MASTER OF APPLIED SCIENCE
in
MECHANICAL ENGINEERING

Ottawa-Carleton Institute for
Mechanical and Aerospace Engineering

ISBN 0-315-93608-8

UNIVERSITÉ D'OTTAWA
UNIVERSITY OF OTTAWA

ABSTRACT

Delayed Hydride Cracking (DHC) occurs in Zr-2.5Nb when certain requirements are met. The mechanism of DHC consists of diffusion of hydrogen to a stress concentrator, such as a crack-tip, precipitation then fracture of a hydride at the crack-tip, and repetition of the process; the crack advances in steps. Incubation times, to the start of cracking and crack-tip hydride morphologies have been measured in pre-cracked cantilever beam specimens tested at applied K_I's up to 20 $MPam^{1/2}$ and temperatures ranging from 100 to 250°C. The incubation time for DHC was found to vary inversely with DHC velocity. Contrary to previous research, the incubation time is highly variable, even for a given temperature and applied K_I, and the crack-tip hydride morphology is much more complicated than the simple model of a single hydride at a crack-tip.

Acknowledgements

This research was funded by the CANDU Owners Group (COG), Working Party 31 - DHC and Fracture, Work Package 3124 - DHC Crack Initiation. COG exists to establish a framework for mutual funding of generic programs related to CANDU nuclear reactor technologies. The four founding members of this group were Atomic Energy of Canada Limited, Ontario Hydro, Hydro-Quebec and New Brunswick Power Commission.

For their support, encouragement and guidance throughout the many years of this study, I am indebted to Dr. A.S. Krausz (University of Ottawa) and Dr. C.E. Coleman (AECL-Research, Chalk River Laboratories) who willingly gave their time to be my supervisors.

Many thanks go to A.J. Lockley, G. Newell, J.C. Owens, D. Weisenberg, V. Ling, A. Timmins, and K. Wells for their invaluable and excellent technical contributions.

I am also pleased to have had the assistance of R.R. Hosbons, M.P. Puls, M. Leger, J.P. Slade, M. Richards and G. Keenleyside for their review and comments of this manuscript.

No project is worth the time or effort without the support of family and friends, thank-you all. Kim, let's get on with something else!

TABLE OF CONTENTS

LIST OF TABLES

LIST OF FIGURES

NOMENCLATURE

a	total depth of notch and crack
AE	total acoustic emissions detected
B	specimen breadth (width at notch)
C_H	hydrogen concentration
D	specimen depth
da/dt	average crack growth rate
g	acceleration due to gravity (9.81 m/s^2)
K_I	stress-intensity factor for mode I
K_{IH}	threshold stress-intensity factor for DHC
l_c	critical crack-tip hydride length for fracture, or fracture surface striation spacing
l_g	distance between specimen notch/crack and centre of gravity of free-end grip
l_h	projected crack-tip hydride length (distance from crack tip to the furthest extent of the crack-tip hydride)
l_w	distance between specimen notch/crack and dead-weight load

L	distance between specimen notch/crack and point of loading
m_g	mass of free-end grip
m_w	mass of dead-weight load
M	total applied bending moment
p	constant of proportionality between AE and ΔA
P	applied load
P.Z.	crack-tip plastic zone size
R	Universal gas constant (8.314 J/mol K)
t_i	incubation time
T	temperature
T_S	solvus temperature
TSS	terminal solid solubility
TSSP	terminal solid solubility for precipitation
ΔA	change in area of fracture surface
σ_y	0.2% yield strength

Chapter 1

INTRODUCTION

1.1 Motivation

It is the responsibility of electric utilities to reliably provide electricity to their customers, who demand that it also be economic (i.e., cheap), safe (both to produce and distribute) and limited in its environmental impact. In North America, industry and private individuals have grown accustomed to this luxury and take for granted the economic growth and high standard of living which have accompanied the utilities' success. The wealth of large rivers in Canada means hydro-electric dams are the first choice for inexpensive electricity production. The CANDU (CANada Deuterium Uranium. Registered trademark of Atomic Energy of Canada

Limited) nuclear reactor system was developed, designed, built, owned and operated in Canada by Atomic Energy of Canada Limited (a federal crown corporation), utilities (such as Ontario Hydro) and many engineering and manufacturing companies as a means of producing electricity competitive in price with the conventional power sources of coal and oil.

Internationally recognized as an outstanding scientific and engineering accomplishment, the CANDU reactor system has posed many challenges. The use of natural uranium fuel in the reactor core motivated the choice of heavy water for moderator and coolant and zirconium alloy tubes as the primary pressure boundary. Extensive research programs over the last forty years have focused on the behaviour of zirconium-based alloys in nuclear reactor environments. These studies continue to improve our understanding of the materials and guide operators and designers towards safer operating procedures and advanced systems.

Identified as the cause of failure in components less than twenty years ago, the mechanism of delayed hydride cracking (DHC) can occur in zirconium alloys when certain conditions are satisfied. Characterising DHC is particularly important because it can occur at stresses less than that of the yield stress of zirconium alloys and with fast crack growth rates, 10^{-9} - 10^{-6} m/s. Although a wide variety of engineering data has been

generated and a model of the complex mechanism developed, only a qualitative description of the fundamental physical process exists. A quantitative understanding of DHC will enhance our knowledge of the behaviour of zirconium alloys under reactor operating conditions. This will contribute to maintaining and improving the performance of CANDU reactors, thereby providing a cost-effective, safe and environmentally sound solution to Canada's long-term electricity needs.

1.2 Objective

Delayed hydride cracking occurs when hydrogen diffuses to a crack-tip region, a brittle zirconium hydride platelet precipitates, grows, and subsequently fractures. Previous studies have clearly established that there is a time delay, referred to as the incubation time, between achieving the conditions necessary for the mechanism and advancement of the crack front, and that uncracked hydrides can exist at the crack-tip. The objectives of this study are: (1) to measure the effects of applied stress and temperature on the incubation time for DHC from a sharp crack, (2) to evaluate the morphology of crack-tip hydrides, and (3) to relate these observations to the established behaviour of DHC, including the existence of a threshold stress-intensity factor below which the mechanism does not

operate, the variation of macroscopic crack growth rates with applied stress-intensity factor and temperature, and the existence of striations on the fracture surface.

Chapter 2

BACKGROUND

2.1 The CANDU Reactor

The CANDU nuclear reactor is one of the most successful electricity generating systems in the world. During the 1980's, CANDU reactors were consistent top performers, with four of the top five reactors in the world to the end of March 1990 (in terms of lifetime load factors for reactors of 150 MWe gross or larger) [1]. The Pt. Lepreau generating station in New Brunswick achieved a 97.5% load factor for the year ending September 1991, placing it first in the world for that period and maintaining its number one position for lifetime performance [2]. In 1990, after more than 25 years of experience producing electricity with

the CANDU system, 43.5% of the electricity used in Ontario was generated at 17 CANDU nuclear reactors [3]. The infrastructure of the Canadian nuclear program includes both public and private corporations with responsibilities for every aspect from uranium mining through research and development, design and construction, operation and maintenance of power stations, to storage and disposal of radioactive waste [4].

In conventional electricity generating stations, combustion of coal, oil or natural gas is used to boil water into steam, which turns a turbine to drive a generator. The difference between this and a nuclear power plant is the use of fission of uranium-235 as the source of heat [5]. At the heart of the CANDU system is a unique reactor core. This core consists of a large vessel, the calandria, containing heavy water moderator (at about 70°C), which is penetrated by about 400 horizontal fuel channels, Figure 1. Each fuel channel consists of two end fittings and a pressure tube into which twelve or thirteen fuel bundles containing natural uranium are placed, Figure 2. The cold-worked Zr-2.5Nb alloy pressure tubes are about 6.3 m long, 103 mm inside diameter and 4.1 mm wall thickness, and are rolled into a mechanical connection with the 403 stainless steel end fittings. Operating at a pressure of about 10 MPa, the heavy water coolant (D_2O) of the primary heat transport system flows

through the pressure tube and over the fuel, increasing in temperature from about 250°C at the inlet end to about 300°C at the outlet end. Each of the pressure tubes is surrounded by a thin Zircaloy-2 calandria tube. The space between the pressure tube and calandria tube, the gas annulus, is filled with dry CO_2 which provides insulation between the tubes as well as an effective means of detecting any D_2O leakage. The gap between the pressure tube and calandria tube of each channel is maintained by annulus gap spacers.

2.2 Pressure Tube Metallurgy

2.2.1 Selecting Zirconium Alloys

The demanding environment of the core of a nuclear reactor requires careful selection of materials. The choice is particularly difficult for a pressure tube, which operates in a high neutron-flux, at elevated temperatures (250 to 300°C), and contains the corrosive D_2O at a considerable pressure (resulting in a tensile hoop stress of about 125 to 150 MPa). This environment dictates that pressure tubes must meet stringent requirements for corrosion resistance, strength and behaviour under irradiation.

Inherent with zirconium alloys is their low thermal-neutron capture cross-section; that is, the low fraction of neutrons absorbed by these materials. The fewer the number of neutrons absorbed, the greater the number of neutrons available to produce fission of the fuel. Although important for all nuclear reactors, neutron economy is vital to the CANDU system because of the choice of natural uranium fuel, which is mostly uranium-238 with only a small fraction (about 0.7%) of the fissionable isotope uranium-235. For this reason, zirconium alloys are used for fuel cladding, reactivity mechanisms and other components (structural and control related), as well as for pressure tubes.

In addition to unalloyed grades of zirconium and those for non-nuclear applications, there are four reactor grade zirconium alloys: Zircaloy-2, Zircaloy-4, Zr-2.5Nb and the less common Zr-2.5Nb-0.5Cu alloy. The Zircaloys are alloys of zirconium with 1.5 wt% tin, while, as its name implies, Zr-2.5Nb is alloyed with niobium, Table 1 [6,7]. The earliest CANDU reactors, the NPD (Nuclear Power Demonstration), Douglas Point and Pickering Units 1 and 2 stations, employed Zircaloy-2 for pressure tubes. After construction of these reactors was committed, development of Zr-2.5Nb provided an alternative that was stronger and more resistant to creep deformation than Zircaloy-2 [8]. This increased strength meant that for the same operating pressure a thinner walled tube

could be used with a significant saving in thermal neutrons and thus greater reactor efficiency. It has subsequently been discovered that the Zr-2.5Nb alloy is also more corrosion resistant, and picks up far smaller quantities of hydrogen isotopes than Zircaloy-2 [9]. (Consistent with the literature, both the single-neutron isotope of hydrogen (i.e., protium) and isotopes of hydrogen collectively will be referred to as hydrogen; any distinction between isotopes will be made where necessary.)

2.2.2 Pressure Tube Fabrication

Ingots of Zr-2.5Nb material are formed from zirconium sponge and a master alloy of zirconium and niobium in an arc-melting process. These ingots are analyzed for chemical composition before being forged into round bars. The round bars are then machined into about 30 hollow billets and extruded into tubes. A total of 20 - 30% cold work is applied to the tubes in a two-stage cold draw, to produce a tube of near-final dimensions. The tubes are finished by a combination of honing, grinding and pickling, prior to being stress relieved. The stress relief process (24 h at 400°C) produces an adherent oxide coating (about 1 μm thick) on the tubes. Throughout the fabrication process, ultrasonic inspections are conducted to ensure that defects are not present in the finished tube [10]. The pressure tube fabrication process is controlled by Canadian

standards and regulations, as well as extensive proprietary specifications. The resulting quality assurance is comparable with that of the aerospace industry.

Zirconium has a hexagonal close-packed atomic lattice structure. As such, zirconium alloys are highly anisotropic, the properties of the material being significantly different in different directions. The cold-extrusion process of pressure tube fabrication results in highly elongated (in the axial direction of the tube) alpha grains about up to 20 μm long, 2 μm wide and less than 1 μm thick [10,11]. Zr-2.5Nb is a two-phase material of primarily the α-phase grains (up to 0.6 wt% Nb) with a grain boundary network of the β-phase (up to 20 wt% Nb). The structure contains many dislocations and is highly textured, with a majority of grains having their basal plane normals in the circumferential direction of the tube.

2.2.3 Fuel Channel Fabrication

Pressure tubes are connected to the end fittings by a mechanical rolled joint, thereby avoiding welded joints in the core of the reactor and the difficult task of periodic inspection of such welds. Using an internal tube expander, the pressure tube is rolled into three grooves on the inside of each end fitting, Figure 3. This process results in compressive residual

hoop stresses in the pressure tube inside the end fitting, and tensile residual stresses immediately beyond the end of the end fitting. A detailed non-destructive inspection of each rolled joint is conducted after installation of the fuel channel in the core of the reactor to ensure that the tensile residual stress region is defect-free.

Chapter 3

DELAYED HYDRIDE CRACKING

3.1 Overview

Hydrogen can damage a wide variety of materials. Extensive studies continue to be made towards establishing a better understanding of both the macroscopic fracture characteristics as well as the fundamental physical processes involved. Most hydrogen damage mechanisms originate from the absorption of hydrogen into the material, but the resultant deterioration of the material can take such forms as blisters (accumulation of hydrogen in a local area on or below the metal surface), hydrogen embrittlement (low material ductility) or hydrogen-induced delayed cracking (fracture of the material below the yield stress, occurring some time after the application

of the stress). One type of hydrogen-induced delayed cracking is known as delayed hydride cracking (DHC).

In the mid-1960's, it was shown that certain zirconium-based alloys, although strong and corrosion resistant, are susceptible to DHC [12,13]. These early studies examined several fracture modes and alloys, including the phenomenon of delayed fracture in Zr-2.5Nb material at room temperature. It was found that: brittle fracture occurs after a delay period from the time of loading, the stress required to cause cracking is less than the yield stress, and there exists a stress below which cracking is not observed. Alloys with greater ductility (lower strength) were observed to be less susceptible to DHC. Subsequently proposed by Westlake [14], the model for DHC in zirconium alloys involves hydrogen diffusion to the region near a stress concentrator, hydride precipitation and growth, and eventually hydride fracture when some critical condition is achieved. The process repeats, advancing the crack front in jumps.

3.2 Service Failures

Zirconium alloys are used in the chemical industry because of their above-average resistance to corrosion in severe chemical environments; however, failures by DHC have occurred [15,16]. In welded structures, stress concentrators in the form of small cracks or voids and high residual stresses provide the necessary conditions for DHC to occur in as short a time as a few weeks, or after as long as 18 months.

By far the greatest number of failures of zirconium alloys by DHC during service have been documented for nuclear reactor components. The first observed failure in Zr-2.5Nb occurred in an experimental fuel sheath assembly [17]. The thin-walled tubular sheath was closed at each end by a welded end cap. The high residual stresses from welding and the sharp angle between the weld upset and the sheath were sufficient to cause failure at room temperature. The role of hydride platelet precipitates at the crack tip was confirmed by metallographic examinations.

3.2.1 Pickering NGS Units 3 and 4 (1974/75)

In 1974 and 1975, several pressure tubes made from Zr-2.5Nb were found to be leaking D_2O into the annulus gap of Units 3 and 4 of the Pickering Nuclear Generating Station (NGS) [18,19]. DHC cracks had initiated on the inside surface of the pressure tubes near the rolled-joint connections to the end fittings and propagated in the radial-axial plane of the tube. Over-extension of the forming tool during fabrication of the joints caused tensile residual hoop stresses as large as 600 MPa in the regions where cracks were observed, Figure 4. The presence of high stresses is not by itself sufficient for DHC to occur. Although the as-manufactured hydrogen concentrations were high enough to cause DHC at room temperature, elevated levels were observed near the rolled-joint regions of the tubes. Metallographic examination of shallow cracks adjacent to the through-wall cracks, which caused the detected leakage, revealed hydrides precipitated at the crack tip. In total, seventy-four of 780 pressure tubes were found to contain cracks, ranging in size from less than 0.5 mm deep and 1 mm long up to through-wall and 15 to 20 mm long, Figure 5. One of the many studies initiated following the discovery of these cracks established that tubes with high tensile strengths were more susceptible to cracking [20], consistent with the findings of Weinstein and Holtz ten years earlier [12]. Also, a higher yield strength might

result in larger residual stresses, which would make DHC initiation more likely.

3.2.2 Bruce NGS Unit 2 (1982)

In 1982, leakage was once again detected in the fuel channels of a CANDU reactor, this time at the Bruce NGS Unit 2 reactor [21]. The fuel channels of this reactor were installed prior to the discovery of the DHC cracks in the Pickering reactors. To minimize the potential for crack initiation in the rolled joints of the Bruce NGS Units 1 and 2 because of high residual stresses from over-extended rollers, these units were stress relieved prior to being commissioned into full-power service. The time between forming the rolled joints and the stress relieving treatment had permitted one crack to initiate in each of the X14 and A14 fuel channel pressure tubes, which eventually led to the detected leakage. A third fuel channel, J11, was also found to be leaking in the rolled-joint region. However, rather than crack initiation from the smooth inside surface of the pressure tube, the crack extended from what appeared as a flap of material on the inside of the pressure tube.

3.2.3 Pickering NGS Unit 3 (1985)

About ten years after the first DHC fractures were discovered at the Pickering NGS, leakage was again detected in the gas annulus system of the Unit 3 reactor. The source of the leakage was determined to be a DHC crack which grew through the wall of the pressure tube in fuel channel F13 and extended to a length of about 28 mm [22]. As with the 1974/75 Pickering NGS failures, this crack was shown to have initiated early in the life of the reactor due to the high residual stresses from rolled-joint forming and the availability of hydrogen. This is the only crack known to have initiated early in the life of the reactor, but which remained in the reactor undetected for such a long period of time.

3.2.4 Bruce NGS Unit 2 (1986)

In 1986, a single pressure tube ruptured at room temperature in the Bruce NGS Unit 2 reactor while the reactor was shut down, and attempts were being made to identify the source of heavy water detected in the gas annulus system. The extensive failure analysis [23] found that a 3.8 m long crack had resulted from the rupture of the N06 pressure tube, which contained a manufacturing flaw. The flaw, a shallow-angle planar lamination at one end of the pressure tube, had preferentially corroded

and cracked along its plane during reactor operation. The stress necessary to initiate DHC was achieved by a combination of the operating hoop stress, the residual stresses from rolled-joint forming and the localized stressing associated with oxide-wedging of the crack. Unlike previously examined fractures which had single-point origins, the manufacturing flaw provided multiple crack-initiation sites. Several cracks initiated in the same plane of the tube (at the end of the flaw), and grew simultaneously, eventually forming one long crack. Cold pressurization of the channel caused unstable (ductile) fracture of the tube.

3.2.5 Pickering NGS Units 1 and 2 (1983)

As previously identified, the effects of hydrogen in a metal can take several forms. Only one failure of a pressure tube has ever occurred by the formation of hydride blisters [24]. The Pickering NGS Units 1 and 2 reactors were originally constructed with pressure tubes made of the Zircaloy-2 alloy and only two annulus gap spacers. Spacers in some of the fuel channels became displaced from their design locations, permitting the hot pressure tube to contact the cooler calandria tube. With ample hydrogen available in these tubes after more than ten years of operation [25], hydrogen diffused down the temperature gradient to these cold spots,

numerous hydrides precipitated, and the local hydrogen concentration increased to the point where the region was transformed into solid zirconium hydride, Figure 6. (This type of blister is not the same as that associated with steel, which can occur as a trapped bubble of hydrogen gas.) In one pressure tube, two adjacent hydride blisters cracked, the cracks grew beyond the brittle blister by DHC, but did not penetrate the tube wall, and unstable fracture occurred when the critical crack length was exceeded.

3.3 The Requirements for DHC

Combining the original model proposed by Westlake [14] with the experiences of cracking in structural applications, the requirements for DHC in zirconium alloys can be defined. Simply stated, DHC requires that: the material be susceptible to the mechanism (most importantly, it must contain sufficient hydrogen to exceed the solubility limit), the component be subjected to a stress, and sufficient time be available for cracking to occur. Let us consider each of these requirements in turn.

3.3.1 Susceptibility

All zirconium alloys are susceptible to DHC, to varying degrees. The likelihood of cracking has been related to the strength of the material [12], which is a function of the alloy, its heat treatment and microstructure. Perhaps the most important contributor to DHC is the presence of sufficient hydrogen in the material to form the brittle zirconium-hydride precipitates (known as hydrides). The equilibrium terminal solid solubility (TSS) limit of hydrogen varies with temperature and is described by the equation [26]:

$$TSS = 1.2 \times 10^{5} \exp\left(-35900 / RT \right) \quad (1)$$

where, TSS is expressed in ppm by weight for the given temperature, T (K), and R is the universal gas constant (8.314 J/mol K). [Equation (1) can be expressed in terms of atomic percent (at%), where the constant in front of the exponential and the numerator of the exponential become 1.1×10^{3} at% and -35800 J/mol, respectively.] This same equation can be used to determine the solvus temperature, T_S, for a given hydrogen concentration, C_H, above which all hydrogen will be in solution at equilibrium. Thus, at the operating temperature of a structure, DHC will

occur only if the solubility limit of hydrogen is exceeded; or, if the structure has a given hydrogen concentration, DHC will only occur at service temperatures below the solvus temperature for that concentration.

The situation is further complicated by observations and theories, which have identified at least two solubility limits: one for precipitation of hydrides (e.g., cooling the material) and one for dissolution of hydrides (e.g., heating the material). The solubility on cooling is given as [27]:

$$TSSP = 4.1 \times 10^4 \exp (-28000 / RT) \qquad (2)$$

where TSSP is the solubility on cooling (precipitation) in ppm by weight. This equation suggests a greater solubility at a given temperature than indicated by the equilibrium TSS of equation (1), thus less hydrogen will be precipitated as hydrides. The existence of various solubility limits has been explained on the basis of the elastic-plastic hydride/matrix accommodation energies [28,29,30].

3.3.2 Stress

The existence of hydrides is necessary but not sufficient for DHC to occur. The successful operation of Zircaloy-2 pressure tubes in the CANDU NPD reactor for about 25 years [31], at the end of that period with deuterium concentrations exceeding 300 ppm (1.3 at%), demonstrates that some other factors are necessary. Service failures of zirconium alloys consistently point to the need for high tensile stresses. High tensile stresses are common in engineered structures because of the need for irregular geometries, such as 90° angles, or the presence of unexpected flaws, such as weld porosity; both result in local stress concentrations. Although careful design and fabrication processes should eliminate these problems, they are sometimes unavoidable or occur without being detected. Even structures and components designed and manufactured to the most stringent specifications and standards, such as in the aerospace or nuclear industries, may be subjected to unusually high stresses. In pressure tubes, the applied stresses resulting from normal-operating and anticipated abnormal or transient pressures are not sufficiently high to cause DHC. However, when combined with other stresses, such as the high residual stresses associated with improper rolling procedures, DHC cracks have initiated at nominally smooth surfaces or at some minor discontinuity or flaw [19].

The situation for hydrogen in zirconium is further exacerbated by the effects of applied stresses. It has been observed that hydrogen, present as an interstitial solute, migrates to regions of high stress. This effect is due to the increased solubility of hydrogen as a result of the hydrostatic stress component of the applied stress [32]. Thus, hydrogen accumulates in a region of locally high stress, such as at a stress concentrator.

The magnitude and direction of the applied stresses will also influence the direction of growth of precipitated hydrides and hence the orientation of the platelets. The usual orientation for hydrides in pressure tubes is with their platelet normals in the radial direction; these are commonly referred to as circumferential hydrides. Tensile hoop stresses cause hydrides to precipitate with their platelet normals in the circumferential direction (radial hydrides), a situation more conducive to DHC resulting in a through-wall crack.

3.3.3 Time

As its name implies, delayed hydride cracking is not an instantaneous process; a susceptible material with sufficient hydrogen will not necessarily crack immediately with the application of a stress. The conditions for DHC must be maintained for a sufficient length of time to permit

migration of hydrogen to the high-stress region of the material, precipitation of a hydride(s) and growth of the hydride(s) to the critical condition for fracture. DHC is both a thermally activated and stress-dependent process, and therefore the length of time required to initiate DHC will depend on the temperature history and the loading conditions.

3.4 The Behaviour of DHC

The requirements for DHC are reflected in the observed behaviour of the mechanism over a range of conditions.

DHC exhibits a three-stage velocity behaviour, Figure 7. The first stage of cracking occurs over a small range of applied stress-intensity factors, where the crack velocity increases dramatically with K_I from negligibly low velocities. In Stage II, however, the crack velocity is observed to be almost independent of the applied stress-intensity factor. The observed Stage I behaviour is believed to be a transition from no cracking occurring at K_I's close to zero to the Stage II regime, rather than being indicative of a change in cracking mechanism. At higher applied K_I's, Stage III, the crack velocity increases rapidly with K_I as greater amounts of unstable fracture occur in conjunction with DHC.

3.4.1 Existence of K_{IH}

No cracking is observed at very low applied stresses; the lowest applied stress-intensity factor at which the cracking occurs is referred to as K_{IH}. With some structural materials, knowledge of the existence of a threshold value below which cracking does not occur can be used to advantage. For example, a stainless steel component subjected to cyclic loading should be designed such that the applied stresses do not exceed the fatigue crack growth threshold. Unfortunately in the case of DHC in Zr-2.5Nb, K_{IH} occurs at such low values that even small stress concentrators can initiate cracking. Although DHC involves the fracture of a hydride platelet, K_{IH} is significantly greater than the fracture toughness observed for solid zirconium hydride, about 1 - 2 $MPam^{1/2}$ [33].

For Zr-2.5Nb pressure tube material, it has been established that there is little or no effect on K_{IH} of hydrogen concentration, test temperature or neutron fluence [22,34]. The range of values reported in the literature, 4.5 - 15 $MPam^{1/2}$, is a result of the test and material conditions. The minimum value of about 5 $MPam^{1/2}$ appears to be valid for all conditions relevant tc pressure tube operation.

3.4.2 Temperature Dependence of Crack Velocity

Several authors have conducted studies to determine the velocity of DHC in Zr-2.5Nb with respect to test temperature in the stress-independent Stage II cracking regime [34 - 38]. In general, the rate of crack growth follows an Arrhenius relationship, for example [38]:

$$\frac{da}{dt} = 6.86 \times 10^{-1} \exp\left(-71500/RT \right) \qquad (3)$$

where da/dt is expressed in m/s. This relationship is only valid when the test temperature is approached from above, or when approached from room temperature for test temperatures up to a critical temperature, about 150 to 180°C, above which the crack growth rate decreases, Figure 8 [38]. The activation energies reported vary from study to study, ranging from about 30 to 72 kJ/mol depending on material condition, the range of temperatures studied, etc. [16,36].

3.4.3 Incubation Time

The time required to fail a component by DHC is the sum of the time to initiate cracking and the time to propagate the crack to unstable

fracture [39]. The characteristic delay between establishing the conditions for DHC and initiation of cracking is called the incubation time, t_i. Using acoustic emission techniques to detect the onset of cracking, Coleman and Ambler [40,41] established that the incubation time for DHC from a sharp crack with an applied stress-intensity factor of 15 $MPam^{1/2}$ followed an Arrhenius relationship when the test temperature was less than 150°C or approached by cooling:

$$t_i = 1.55 \times 10^{-9} \exp (71400 / RT) \quad (4)$$

where t_i is in hours. At temperatures above 150°C (423 K) and when the test temperature was approached by heating, the incubation time was significantly longer than predicted by equation (4), Figure 9. In the same study, the incubation time increased significantly with decreasing applied K_I's, Figure 10.

Coleman and Ambler subsequently used the detection of cracking by acoustic emission to establish the effective solvus temperature of hydrogen in Zr-2.5Nb [42,43]. For specimens containing 0.018 to 0.18 at% hydrogen and at applied K_I's of 15 - 20 $MPam^{1/2}$, the incubation times for DHC were established over a range of temperatures; the highest temperature at

which cracking was detected was defined as the effective solvus temperature. Because these studies focused on determining the solvus temperature, only a limited amount of the incubation time data was presented, for example Figure 11. Incubation times at temperatures more than 10°C below the solvus temperature were typically less than 5 hours in this example.

More recently, incubation times were determined during studies of the hydride growth kinetics at crack tips [44,45]. Shalabi confirmed the observations of Coleman and Ambler of decreasing incubation times with increasing temperature (at an applied K_I of 15 $MPam^{1/2}$), increasing incubation times at lower applied K_I's and increased incubation time when the test temperature of 225°C (498 K) was approached by heating rather than cooling. Reported incubation times vary from less than 0.02 h to greater than 25 h, depending on the conditions.

3.4.4 Fracture Surface Striation Spacing

Macroscopically, DHC fracture surfaces are smooth, indicating a brittle failure process; on a microscopic scale, cleavage-type fracture features predominate [39]. Some researchers have observed striations on DHC fracture surfaces and found these to be narrow bands of ductile tearing

between cleavage fracture regions [36,46]. These fracture surface features have been attributed to the brittle fracture of hydrides and the ductile tearing of narrow regions of adjacent metal. It has been reasoned that the distance between striations (or striation spacing) represents the critical length for fracture of the crack-tip hydride. Striation spacing has been found to increase with temperature, Figure 12, and as the applied K_I approaches K_{IH}, Figure 13 [47].

3.5 The Mechanism of DHC

The current model for the physical processes which occur during DHC in zirconium alloys with all the necessary requirements is, Figure 14:

- diffusion of hydrogen to the crack-tip (or flaw) region,
- accumulation of sufficient hydrogen to form a zirconium hydride precipitate(s),
- growth of the hydride,
- achievement of the critical condition for hydride fracture,
- fracture of the hydride, and
- repetition of the above process.

A mathematical model for DHC in zirconium alloys, particularly pressure tube material, was first proposed by Dutton and Puls to derive a quantified expression for DHC crack velocity [48]. The driving forces considered by this early model were those associated with diffusion of hydrogen up the stress gradient to the highly stressed region at the crack tip, and the formation of the hydride precipitate at the tip of the crack. Refinements to the original model have attempted to account for the transition from negligibly small crack velocities at K_I less than 10 $MPam^{1/2}$ to K_I independent behaviour, and introduced the concept of a critical hydride length, l_c, consistent with the observation of striations on fracture surfaces [32,49,50]. More recently, the model has been reviewed and modifications implemented to more closely match experimental observations, such as the dependence of crack velocity on the direction of approach to the test temperature and a constant crack-tip hydride thickness [51,52]. Details of the mathematical formulation of this model are not necessary for the work of this thesis; it is sufficient to note here that the model appears to account for many of the behaviours observed for DHC, but with varying degrees of success and validity.

One aspect of DHC not yet incorporated by the model is a detailed physical description and mathematical formulation of the criteria for the fracture process occurring at the crack tip. The experimental evidence of

intermittent acoustic emissions [41], discrete potential drop changes [46], and fracture surface striations [36,46] confirms that DHC is a step-by-step process. Crack velocities derived from the mathematical model are based on continuous fracture of the crack-tip hydride (lying in the plane of the fracture) as it forms, or based on the time required to achieve the critical hydride length; as such, the predicted velocities represent average crack growth rates. During testing, measurements of average macroscopic phenomena are relatively easy in comparison to in-situ observation of the microscopic processes of hydride formation, growth and fracture [53]. Thus, it is understandable that the quantitative model is, as yet, incomplete in this respect.

It is fundamental to advancing our understanding of the mechanism of DHC, and hence our ability to model the process, that we quantify the basic physical parameters of crack-tip hydride precipitation, growth and fracture. The objectives of this study are: (1) to measure the effects of applied stress and temperature on the incubation time for DHC from a sharp crack, (2) to evaluate the morphology of crack-tip hydrides, and (3) to relate these observations to the established behaviour of DHC, including the existence of a threshold applied stress-intensity factor below which the mechanism does not operate, the variation of macroscopic crack

growth rates with applied stress-intensity factor and temperature, and the existence of striations on the fracture surface.

Chapter 4

EXPERIMENTAL PROCEDURE

4.1 Material

Specimens for the current study were machined from portions of three pressure tubes. These pressure tubes are identified as N631B, C148 and H737. Although manufactured at different times, the chemical composition of the portions of the ingots from which each of these tubes were made meets the specification for Zr-2.5Nb pressure tubes to be used in the core of a CANDU reactor [54], Table 2, with the small exception of the hafnium concentration of tube N631B.

The mechanical properties of these pressure tubes were determined at the time of manufacture and are summarized in Table 3. As with the chemical composition, the mechanical properties meet the specifications for CANDU pressure tube material [54].

4.2 Specimen Preparation

Material was machined into notched cantilever beam specimens from finished pressure tubes. This is a common specimen choice for testing CANDU pressure tube material, because of the small size of specimen and because study of cracking in the radial-axial plane of the tube is easily accommodated. The approximate size of the specimens was 38 mm long, tube wall thickness deep and 3.5 to 4.5 mm wide, with a 45°, 0.5 mm deep notch across the width of the specimen at its middle, Figure 15. Only the curved specimen geometry was used.

Pressure tubes are manufactured with less than 20 ppm (0.19 at%) hydrogen. This concentration of hydrogen is insufficient to permit delayed hydride cracking at reactor operating temperatures (about 200 - 300°C), and therefore hydrogen was added to the finished cantilever beam specimens prior to testing. The machined specimens were sand-blasted to

provide an oxide-free surface of increased area, then placed into a hydriding apparatus [55] which was then evacuated and filled with hydrogen gas. The specimens were heated to 400°C and the hydrogen gas pressure monitored as hydrogen was absorbed into the surface of the specimen. A homogenizing treatment (400°C for 72 hours in a vacuum of $<10^{-5}$ torr) equilibrated the hydrogen within the specimen. The different hydride structures of the as-received, as-hydrided and homogenized materials are shown in Figure 16. Although the amount of hydrogen introduced into each specimen was monitored by the pressure drop during hydriding, chemical analysis was conducted on each specimen after homogenizing or testing to determine the total hydrogen concentration. The desired total hydrogen concentration was 50 ± 5 ppm.

Each specimen was pre-cracked by DHC before testing to produce a sharp crack at the root of the notch. This is similar to fatigue pre-cracking used for fracture toughness tests [56]. Pre-cracking employed an apparatus and procedure similar to that of the test program itself, except that a computer-controlled load-cell provided cracking with a gradually reducing load until no cracking was detected by acoustic emission for 24 to 48 hours [57]. This technique provided a crack tip ahead of which only a very small zone experienced plastic deformation, as well as a measure of K_{IH} for each specimen.

Specimens tested early in this work were loaded to the desired test stress-intensity factor based on an estimate of the crack depth from the total number of acoustic emissions detected. After the first several tests, it was realized that the desired K_I could be more accurately achieved if the crack depth was determined metallographically prior to loading. This is reasonable, considering the variation in calibration constants relating AE counts to fracture surface area found in the literature [57,58,59]. Using metallography to determine the crack depth required a larger specimen size, 4.5 mm wide, to accommodate material removal during the grinding and polishing stages of metallography. To measure the crack depth in the plane-strain region of the specimen, rather than the plane-stress region close to the specimen edges, about 0.3 - 0.5 mm was removed from each side of the specimen.

4.3 Apparatus

The test apparatus used in the current study consisted of a load-frame, the acoustic emission and temperature control systems and a chart recorder, Figure 17. The load-frame consisted of two 5/16" (about 8 mm) thick steel plates welded together at right angles; additional bracing was added to the vertical plate to prevent distortion of the load-

frame when the specimen was loaded, Figure 18. The fixed-end specimen grip was screwed to the vertical plate of the load-frame. The test specimen was held securely between the fixed-end and free-end grips with an unsupported length of 12 mm; the specimen notch was positioned at the mid-point of the unsupported length. The load applied to the specimen was the sum of the contributions from the free-end grip and the dead-weight load, Figure 19. The dead-weight load comprised a stainless steel beaker (with a handle) filled with small lead pieces and shot, which could be easily added or removed to alter the mass of the dead-weight load, as necessary.

During testing, the specimen and immediately adjacent portions of the grips were enclosed in a furnace consisting of an insulated box with two 240 W heaters. The furnace temperature was controlled by a sensing thermocouple (T/C 1) and an Omega temperature controller (Model CS-4001). The specimen temperature was monitored by a thermocouple (T/C 2) placed in the notch of the specimen, Figures 19 and 20. Type-K (chromel-alumel) thermocouples were used.

Acoustic emissions were monitored using a system of Dunegan-Endevco components. A Model D9203 transducer was attached to the fixed-end specimen grip, Figures 18 and 19. This model of transducer is most

sensitive in the 0.1 to 0.3 MHz range. The signal from the transducer was processed through a Model 1801-190B pre-amp (fixed gain of 40 dB), a Model 302A signal conditioner (two channel, variable gain of 0 to 60 dB) and a Model 303 counter (two channel, 0 to 999 999 counts). The conditioner gain was set between 40 and 45 dB, giving a total gain of 80 to 85 dB. The counter displayed the total number of acoustic emission wave peaks detected.

The specimen temperature and total number of acoustic emission counts were recorded on a three-pen Yokogawa chart recorder (Model 305631); the third channel of the chart recorder was not used.

4.4 Test Procedure

4.4.1 Determination of Load for Required K_I

The stress-intensity factor, K_I, at the tip of a crack in a cantilever beam loaded as in these experiments, is given by:

$$K_I = \frac{4.12\ M \left[\alpha^{-3} - \alpha^{3} \right]^{1/2}}{B\ D^{3/2}} \qquad (5)$$

where M is the total applied bending moment, B is the specimen breadth (width at notch), D is the specimen depth and α is (1 - (a/D)), where a is the total depth of the notch and crack. This equation is a modification of the equation of Kies, et. al. [60] with the bending moment generalized (represented by M) rather than expressed as PL/2, where P is the load and L is the distance between the notch/crack and the loading point. Equation 5 is not the only formula for the stress-intensity factor at a crack tip in a notched beam in bending. For example, for a single-edge-cracked specimen in pure bending [61]:

$$K_I = \frac{6\,M}{B\,D^2}\sqrt{\pi\,a}\;F_I(\alpha) \qquad (6)$$

where α = a/D and $F_I(\alpha) = 1.122 - 1.40\alpha + 7.33\alpha^2 - 13.08\alpha^3 + 14.0\alpha^4$. By rearranging equations (5) and (6) to provide expressions for K_I/M in terms of a/D, the difference between the two equations is found to be less than ± 3% for $0.16 < a/D < 0.57$. Equation (5) has been used in this study for consistency with the work of previous researchers [39].

For the cantilever beam test configuration, the total bending moment was achieved by the combined loads of the free-end grip and the dead-weight. Thus, M can be expressed as:

$$M = (g\, m_g l_g + g\, m_w l_w) \qquad (7)$$

where, g is the acceleration due to gravity (9.81 m/s^2), $gm_g l_g$ is the bending moment of the free-end grip (mass m_g with a centre of gravity at a distance l_g from the specimen notch) and $gm_w l_w$ is the bending moment of the dead-weight load (mass m_w at a distance l_w from the specimen notch). The K_I achieved at the crack tip due to the free-end grip alone was typically less than 4 $MPam^{1/2}$. To produce the desired K_I, the required dead-weight load was calculated by rearranging the above equations, giving:

$$m_w = \left[\frac{K_I\, B\, D^{3/2}}{\left(\alpha^{-3} - \alpha^{3} \right)^{1/2}} - g\, m_g l_g \right] / g\, l_w \qquad (8)$$

During the course of this study, this equation was solved by hand (with the aid of a calculator), with a short BASIC computer program or by using a LOTUS 123 (Registered trademark of Lotus Corporation) spreadsheet.

4.4.2 Determination of Incubation Time

The specimen was placed into a test rig and covered by the furnace. The temperature was increased to 320 - 360°C and held for about 16 - 24 hours (typically overnight). Because the solvus temperature for 50 ppm hydrogen is about 280°C, this treatment permitted time for all of the hydrogen to go into solid solution; i.e., there will be no hydrides remaining. The temperature was then lowered to the test temperature. During and immediately following the reduction in temperature, acoustic emissions were often detected. These emissions are believed to be associated with small movements of the specimen, grips, or other portions of the test rig relative to each other. The specimen and test rig were allowed to stabilize for 1 - 2 hours before the dead-weight load was applied. The specimen was monitored until cracking began, as detected by repeated bursts of acoustic emissions. The incubation time, t_i, is defined as the time between the application of the dead-weight load and the first detected burst of acoustic emissions from cracking, Figure 21.

Once cracking began, the load was removed (acoustic emissions stopped) and the temperature was returned to 320 - 360°C and again held overnight in preparation for the next determination of the incubation time.

When no further testing of a specimen was required, it was air-cooled in the specimen grips with the furnace removed.

4.4.3 Crack-tip Hydride Morphology

The morphology of crack-tip hydrides (i.e., size, shape, position and orientation) was evaluated by metallographic examination of the hydrides in front of a propagating crack. DHC was initiated in each specimen and allowed to continue until a total of about 30 000 acoustic emission counts were recorded. This ensured that cracking occurred across all or most of the crack front. With the dead-weight load still applied, the specimen was ice-water quenched to room temperature to stop the cracking process and "freeze" the hydride structure present at the crack tip, while cracking was occurring at the test temperature. Each specimen was then metallographically prepared and examined at several transverse planes (planes whose normals are in the axial direction of the pressure tube).

4.4.4 Metallographic Preparation and Examination

Specimens were metallographically prepared for examination of either the depth of the crack at the notch or the existence of hydrides. A cold-mounting plastic material was used, rather than Bakelite, to limit any

heating which might have affected the hydride structure of the specimen. Each mounted specimen was first rough-ground to a level surface on 80 - 100 grit paper and then ground on progressively finer grit papers (240, 320, 400 or 500 and 600) using water or varsol as a lubricant.

The specimen was then polished using a 6 μm diamond paste or suspension, followed by colloidal silica and finally an attack polish. This process reduces the amount of edge-rounding and material smearing and provides a true polished surface along the crack. Careful attention to preparation is vital to the study of crack-tip hydrides because of the fineness of the cracks, the small size of the hydrides and possible confusing observations associated with the presence of the crack. The attack polish consists of Cr_2O_3 in water and a 0.5% HF solution used alternately to remove the final worked layer (from polishing). In the as-polished condition, the crack in a specimen was extremely tight and hydrides were not usually seen. (During this study, the addition of an automatic polisher to the metallography laboratory's equipment greatly enhanced the quality and speed of specimen preparation, primarily through the application of higher and more uniform loads than can be achieved by hand. Some changes in the specimen preparation technique were required, but these were not significant.)

To reveal the hydride structure, specimens were etched for 5 - 10 s with a cotton swab and a solution of concentrated HNO_3, lactic acid and HF in the ratio 9:9:1 by volume, respectively. This is similar to one of two etchants recommended for the examination of hydrides in zirconium alloys, and the one preferred for zirconium-niobium alloys [62]. In addition to etching the hydrides, this treatment opened the crack by preferentially etching the crack edges. It was important to thoroughly rinse the specimen, allowing sufficient time to wash any etchant from within the crack which might leach out, resulting in over-etching the specimen in the region of the crack or staining of the sample. A correctly ground, polished and etched specimen revealed the crack and the crack-tip hydride with no ambiguity.

Each metallographically prepared sample was examined at several magnifications, typically 100, 500 and 1000 times, in both the as-polished and etched conditions; photographs were normally taken at magnifications of 100 and 1000 times only. This combination of examinations was necessary to determine the depth of the crack and observe the hydride at the tip of the crack.

4.5 Post-test Measurements and Analysis

4.5.1 Applied Stress-Intensity Factor

The applied stress-intensity factor was calculated for each metallographic plane examined, using the crack depth measured at that plane and equation (5). The mean and standard deviation of the calculated K_I's was determined for each specimen.

4.5.2 Incubation Times

From the record of the accumulated acoustic emission counts with time, the incubation time, t_i, was determined as the time from the application of the dead-weight load until the first burst of acoustic emissions associated with cracking. Establishing the time at which the first burst of acoustic emissions from cracking was detected was not normally difficult, but could be complicated by noise from unknown or external sources or "free-counting". Noise from DHC is identified by intermittent bursts of varying numbers of counts, recall Figure 11, whereas noise from unknown and external sources occurs as individual bursts of a large number of counts, and free-counting is characterized by numerous bursts of only a small number of counts.

4.5.3 Crack-tip Hydride Size

The crack-tip hydride size was measured from the 1000 X magnification photos taken during the metallographic examinations. The hydride length, l_h, is the distance from the crack tip to the furthest extent of the crack-tip hydride. If the crack-tip hydride does not lie immediately ahead of the crack or is oriented in other than the crack plane, l_h is the distance from the crack tip to the furthest extent of the projection of crack-tip hydride(s) onto the crack plane, Figure 22. Any gap between the crack tip and the crack-tip hydride was also measured, using a similar projection onto the crack plane if necessary. The width of the hydride was not considered in this study.

Chapter 5

EXPERIMENTAL RESULTS

5.1 Procedure Parameters

5.1.1 Hydride Dissolution Temperature

Each test conducted in this study relied on a number of assumptions inherent in the test procedure. The first assumption was that the overnight hold temperature exceeds the solvus temperature by a sufficient amount to allow for dissolution of all hydrides in the specimen. The complete dissolution of hydrides is necessary to remove any near-crack-tip hydrides present as a result of previous testing. In this way, the

specimen is rejuvenated and crack initiation is from a crack without any influence of hydrides near the crack tip.

Two specimens, N631B-1 and N631B-3, were tested to show the effect of varying the overnight hold temperature between 320 and 360°C. Each specimen was placed into an experimental apparatus and heated to the desired hold temperature, then ice-water quenched to room temperature the following morning, about 16 - 20 hours later. Large circumferential hydrides (the common orientation for hydrides in pressure tube material) were observed in decreasing size and number with increasing hold temperature, Figure 23. At 360°C, all of the large circumferential hydrides were either completely dissolved or significantly reduced in size. Small point hydrides were also observed. These point hydrides form when the material is quenched to room temperature and hydrogen comes out of solution, but does not have sufficient time to diffuse any significant distance to form the larger circumferential flake hydrides. Post-test hydrogen analyses showed that these specimens contained about 85 ppm (0.76 at%) hydrogen, significantly more than the desired 50 ppm (0.45 at%). The equilibrium solvus temperature for 50 ppm is about 282°C compared with 322°C for 85 ppm, therefore it is not surprising that dissolution required 360°C, exceeding the solvus temperature by only about 40°C.

One specimen of the C148 material, C148-A1, was tested in a similar manner to the two N631B specimens. An overnight hold temperature of 320°C resulted in some dissolution of the large circumferential hydrides; the remaining structure consisted of numerous small hydrides between large circumferential hydrides. At 340, 350 and 360°C, the size of the remaining circumferential hydrides decreased with increasing temperature. An overnight hold temperature of 350°C almost completely dissolved the large hydrides; however, 360°C was again found to be the most effective for complete dissolution, Figure 24. Post-test analysis of C148-A1 showed the specimen to contain about 75 ppm (0.67 at%) hydrogen, which has a corresponding equilibrium solvus temperature of 312°C.

Previous studies of the decomposition of hydrides in Zr-2.5Nb [63] showed that material containing 30 ppm (0.27 at%) hydrogen would require about 3000 s (0.85 h) at 300°C, or 100 s (0.03 h) at 350°C, to completely dissolve large circumferential flake hydrides, whereas material containing 60 ppm (0.54 at%) would require about 1700 s (0.47 h) at 350°C. Interpolation and extrapolation of the data from this earlier work suggests that for material containing 60 ppm hydrogen, complete dissolution of hydrides will occur in 6×10^4 s (16.7 h) at 320°C (exceeding the equilibrium solvus temperature by only 25°C). Tests of the N631B and C148 materials are consistent with this previous work. For specimens

containing 50 ppm hydrogen, an overnight hold temperature of either 320 or 360°C was considered sufficient for hydride dissolution.

5.1.2 Acoustic Emission Calibration

In the current study, DHC was monitored by acoustic emission, acoustic emissions being detected only when cracking was occurring. Crack extension was kept to a minimum by removing the dead-weight load when only a limited number of emissions had been detected. The number of acoustic emissions has been shown to be proportional to the area of fracture surface created [57,58,64,65]:

$$AE = p\ \Delta A \tag{9}$$

where AE is the total number of acoustic emissions detected, p is the constant of proportionality and ΔA is the area of fracture surface created. For a known specimen width, the average advance of the crack front across the specimen can be determined if the constant is known. The number of acoustic emissions detected per unit of crack extension will depend on such factors as the amplifier settings, the sensitivity of the transducer, the location of the transducer relative to the crack, and the

attenuation of the acoustic emission as it travels through the specimen grips. It was therefore necessary to establish the constant of proportionality for the experimental apparatus used in this study.

Four specimens of C148 material, C148-A2 through C148-A5, were cracked in several stages by dead-weight loading at 200°C with applied K_I's of 10 - 15 $MPam^{1/2}$, Table 4. The specimens were then fractured open for examination of the fracture surfaces. Where possible, the area of fracture surface associated with a stage of cracking was determined (by fracture surface oxide colours and crack-arrest lines) and the constant of proportionality calculated, expressed as acoustic emission counts per unit area. The constant of proportionality varied from 6 to 40 x 10^4 counts/mm^2, and with all tests combined the average was 14 x 10^4 counts/mm^2.

Two additional specimens, C148-A11 and C148-A14, were cracked by load-reduction from 17 $MPam^{1/2}$ to K_{IH} at 200°C and then fractured open for examination of the DHC fracture surface. The average constant of proportionality was about 2.5 x 10^4 counts/mm^2. This average is significantly different from that of the dead-weight tests, likely because a different experimental apparatus was used.

The constant of proportionality for acoustic emissions from DHC has been reported as 2.4×10^3 counts/mm^2 by Arora and Tangri [64,65], 6.8×10^4 counts/mm^2 by Sagat et. al. [57], and 5×10^5 counts/mm^2 by Coleman [59]. The results of the current study fall within these values but are closer to those of Coleman and Sagat, consistent with the similarity of the type of test apparatus used. It is clear from the observed variation that relying on an average constant of proportionality may result in some significant error in the crack depth. From test to test, the constant of proportionality for a single specimen is reasonably constant (e.g., specimen C148-A5, Table 4) and therefore if accurate crack depths can be determined (by metallography or fracture surface examinations) at the beginning and end of a test, then intermediate crack depths can be estimated. This consistency for a given specimen enables an estimate of the applied stress-intensity factor to be made for each incubation time test when several determinations were made, without the need for metallography between each test.

5.1.3 Threshold Stress-Intensity Factor

Finally, it is important to know the threshold stress-intensity factor, K_{IH}, for each specimen, as this is fundamental to the behaviour of DHC. Pre-cracking specimens by load-reduction until no acoustic emissions are

detected for an extended period of time provides not only an almost residual-stress-free crack-tip zone but also an estimate of K_{IH}. The value of K_{IH} was estimated from the final applied load and the crack depth estimated from acoustic emission or measured by metallography or examination of the fracture surface. As noted above, measurements of the crack depth provide for more accurate calculations of K_{IH} than crack depths estimated from acoustic emissions.

For specimens C148-A11 and C148-A14, the maximum crack depth was determined by examination of the fracture surfaces after cracking by load-reduction and K_{IH} was calculated to be about 11.5 $MPam^{1/2}$, Table 5. All other K_{IH} values were calculated using the average crack length from two metallographic examinations made after pre-cracking, or from estimates of the crack depth based on acoustic emissions. The average K_{IH}'s are 10 and 9 $MPam^{1/2}$ (± 1 $MPam^{1/2}$) for C148 and H737 materials, respectively. These values are higher than the generally accepted lower bound value of K_{IH} for Zr-2.5Nb of 4.5 $MPam^{1/2}$, but consistent with some higher reported values [32,34].

5.2 Incubation Times

Every specimen tested produced at least one value of the incubation time, t_i, for DHC from a sharp crack; several specimens were tested repeatedly, yielding as many as 23 t_i's. A summary of the t_i's determined is provided in Tables 6 through 8. Most specimens were tested on cooling to 150 or 200°C and with applied K_I's ranging from 10 to 20 $MPam^{1/2}$. The average t_i for each specimen ranged from about 0.1 to 1.5 h for all test conditions. Four specimens provided results worth individual attention.

One specimen is N631B-2, which was to be tested at an applied K_I of 8 $MPam^{1/2}$, within 1 $MPam^{1/2}$ of K_{IH}, on cooling to 225°C. Several initial attempts to determine t_i were unsuccessful, with no cracking being detected after as much as 14 days. A single test was then conducted with the stress-intensity factor increased by about 3 $MPam^{1/2}$; DHC was initiated without difficulty. The remainder of the tests on this specimen were conducted with an applied K_I of about 9 $MPam^{1/2}$. The first three incubation times determined were quite long compared with later tests, Figure 25. This result is interpreted as illustrating the effect of residual compressive stresses at the crack tip. When a specimen is loaded, some plastic deformation will occur at the crack tip. If the load is then reduced, this plastically deformed region experiences a compressive stress,

which reduces both the rate of diffusion of hydrogen to the crack-tip region and therefore the crack-tip hydride growth rate, and the magnitude of the tensile stress at the crack tip, which is necessary to fracture the crack-tip hydride. It is not until crack extension advances the crack front through the zone of plastically deformed material that the observed incubation times become relatively constant. It was this result that identified the need to pre-crack specimens by load-reduction to K_{IH}.

Specimen C148-A16 produced results similar to those of N631B-2, but for different reasons. The C148-A16 specimen was to be tested at an applied K_I close to K_{IH} (cooling to 200°C). The dead-weight load required was determined from an estimate of the crack depth based on the cumulative acoustic emissions detected during pre-cracking by load reduction. Initial tests to determine the incubation time found no cracking after 8 - 24 hours. The applied load was then increased in steps of about 1 $MPam^{1/2}$ until cracking was observed at an applied K_I about 4 $MPam^{1/2}$ higher than first applied. The first incubation time determined was 12.1 hours with an applied K_I within 1 $MPam^{1/2}$ of K_{IH}. Using the same dead-weight load, subsequent t_i's became progressively shorter as the applied K_I increased slightly with each crack advance, Figure 26. The average of the last seven t_i's was 0.3 h. This specimen illustrates not only the effect of incubation times being longer at applied

K_I's close to K_{IH}, but the need to accurately determine the crack length to ensure the desired K_I is achieved.

Two specimens, H737-B19 and H737-B20, were tested with applied K_I's of about 15 $MPam^{1/2}$ on cooling to several different temperatures. Rather than providing a large statistical sample, the focus of testing these specimens was to evaluate the effect of temperature on the incubation time. Test temperatures were selected at random from between 100 and 275°C (25°C intervals), with eight tests being completed on each specimen, Table 9. Incubation times were determined for all test conditions except for the one test conducted at 275°C, where no cracking was detected after 20 hours. The amount of cracking for each test was limited to a few thousand acoustic emission counts to limit the increase in the applied K_I due to crack growth, but sufficient to ensure that DHC was occurring (rather than the detection of background noise, etc.).

5.3 Crack-tip Hydride Morphologies

More than 1000 photographs were taken during this study and it would be impractical and of limited use to reproduce all of them here. The lower-magnification photographs (100 times) were used to determine the

depth of the crack beyond the notch root and therefore the approximate K_I at that location. The higher magnifications (500 and 1000 times) were needed for examination of the crack-tip hydride morphology because of the short length of these hydrides, typically less than 50 μm. The as-polished and etched conditions were both necessary to determine the crack-tip hydride length; hydrides are not generally observed in the as-polished condition, and some ambiguity as to the extent of cracking can exist if only the etched condition is relied upon. Measurements can also be complicated by the observed sub-structure of the crack-tip hydrides to be aligned accumulations of smaller hydrides, Figure 27.

The projected crack-tip hydride lengths, l_h, have been summarized with the average final applied stress-intensity factor for each specimen, Table 10.

Chapter 6

DISCUSSION

6.1 Incubation Times

The earliest published data for the incubation time of DHC from a sharp crack is that of Ambler and Coleman [40], where a single specimen was tested with an applied crack-tip stress-intensity of about 15 $MPam^{1/2}$ at temperatures ranging from 100 to 250°C. These incubation times were found to follow an Arrhenius relationship when the test temperature was approached from above, equation (4). In the same work, the incubation time was observed to increase significantly with decreasing applied K_I, particularly for $K_I < 12$ $MPam^{1/2}$. More recently, Arora and Tangri [65] and Shalabi [45] have reported incubation times for DHC at K_I's of 5 to

20 $MPam^{1/2}$ over a temperature range of 100 to 250°C for both cooling and heating to the test temperature, Table 11. For temperatures less than 150°C, the direction of approach to the test temperature does not affect the incubation time and therefore both are included in Table 11.

6.1.1 Variation with Applied K_I

The works of previous researchers are consistent in their finding that, below 15 $MPam^{1/2}$, the incubation time for DHC increases with a decrease in the applied stress-intensity factor. At K_I's close to the threshold stress-intensity factor, the incubation time can increase by several orders of magnitude. At K_I's above 15 $MPam^{1/2}$, there appears to be no effect of changing the applied stress-intensity factor, although the variation in observed incubation times is large.

In the current study, applied stress-intensity factors ranged from 9 to 20 $MPam^{1/2}$, with most of the tests conducted between 10 and 15 $MPam^{1/2}$, Figure 28. Observed incubation times varied from as short as 0.003 hours (12 seconds) to as long as 12 hours. No significant increase in incubation time was observed with decreasing applied K_I's, and the variation in incubation times was more than two orders of magnitude at all K_I's. This result is not completely inconsistent with previous studies.

Both Ambler and Coleman [40] and Arora and Tangri [65] observed orders of magnitude increases in the incubation time only at K_I's less than 10 $MPam^{1/2}$ or within about 2 $MPam^{1/2}$ of K_{IH}. In the current study, it was difficult to achieve a desired stress-intensity factor within about ± 1 $MPam^{1/2}$ due to the variation in crack depth across the specimen and without destructively examining a specimen to determine the crack depth. As a result, very few incubation times were obtained close to the K_{IH}'s determined by load-reduction, and the near-K_{IH} effect may have been overshadowed by the variability observed. As previously noted, the effect of applied K_I was observed for one specimen in this study, C148-A16, confirming the sensitivity of the incubation time to K_I within 1 $MPam^{1/2}$ of K_{IH}, Figure 26.

6.1.2 Variation with Temperature

For the current study, with no correlation observed between incubation time and applied K_I, the effects of temperature can be considered using the results of all tests combined without regard to the applied stress-intensity factor. Considering all data, except the H737-B19 and B20 specimen results, there was no apparent relationship between incubation time and the test temperature, Figure 29. Individual specimens were tested at only one temperature and the data at 225 and 250°C are for

single specimens only, thereby introducing the possibility that specimen-to-specimen variations might hide temperature effects. Furthermore, at 200°C, where the majority of the tests were conducted, the variation in incubation time is so great, almost three orders of magnitude, that any general trend is likely to be difficult to determine without having a greater sample of results over a wider temperature range. These findings are in contrast to the results of Ambler and Coleman [40] and Shalabi [44], who have established clear relationships with little variability between t_i and test temperature, respectively.

Specimens H737-B19 and H737-B20 were tested specifically to examine the variation of t_i with temperature at an applied K_I of about 15 $MPam^{1/2}$. Whereas Ambler and Coleman tested only one specimen and conducted only a single test at each temperature, in the current study multiple tests with the same conditions performed to measure the variability in t_i. As demonstrated by the first test result for each specimen (recall Table 9), both at 150°C (1000/T = 2.36), the incubation time can vary by more than an order of magnitude. From these two specimens, the incubation time can be described by an Arrhenius relationship:

$$t_i = 2.51 \times 10^{-8} \exp (61300 / RT) \qquad (10)$$

where t_i is given in hours, Figure 30.

Additional studies by Coleman and Ambler [42,43] used incubation times to establish the effective solvus temperatures for various hydrogen concentrations in Zr-2.5Nb. It was observed that the incubation time increases significantly at temperatures close to the solvus temperature, T_S. The incubation time data presented in their papers on this work is limited; however, data for specimens containing between 25 and 75 ppm hydrogen (0.23 and 0.67 at%) have been extracted from the original records of these experiments [66]. For comparison with the results of the current work, only data for temperatures sufficiently below T_S that they are unaffected by the solubility limit have been considered. Although some variability in the incubation time for a given temperature is observed, the results can be reasonably well fitted by an Arrhenius relationship:

$$t_i = 1.47 \times 10^{-6} \exp (52600 / RT) \qquad (11)$$

where t_i is given in hours, Figure 31. The activation energies of the above relationships (the constant in the exponential term) and of equation

(4) are comparable in magnitude but opposite in sign to those established for DHC velocity.

From the model of DHC, it is expected that the incubation time would follow an Arrhenius relationship, as shown above. The incubation time is assumed to be the time required to grow a crack-tip hydride to a critical length, and the rate of growth is directly proportional to the rate of diffusion of hydrogen into the near crack-tip zone. The solution to the diffusion equations is of the form of an exponential. In this respect then, the incubation time data confirm the qualitative model of delayed hydride cracking and supports the mathematical formulation of the existing quantitative model [52].

6.1.3 Correlation with Crack Growth Behaviour

In general, K_{IH} has not been defined by infinitely long incubation times, but rather by the reduction by several orders of magnitude of the crack growth velocity. The mechanism of DHC requires time to precipitate and grow the crack-tip hydride until it fractures; therefore, it is reasonable to consider that incubation time might mirror the behaviour of crack velocity in an inverse relationship. Indeed, the results of this current work combined with previous crack-growth studies show that: for a given

temperature, incubation times increase and crack growth velocities decrease as K_I is decreased towards K_{IH}, and, for a given applied stress-intensity factor, the incubation time decreases and crack growth velocity increases with increasing temperature.

In the Stage II regime of crack growth, where crack velocity is independent of the applied K_I, the variability of incubation times observed in the current study (two orders of magnitude or more) is greater than the variability reported for crack growth velocity (typically less than one order of magnitude). This is despite the apparent agreement of the two parameters in terms of comparable activation energies. A direct comparison is not necessarily valid. Incubation time studies consider the period from achieving the conditions needed for DHC until cracking first occurs, while DHC velocity studies consider an advancing crack front. The differences between these two situations being that the former requires hydrogen gradients to be established while the later already has these gradients established and might be influenced by the presence of the previously fractured crack-tip hydride.

The cantilever beam specimens used in this current work are wider, and therefore the crack front is longer, than the dimensions of a typical crack-tip hydride platelet. Thus, more than one hydride will exists along the

crack front at a time shortly after the conditions necessary for DHC are achieved. In incubation time studies, t_i is the time required to precipitate and grow to a critical size only the first hydride which cracks; i.e., the time at which the first acoustic emission burst is detected. At other positions along the crack front, other hydrides have precipitated and grown, perhaps at different times and rates depending on local conditions. These other hydrides have not yet achieved the critical condition for cracking. The incubation time determined is therefore not an average value, and will be influenced by the highly probabilistic nature of precipitation. In comparison, in tests to establish the DHC velocity behaviour, advances of the crack front are averaged across the specimen thickness and velocities calculated are average values.

Once DHC is occurring, the times between acoustic emission bursts are much shorter than for the initial incubation time, recall for example Figure 11. This not only indicates the step-wise nature of DHC, as has been noted by other researchers [37,39,64], but could be interpreted as the sum of the effects of numerous hydrides at the crack front. Each acoustic emission burst represents an advance of only a short section of the crack front.

This is not to say that the incubation time studies are not useful. The time required to start cracking once the conditions for DHC are achieved is important for determining the time required to propagate a crack until leakage of heavy water into the annulus gap, where it can be detected. Assessments of the fitness-for-service of pressure tubes have assumed that initiation of DHC is instantaneous, i.e. the incubation time is equal to zero, because of the sometimes short and large variability in measured incubation times. In relation to the fundamentals of the DHC mechanism, incubation time tests may lead to a better understanding of what governs the fracture behaviour of a crack-tip hydride. Advancement of the existing mathematical model for DHC will necessitate consideration of local crack-tip conditions as well as the macroscopic average behaviours. However, the current work has clearly established the large variability of t_i. An appreciation of this variability must be brought to any study which attempts to use t_i in defining DHC characteristics or when making quantitative comparisons with average behaviours.

6.2 Crack and Hydride Configurations

6.2.1 Crack Paths

The objective of pre-cracking fracture specimens is to create a sharp uniformly-deep crack-front from which to study the fracture behaviour of the material. Pre-cracking should sufficiently advance the crack from the starter-notch, and use smaller stress intensity factors than those of the fracture test, such that there is no effect of either. The cantilever beam specimen used in the current work is considered a plane-strain specimen because the width of the specimen is significantly larger than the region of plane-stress which unavoidably exists at the specimen edges. In a few specimens, fractographic examinations showed that the crack front in the plane-stress region was not as deep as in the plane-strain region at the centre of the specimen. Metallography of some specimens revealed that in the plane-stress region, several long hydrides were present and no crack growth had occurred from the starter-notch, Figure 32. This observation is consistent with the crack-tip hydride growing under the influence of the plastic strains at a stress concentrator, which occur over a larger volume for plane-stress than plane-strain conditions, and emphasizes the importance of the crack-tip stress state on hydride fracture.

Most specimens in the current study had a well-behaved crack propagating from the root of the notch; that is, the crack was connected to the notch and had propagated in a flat plane. This is the desired condition, which is observed metallographically as a straight crack perpendicular to the surface of the specimen. All specimens showed some deviations of the crack path from a single flat plane, but in general these were only slight deviations and the crack re-aligned itself. One of the most striking examples of an irregular crack path was that of the H737-B4 specimen, Figure 33. Numerous crack branches and fracture of circumferential hydrides perpendicular to the crack propagation direction resulted in the irregular path observed. Despite the apparent irregularity of the crack path, neither the incubation times nor the crack-tip hydride lengths for this specimen were significantly different than those of other specimens.

6.2.2 Crack-tip Hydride Morphologies

Throughout previous studies, metallographic examinations have provided evidence of hydrides preferentially precipitated near crack tips to support the findings of the existence of delayed hydride cracking. The classic picture of delayed hydride cracking is one of a single hydride lying in the plane of the crack and immediately adjacent to the crack tip, Figure 34. This picture is one of the basic assumptions of the quantitative

mathematical model for DHC. The model does not consider the case of more complex crack-tip hydride parameters (i.e., number, size, shape, position and orientation), as found in previous studies [36,46] or the current work.

In the current study, more than 125 crack-tip regions were examined on 18 specimens. The crack-tip hydride configurations observed ranged from no crack-tip hydride to arrangements of several hydrides at various angles to the crack plane. In an attempt to summarize these observations, five crack-tip hydride classifications are suggested:

(1) hydride(s) lying roughly in the plane of the crack,

(2) hydride(s) lying at an angle to the crack plane, typically 30 - 35°,

(3) hydride(s) lying perpendicular to the plane of the crack (this hydride(s) may be cracked and may have small hydrides parallel to the crack plane associated with either the ends of the main hydride(s) or lying beneath the hydride perpendicular to the crack),

(4) a combination of the three types described above, with a short hydride perpendicular to the crack plane and other hydrides lying closer to the plane of the crack, and

(5) numerous hydrides lying in several orientations and forming a complex arrangement.

Each of these classifications is illustrated in Figure 35. The most common configurations are those of one or two hydrides close to the crack tip and parallel or at a small angle to the crack -plane, Types 1 and 2 above. Modelling of DHC using the configuration of a single hydride parallel to the crack plane has been extremely successful in predicting average behaviours. The deviations of the model from the observed behaviours may be due in part to the more complex crack-tip hydride configurations which exist and will affect both the hydride growth and fracture criteria.

In their work on DHC in Zircaloy-2, Mills and Huang [67] observed that the first hydride to precipitate did so at a position slightly ahead of the crack tip, where the triaxial stresses are greater than at the crack tip. A similar observation was made in the current work, with some hydrides found not connected to the crack. The gaps observed were typically up to 4 μm for single hydrides near the crack tip (Types 1 and 2 above). In cases where the crack intersected a hydride perpendicular to the crack path (Type 3 above), the gap between the perpendicular hydride and the hydride that subsequently precipitates parallel to the crack plane was typically 15 to 20 μm (ranging from 10 to 40 μm). In both cases, continued propagation of the crack front results in fracture of the gap material. From the current work, it is not clear whether this closing of

the gap is the result of the advance of the crack, backward fracture after that of the crack-tip hydride (either by ductile tearing or hydride growth and brittle fracture) or lateral fracture from adjacent portions of the crack.

When a crack propagates in the through-thickness (radial) direction and the applied stress is in the hoop (circumferential) direction, as in the current work, the crack propagation direction is perpendicular to the common hydride platelet orientation away from the notch/crack region. It is therefore not surprising that the crack intersects such a hydride(s); the Type 3 crack-tip hydride configuration identified above is likely the result of this condition. Fracture of these perpendicular hydrides is expected because of the triaxial stress state at the crack tip [68] and produces secondary cracking [69] or T-shaped crack-tips. As is evident from the position of subsequent crack-tip hydrides observed in the current work, fracture of hydrides perpendicular to the crack plane will influence the crack-tip conditions and hence local DHC behaviour. Logically, material containing a greater amount of hydrogen present as hydrides will exhibit Type 3 crack-tip hydride morphology (or T-shaped crack-tip) more often than material with less hydrogen present as hydrides. A T-shaped crack-tip can increase the volume of the plastic zone and therefore affect not only the crack-tip hydride morphology but increase the incubation time,

similar to the observed effect of the plane-stress region to support larger un-cracked hydrides. The presence of hydrides perpendicular and close to the crack front will be probabilistic and therefore account, at least in part, for the observed variability in t_i.

However complex the crack-tip hydride morphology and stress state may be, mathematical modelling requires quantifiable criteria for crack-tip hydride fracture.

6.3 Projected Crack-tip Hydride Length

The existing mathematical models for DHC have considered that it is the length of the crack-tip hydride ahead of and parallel to the crack which will determine the critical condition for fracture. Despite the fundamental nature of the crack-tip hydride condition to the DHC mechanism, very few studies have attempted to quantify the critical crack-tip hydride length. The earliest work, by Coleman [70], found that at 75°C hydrides existing near the crack tip prior to cracking were up to 30 μm long, but after cracking started the maximum crack-tip hydride length was only 15 to 20 μm long. Later, Coleman and Ambler [42] found that at 185°C crack-tip hydrides up to 28 μm were present when a specimen was

quenched after testing the specimen for only 80% of the established incubation time. Based on this experiment, Shalabi [45,71] conducted numerous tests to predict the critical hydride length based on extrapolation of intermediate hydride lengths (i.e., for times less than t_i) for temperatures ranging from 100 to 225°C at 10 and 15 $MPam^{1/2}$, Table 12. For example, at 200°C and 15 $MPam^{1/2}$, Shalabi predicted a critical crack-tip hydride length of about 22 μm.

It has been more common to consider the striation spacing data derived from fractographic examinations of DHC fracture surfaces and assume that this spacing represents the incremental jumps of the crack front by DHC and the critical crack-tip hydride length, l_c. The observed trend of all striation spacing data (crack-growth in the axial direction in the tube) is of an increasing spacing with temperature, Figure 12 [36,46,49]. Considering the lower and upper bounds of the data, the striation spacings at 150 - 200°C would be expected to vary between 5 and 25 μm. The effect of increasing the applied crack-tip stress-intensity factor has also been considered [47], indicating an increasing spacing with a decrease in K_I, Table 13.

6.3.1 Variation with Applied K_I

In the current work, the projected crack-tip hydride lengths, l_h, were determined from metallographic sectioning of specimens which were quenched while cracking. Each plane examined represents the local condition, while all examinations considered together should illustrate the full range of crack-tip hydride possibilities and suggest the average crack-growth behaviour. Consideration of all data presents a confusing picture, Figure 36. The range of the data, from 2 to greater than 100 μm, supports the concept of multiple hydrides precipitating, growing, and fracturing at different times at different positions along the crack front; recall a similar conclusion from the acoustic emissions occurring during DHC, section 6.1.3.

The shortest hydride lengths observed represent positions where the crack front has recently advanced and the subsequent precipitation and growth of a new crack-tip hydride has only just started. Not shown in Figure 36 are the numerous observations of no crack-tip hydride. The largest crack-tip hydrides observed approach the limit of the largest hydride which can be formed at the crack tip which will not fracture. It is not necessarily correct to assume that this maximum hydride length is equal to the critical hydride length for fracture. If we consider that only part of the

crack front is advancing as an individual crack-tip hydride fractures, then a redistribution of the stresses at the crack tip will occur. The crack-tip stress-intensity factor will vary across the crack front and in some regions the necessary stress-state condition to fracture the hydride may not exist. An increase in the local crack-tip plastic-zone size will allow the hydride to grow to a longer-than-average length before fracture.

Nor can it simply be assumed that the average crack-tip hydride length is equal to the critical length, because this average will be reduced by the hydrides which have only grown to a fraction of their critical length. It is more likely that the average critical hydride length, l_c, is equal to the value of an upper confidence level or fraction of all observed values of l_h, for example the value of the mean length plus one standard deviation. By the above rationalisation, it is necessary to consider the distribution of observed hydride lengths with respect to both temperature and applied stress-intensity factors.

6.3.2 Variation with Temperature

As a first step in evaluating the projected crack-tip hydride lengths determined in the current study, it is worth noting that there is a significant difference between 150 and 200°C in terms of the fraction of

observations showing no crack-tip hydride; 11 of 36 and only 6 of 92 observations showed no hydride at 150°C and 200°C, respectively. One explanation for the larger fraction of zeros at 150°C can be found from the metallographic findings, that in most cases these zero hydride lengths are associated with the crack intersecting a hydride perpendicular to and in front of the crack, i.e. Figure 35, Type 3 hydride configuration. The likelihood of this occurring is greater at the lower temperatures because of the lower solubility of hydrogen and the resultant greater number and size of hydrides present in the material. With a specimen concentration of 50 ppm (0.45 at%), about 17 ppm will be present as hydrides when cooled to 200°C, but this increases to 36 ppm on cooling to 150°C (equation (2)). These zero crack-tip hydride values should be disregarded when defining l_c, but in so doing the statistical sample at 150°C becomes quite small.

To evaluate the temperature dependence of l_h, the data of the current study have been grouped according to stress-intensity factor range, Table 14. By considering the average plus one standard deviation calculation, it can be observed that l_c increases with both temperature and stress-intensity factor, Figure 37.

6.3.3 Comparison with Previous Research

The crack-tip hydride lengths observed in the current work were similar to the findings of previous research, the average lengths being of the order of a few tens of micrometers. The results of previous studies of the critical crack-tip hydride length or the fracture surface striation spacings showed an increase with temperature which was also observed in the current work. While the average crack-tip hydride size, about 20 - 30 μm, in the current work was consistent with previous work, numerous hydrides were also observed at much longer lengths, up to about 80 μm. These differences suggest that the average critical hydride size is reflected on fracture surface by the striation spacing, but that in some regions longer hydrides can exist. Finer striation spacings than the observed crack-tip hydride lengths may be related to the observed aligned-accumulation-of-smaller-hydrides structure of the crack-tip hydride.

The correlation of striation spacing with critical hydride size does not appear to hold when the effect of applied stress-intensity factor is considered. In the current work, l_c is observed to increase with applied K_I, doubling with a change in K_I from 12 MPam$^{1/2}$ to 18 MPam$^{1/2}$. However, Amouzouvi found the opposite effect of K_I on striation spacing; that is, an increase with decreasing K_I. In earlier work, Simpson and Puls

[34,46] were unable to determine whether any K_I dependence existed for striation spacing because "... on some specimens, l_c increased with increasing K while, on others, it decreased or showed no clear effect at all" [46]. Thus, the assumption by previous researchers that the striation spacing is indicative of the critical hydride length for fracture has proved reasonable (as illustrated by the ability of the mathematical model to predict average macroscopic behaviours such as DHC velocity) only because the striation spacing and the critical hydride length are of the same order of magnitude, and not necessarily because the crack-tip hydride always fractures at a given size, producing a uniform striation spacing.

In an attempt to understand the conditions necessary to fracture a crack-tip hydride, consideration has also been given as to whether or not the hydride exists only within the crack-tip plastic zone, or extends beyond this region. Using the Rice-Johnson model for the plastic zone size [72]:

$$P.Z. = 0.032 \left[\frac{K_I^2}{\sigma_y^2} \right] \qquad (12)$$

where σ_y is the yield stress of the material (about 650 MPa at 150°C and 615 MPa at 200°C) by the empirical relationship σ_y = 1088 - 1.02 T [52], the plastic zone size is expected to increase from about 9 to 35 μm between 10 and 20 MPam$^{1/2}$ (at 200°C). The variation of the yield stress between 100 and 250°C does not have as large an effect on the plastic zone size as does the range of applied K_I's (10 to 20 MPam$^{1/2}$). Comparing this plastic zone size with the crack-tip hydride sizes observed in the current work suggests that hydride growth beyond the plastic zone is necessary for hydride fracture. This simple approach does not take into account the effect of the volume expansion associated with hydride formation [73] on the crack-tip stress state. Hydride precipitation will reduce the magnitude of the tensile stresses adjacent to the crack-tip hydride, but increase the stress ahead of the hydride, thereby increasing the extent of the plastic zone in the crack plane. The magnitude of this effect has been estimated to be significant, almost doubling the distance from the crack tip at which plastic strains exist [74]. What can be deduced from the current work is that the crack-tip hydride precipitates within the plastic zone and grows to a length approximately the same size or slightly greater than that of the plastic zone.

Chapter 7

CONCLUSIONS

In the current study, the incubation times, t_i, and projected crack-tip hydride lengths, l_h, were observed to be affected by temperature and the applied stress-intensity factor as follows:

- t_i increases with a decrease in temperature,
- t_i does not vary significantly with applied K_I in the range of 10 to 20 $MPam^{1/2}$,
- t_i increases significantly at K_I's approaching K_{IH} from above,
- l_h increases with increasing temperature, and
- l_h increases with increasing applied K_I in the range of 10 to 20 $MPam^{1/2}$.

To aid in the interpretation of these results:

- t_i is described by an Arrhenius relationship with an activation energy equal in magnitude but opposite in sign to that established for DHC velocity, and
- a classification system of five crack-tip hydride morphologies has been proposed.

Assuming that the incubation time is the time to precipitate and grow a crack-tip hydride to the critical condition for fracture, and DHC velocity is therefore proportional to l_h divided by t_i, the above results confirm the standard model for DHC. Specifically:

- precipitation and growth of the crack-tip hydride(s) is governed by diffusion of hydrogen to the crack-tip region,
- the critical condition for fracture of the crack-tip hydride appears to be dependent upon the crack-tip stress state and may be a function of the plastic zone size,
- the macroscopic behaviours of DHC velocity and the spacings of striations on DHC fracture surfaces are the average of numerous local crack-tip events, and

- the variability observed in t_i and crack-tip hydride morphologies, and hence DHC velocity, is the result of the probabilistic nature of hydride precipitation and the variety and complexity of local crack-tip conditions.

Contrary to previous research and the mathematical DHC model, the incubation time for DHC is highly variable even for a given temperature and applied K_I condition, and the crack-tip hydride morphology is much more complicated than the simple model of a single hydride at the crack-tip.

Chapter 8

RECOMMENDATIONS

Based on the work of the current study, several areas of research are identified as being worthy of further work. These are:

- assess factors, such as hydrogen concentration or matrix microstructure, which might cause the large specimen-to-specimen variation for incubation times while a single specimen follows an Arrhenius relationship with temperature,
- determine both crack-tip hydride lengths and striation spacings for individual specimens, to establish whether or not a correlation exists,

- evaluate incubation times, crack-tip hydride lengths and striation spacings at K_I's close to K_{IH} to improve the understanding of the physical process which results in this threshold behaviour,
- consider the effect of the direction of approach to the test temperature (i.e., cooling versus heating) in terms of the amount of hydrogen available in solid solution for DHC and the effect on incubation time, crack-tip hydride length and striation spacing,
- review the crack-tip stress state, particularly the plastic zone size in the crack plane and the angle of maximum plastic zone size, for interpretation of the crack-tip hydride length and orientation, and striation spacing, and
- measure the distributions of acoustic emission burst size (number of ring-down counts) and time between events and relate these to the DHC velocity behaviours, such as the effect of temperature and the existence of K_{IH}.

REFERENCES

[1] L. Howles. Power Plant Performance: Performance to end March 1990. Nuclear Engineering International, 35(434):17-19 (1990).

[2] L. Howles. Power Plant Performance: Load Factors to end Sept 1991. Nuclear Engineering International, 37(451):45-47 (1992).

[3] Ontario Hydro Annual Report 1990.

[4] Datafile: Canada. Nuclear Engineering International, 35(433):47-54 (1990).

[5] J.A.L. Robertson. Nuclear Power in Canada: The CANDU System. AECL Report, AECL-6328, revision 2 (1990).

[6] American Society for Testing and Materials. Standard Specification for Wrought Zirconium and Zirconium Alloy Seamless and Welded Tubes for Nuclear Service. ASTM B353-89

[7] Society of Automotive Engineers, Inc. and American Society for Testing and Materials. Metals and Alloys in the Unified Numbering System, 4th edition (1986).

[8] E.F. Ibrahim and B.A. Cheadle. Development of Zirconium Alloys for Pressure Tubes in CANDU Reactors. Canadian Metallurgical Quarterly, 24(3):273-281 (1985).

[9] V.F. Urbanic and B. Cox. Long-Term Corrosion and Deuteriding Behaviour of Zircaloy-2 Under Irradiation. Canadian Metallurgical Quarterly, 24(3):189-196 (1985).

[10] B.A. Cheadle, C.E. Coleman and H. Licht. CANDU-PHW Pressure Tubes: Their Manufacture, Inspection and Properties. Nuclear Technology, 57:413-425 (1982 June).

[11] B.A. Cheadle and C.E. Ells. Crack Initiation in Cold-Worked Zr-2.5 wt% Nb by Delayed Hydrogen Cracking. Proceedings of the Second International Congress on Hydrogen in Metals, Paris, France, 1977. Paper 3C8.

[12] D. Weinstein and F.C. Holtz. Susceptibility of Zirconium Alloys to Delayed Failure Hydrogen Embrittlement. Transactions of the American Society for Metals, 57:284-293 (1964).

[13] G. Ostberg. Some Observations on the Ductility of Zirconium Alloys, with Special Reference to the Effect of Hydrogen. Journal of the Institute of Metals, 93:223-228 (1964-65).

[14] D.G. Westlake. A Generalized Model for Hydrogen Embrittlement. Transactions of the American Society for Metals, 62:1000-1006 (1969).

[15] J.R. Ambler. Failure Analysis on a Chemical Waste Pipe. Process Industries Canada, 69(3):40 (1985).

[16] B.A. Cheadle, C.E. Coleman and J.F.R. Ambler. Prevention of Delayed Hydride Cracking in Zirconium Alloys. In Zirconium in the Nuclear Industry: Seventh International Symposium, (R.B. Adamson and L.F.P. Van Swam, eds.), American Society for Testing and Materials. ASTM STP 939, pp. 224-240 (1987).

[17] C.J. Simpson and C.E. Ells. Delayed Hydrogen Embrittlement in Zr-2.5 wt% Nb. Journal of Nuclear Materials, 52:289-295 (1974).

[18] P.A. Ross-Ross, J.T. Dunn, A.B. Mitchell, G.R. Towgood and T.A Hunter. Some Engineering Aspects of the Investigation into the Cracking of Pressure Tubes in the Pickering Reactors. Paper presented at Annual Congress of the Engineering Institute of Canada, Winnipeg, Manitoba, 1975. AECL Report, AECL-5261 (1976).

[19] E.C.W. Perryman. Pickering Pressure Tube Cracking Experience. Nuclear Energy, 17(2):95-105 (1978).

[20] B.A. Cheadle and G.N. Williams. Computer Assisted Analysis of Cracking in Zr-2.5 wt% Nb Pressure Tubes. The American Society of Mechanical Engineers, New York, NY. ASME Publication, 78-PVP-42 (1978).

[21] J.T. Dunn and A.H. Jackman. Replacement of a Cracked Pressure Tube in Bruce GS Unit 2. Presented to the Canadian Nuclear Society, Toronto, Ontario. AECL Report, AECL-7537 (1882).

[22] G.D. Moan, C.E. Coleman, E.G. Price, D.K. Rodgers and S. Sagat. Leak-Before-Break in the Pressure Tubes of CANDU Reactors. International Journal of Pressure Vessels and Piping, 43:1-21 (1990).

[23] D.K. Rodgers, C.E. Coleman and R.R. Hosbons. Fracture of a Core Component in a Nuclear Reactor. Proceedings of the International Conference on Failure Analysis, ASM International, Montreal, Quebec, 1991.

[24] G.J. Field, J.T. Dunn and B.A. Cheadle. Analysis of the Pressure Tube Failure at Pickering NGS "A" Unit 2 Nuclear Systems Department. Canadian Metallurgical Quarterly, 24(3):181-188 (1985).

[25] V.F. Urbanic, B.D. Warr, A. Manolescu, C.K. Chow and M.W. Shanahan. Oxidation and Deuterium Uptake of Zr-2.5Nb Pressure Tubes in CANDU-PHW Reactors. In Zirconium in the Nuclear Industry: Eight International Symposium, (L.F.P. Van Swam and C.M. Eucken, eds.), American Society for Testing and Materials. ASTM STP 1023, pp. 20-34 (1989).

[26] J.J. Kearns. Terminal Solubility and Partitioning of Hydrogen in the Alpha Phase of Zirconium, Zircaloy-2 and Zircaloy-4. Journal of Nuclear Materials, 22:292-303 (1967).

[27] M. Jovanovic, A. Stern, H. Kneis, G.C. Weatherly and M. Leger. Thermal Diffusion of Hydrogen and Hydride Precipitation in Zr-Nb Pressure Tube Alloys. Canadian Metallurgical Quarterly, 27(4):323-330 (1988).

[28] M.P. Puls. On the Consequences of Hydrogen Supersaturation Effects in Zr Alloys to Hydrogen Ingress and Delayed Hydride Cracking. Journal of Nuclear Materials, 165:128-141 (1989).

[29] M.P. Puls. The Effects of Misfit and External Stress on Terminal Solid Solubility in Hydride-Forming Metals. Acta Metallurgica, 29:1961-1968 (1981).

[30] M.P. Puls. Elastic and Plastic Accommodation Effects on Metal-Hydride Solubility. Acta Metallurgica, 32:(8)1259-1269 (1984).

[31] C.E. Coleman, B.A. Cheadle, A.R. Causey, C.K. Chow, P.H. Davies, M.D. McManus, D.K. Rodgers, S. Sagat and G. van Drunen. Evaluation of Zircaloy-2 Pressure Tubes from NPD. In Zirconium in the Nuclear Industry: Eighth International Symposium, (L.F.P. Van Swam and C.M Eucken, eds.), American Society for Testing and Materials. ASTM STP 1023, pp. 35-49 (1989).

[32] R. Dutton, K. Nuttall, M.P. Puls and L.A. Simpson. Mechanisms of Hydrogen Induced Delayed Cracking in Hydride Forming Materials. Metallurgical Transactions A, 8A:1553-1562 (1977).

[33] L.A. Simpson and C.D. Cann. Fracture Toughness of Zirconium Hydride and Its Influence on the Crack resistance of Zirconium Alloys. Journal of Nuclear Materials, 87:303-316 (1979).

[34] L.A. Simpson and M.P. Puls. The Effects of Stress, Temperature and Hydrogen Content on Hydride-Induced Crack Growth in Zr-2.5 Pct Nb. Metallurgical Transactions A, 10A:1093-1105 (1979).

[35] L.A. Simpson and C.D. Cann. The Effect of Microstructure on Rates of Delayed Hydride Cracking in Zr-2.5%Nb Alloy. Journal of Nuclear Materials, 126:70-73 (1984).

[36] K.F. Amouzouvi and L.J. Clegg. Effect of Heat Treatment on Delayed Hydride Cracking in Zr-2.5 Wt Pct Nb. Metallurgical Transactions A, 18A:1687-1694 (1987).

[37] L.A. Simpson and K. Nuttall. Factors Controlling Hydrogen Assisted Subcritical Crack Growth in Zr-2.5Nb Alloys. In Zirconium in the Nuclear Industry, (A.L. Lowe and G.W. Perry, eds.), American Society for Testing and Materials. ASTM STP 633, pp. 608-629 (1977).

[38] J.F.R. Ambler. Effect of Direction of Approach to Temperature on the Delayed Hydrogen Cracking Behavior of Cold-Worked Zr-2.5Nb. In Zirconium in the Nuclear Industry: Sixth International Symposium, (D.G. Franklin and R.B. Adamson, eds.), American Society for Testing and Materials. ASTM STP 824, pp. 653-674 (1984).

[39] C.E. Coleman and J.F.R. Ambler. Susceptibility of Zirconium Alloys to Delayed Hydrogen Cracking. In Zirconium in the Nuclear Industry, (A.L. Lowe and G.W. Perry, eds.), American Society for Testing and Materials. ASTM STP 633, pp. 589-607 (1977).

[40] J.F.R. Ambler and C.E. Coleman. Acoustic Emission During Delayed Hydrogen Cracking In Zr-2.5 wt% Nb Alloy. Proceedings of the Second International Congress on Hydrogen in Metals, Paris, France, 1977. Paper 3C10.

[41] C.E. Coleman and J.F.R. Ambler. Delayed Hydrogen Cracking In Zr-2.5wt%Nb Alloy. Reviews on Coatings and Corrosion, III(2-3):105-157 (1979).

[42] C.E. Coleman and J.F.R. Ambler. Solubility of Hydrogen Isotopes in Stressed Hydride-Forming Metals. Scripta Metallurgica, 17(1):77-82 (1983).

[43] C.E. Coleman and J.F.R. Ambler. Measurement of Effective Solvus Temperature of Hydrogen in Zr-2.5wt%Nb Using Acoustic Emission. In Hydrogen in Metals, The Metallurgical Society of the Canadian Institute of Mining and Metallurgy Annual Volume, 1978.

[44] A.F. Shalabi. Initiation of Delayed Hydride Cracking in Zirconium-2.5 wt% Niobium Pressure Tubes. Ph.D. Thesis, University of New Brunswick, Department of Mechanical Engineering (1988).

[45] A.F. Shalabi and D.A. Meneley. Initiation of Delayed Hydride Cracking in Zirconium-2.5 wt% Niobium. Journal of Nuclear Materials, 173:313-320 (1990).

[46] L.A. Simpson. The Critical Propagation Event for Hydrogen-Induced Slow Crack Growth in Zr-2.5%Nb. In Mechanical Behaviour of Materials, Volume 2 (K.J. Miller and R.F. Smith, eds.), ICM3, Cambridge, England, 1979. Pergamon Press, Oxford and New York, pp. 445-455.

[47] K.F. Amouzouvi and L.J. Clegg. Peak Amplitude Distribution of Acoustic Emission Events During Delayed Hydride Cracking of Zr-2.5% Nb Alloy. In Fracture Mechanics, Proceedings of an International Symposium, Winnipeg, Manitoba, 1987. Volume 6, Proceedings of the Metallurgical Society of the Canadian Institute of Mining and Metallurgy, pp. 107-118.

[48] R. Dutton and M.P. Puls. A Theoretical Model for Hydrogen Induced Sub-Critical Crack Growth. In Effect of Hydrogen on Behavior of Materials, (A.W. Thompson and I.M. Bernstein, eds.), Proceedings of an International Conference, Moran, Wyoming, 1975. The Metallurgical Society of the American Institute of Mining, Metallurgical and Petroleum Engineers, pp.516-528 (1976).

[49] R. Dutton, C.H. Woo, K. Nuttall, L.A. Simpson and M.P. Puls. The Mechanism of Hydrogen-Induced Delayed Cracking in Zirconium Alloys. Proceedings of the Second International Congress on Hydrogen in Metals, Paris, France, 1977. Paper 3C6.

[50] M.P. Puls, L.A. Simpson and R. Dutton. Hydride-Induced Crack Growth in Zirconium Alloys. In Fracture Problems and Solutions In the Energy Industry, (L.A. Simpson, ed.). Pergamon Press, Oxford and New York, pp. 13-25, (1982).

[51] R.L. Eadie and R.R. Smith. Modelling Delayed Hydride Cracking in Zirconium Alloys. Canadian Metallurgical Quarterly, 27(3):213-223 (1988).

[52] M.P. Puls. Effects of Crack Tip Stress States and Hydride-matrix Interaction Stresses on Delayed Hydride Cracking. Metallurgical Transactions A, 21A:2905-2917 (1990).

[53] C.D. Cann and E.E. Sexton. An Electron Optical Study of Hydride Precipitation and Growth at Crack Tips in Zirconium. Acta Metallurgica, 28:1215-1221 (1980).

[54] Canadian Standards Association. Material Standards for Reactor Components for CANDU Nuclear Power Plants. National Standard of Canada, CAN/CSA N285.6 Series 88 (1988).

[55] E.E. Sexton. A Technique for Low Temperature hydriding of Zirconium Alloys. AECL Report, AECL-2511 (1965).

[56] American Society for Testing and Materials. Standard Test Method for Plane-Strain Fracture Toughness of Metallic Materials. ASTM E399-83.

[57] S. Sagat, J.F.R. Ambler and C.E. Coleman. Application of Acoustic Emission to Hydride Cracking. Presented at 29th Acoustic Emission Working Group Meeting, Kingston, Ontario, 1986. AECL Report, AECL-9258.

[58] A. Arora and K. Tangri. Methods of Structural Integrity Evaluation by Acoustic Emission. International Journal of Fracture, 15:R93-R95 (1979).

[59] C.E. Coleman. Effect of texture on Hydride Reorientation and Delayed Hydrogen Cracking in Cold-Worked Zr-2.5Nb. In Zirconium in the Nuclear Industry: Fifth Conference, (D.G. Franklin, ed.), American Society for Testing and Materials. ASTM STP 754, pp. 393-411 (1982).

[60] J.A. Kies, H.L. Smith, H.E. Romine and H. Bernstein. Fracture Testing of Weldments. In Fracture Toughness Testing and Its Application, American Society for Testing and Materials, ASTM STP 381, pp. 328-356 (1964).

[61] Stress Intensity Factors Handbook (Y. Murikami, ed.). Pergamon Press, Tokyo, p. 11 (1987).

[62] American Society for Metals. Metallography and Microstructures, ASM Handbook, 9th edition, Volume 9, Metals Park, Ohio (1985).

[63] C.E. Ells, B.A. Cheadle, C.E. Coleman and J.H. van der Kuur. The Decomposition of Hydrides in Zirconium Alloys. Proceedings of the Third International Congress on Hydrogen and Materials, Paris, France, 1982.

[64] A. Arora and K. Tangri. Acoustic Emission: A Means of Measuring Crack Growth at Elevated Temperatures. Experimental Mechanics, 21(7):261-267 (1981).

[65] A. Arora and K. Tangri. Acoustic Emission Studies of Nucleation and Propagation of Subcritical Cracks. International Advances in Nondestructive Testing, 8:217-236 (1981).

[66] C.E. Coleman. Unpublished data from hydrogen solubility experiments, see references 42 and 43. Atomic Energy of Canada Limited, AECL Research, Chalk River, Ontario.

[67] J.W. Mills and F.H. Huang. Delayed Hydride Cracking Behavior for Zircaloy-2 Plate. Engineering Fracture Mechanics, 39(2):241-257 (1991).

[68] L.A. Simpson. Criteria for Fracture Initiation at Hydrides in Zirconium-2.5 Pct Niobium Alloy. Metallurgical Transactions A, 12A:2113-2124 (1981).

[69] B.J.S. Wilkins and K. Nuttall. Secondary Cracking in Hydrided Zr-2.5 wt% Nb Alloys. Journal of Nuclear Materials, 75:125-130 (1978).

[70] C.E. Coleman. Susceptibility of Cold-Worked Zirconium-2.5 wt% Niobium Alloy to Delayed Hydrogen Cracking. AECL Report, AECL-5260 (1976).

[71] A.F. Shalabi and D.A. Meneley. Modelling of Delayed Hydride Crack Initiation. Journal of Engineering Materials and Technology, Transactions of the American Society of Mechanical Engineers, 113:443-448 (1991).

[72] J.R. Rice and M.A. Johnson. The Role of Large Crack Tip Geometry Changes in Plane Strain Fracture. In Inelastic Behavior of Solids, (M.F. Kanninen, W.G. Adler, A.R. Rosenfield and R.I. Jaffee, eds.). McGraw-Hill Book Co., New York, NY, pp. 641-672 (1970)

[73] G.J.C. Carpenter. The Dilatational Misfit of Zirconium Hydrides Precipitated in Zirconium. Journal of Nuclear Materials, 48:264-266 (1973).

[74] R.L. Eadie and F. Ellyin. The Effect of Hydride Precipitation in the Stresses Near the Crack tip in a Delayed Hydride Crack in Zirconium-2.5% Niobium. Scripta Metallurgica, 23:585-592 (1989).

Table 1 - Alloying Elements for Common Reactor Grade Zirconium Alloys[1].

ELEMENT	COMPOSITION (wt%)		
	Zircaloy-2 (UNS R60802)	Zircaloy-4 (UNS R60804)	Zr-2.5Nb (UNS R60901)
Tin	1.20 - 0.70	1.20 - 1.70	-
Iron	0.07 - 0.20	0.18 - 0.24	-
Chromium	0.05 - 0.15	0.07 - 0.13	-
Nickel	0.03 - 0.08	-	-
Niobium[2]	-	-	2.40 - 2.80
Oxygen	[3]	[3]	0.09 - 0.13
Fe + Cr + Ni	0.18 - 0.38	-	-
Fe + Cr	-	0.26 - 0.37	-

1 Maximum impurity concentrations are also specified.

2 Niobium is also known as Columbium (Cb).

3 Oxygen concentration is only required as specified in the purchase order.

Table 2 - Chemical Composition of CANDU Zr-2.5Nb Pressure Tube Material [53].

ELEMENT	PRESSURE TUBE			
	SPECIFICATION	N631B	C148	H737
Zirconium	Balance	Balance	Balance	Balance
Niobium	2.4 - 2.8 wt%	2.7	2.5	2.6
Oxygen	900 - 1200 ppm	1050	1030	1060
Impurities: (maximum ppm)				
Aluminum	75	47	67	38
Boron	0.5	<0.2	<0.2	<0.25
Cadmium	0.5	<0.3	<0.25	<0.25
Carbon	270	160	140	140
Chromium	200	90	<80	<80
Cobalt	20	<5	<10	<10
Copper	50	25	<25	<25
Hafnium	50	87	30	<40
Hydrogen	20	3	<5	9
Iron	1500	980	480	590
Lead	130	<5	<50	<25
Magnesium	20	<10	<20	<10
Manganese	50	<10	<25	<25
Molybdenum	50	<10	<25	<25
Nickel	70	16	<35	<35
Nitrogen	65	42	33	35
Silicon	120	51	74	<60
Tantalum	200	<200	<200	<200
Tin	100	20	30	<25
Titanium	50	<50	<25	<25
Tungsten	100	25	<25	<25
Uranium	3.5	0.5	<0.5	1.1
Vanadium	50	<5	<25	<25

Table 3 - Tensile Properties of CANDU Zr-2.5Nb Pressure Tube Material at 300°C (573 K) [53].

PROPERTY	PRESSURE TUBE			
	SPECIFICATION	N631B	C148	H737
0.2% Yield (MPa)	≥ 330	366	352	424
Ultimate (MPa)	≥ 480	527	499	504
Elongation (%)	≥ 12	16	13	14

Table 4 - Constant of Proportionality Between Acoustic Emissions Detected and Fracture Surface Area Created.

SPECIMEN	STAGE	ACOUSTIC EMISSIONS (total)	FRACTURE AREA (mm^2)	CONSTANT (10^4 counts/mm^2)
CRACKING BY LOAD-REDUCTION				
C148-A11	1	98 904	3.21	3.1
C148-A14	1	65 620	3.36	2.0
CRACKING BY DEAD-WEIGHT LOADING				
C148-A2	1	50 000	0.42	11.9
	2-7	100 000	0.88	39.8
C148-A3	1	100 000	1.70	5.9
	2	98 010	0.98	10.0
	3	98 360	1.25	7.9
C148-A4	1-2	277 600	1.63	17.0
	3	75 600	0.62	12.2
C148-A5	1-2	152 000	1.12	13.6
	3	52 000	0.62	16.8

Table 5 - Threshold Stress-Intensity Factors for DHC (K_{IH}) as Determined by Load Reduction.

SPECIMEN	TEMPERATURE (°C)	K_{IH} ($MPam^{1/2}$)	METHOD OF DETERMINING CRACK DEPTH
C148-A11	200	11.5	Fracture Surface
C148-A14	200	11.2	Fracture Surface
C148-A17	200	10.2	Acoustic Emission
C148-A18	200	11.3	Acoustic Emission
C148-A19	200	7.9	Acoustic Emission
C148-A20	200	8.8	Acoustic Emission
C148-A22	200	8.5	Acoustic Emission
C148-A24	250	12.2	Metallography
C148-A26	250	9.3	Acoustic Emission
H737-B3	200	8.0	Metallography
H737-B6	200	9.7	Metallography
H737-B7	200	9.6	Metallography
H737-B8	200	9.3	Metallography
H737-B9	200	9.4	Metallography
H737-B10	200	9.3	Metallography
H737-B11	200	9.8	Metallography
H737-B12	200	8.7	Metallography
H737-B13	200	11.6	Metallography
H737-B14	200	9.2	Metallography
H737-B15	200	7.6	Metallography
H737-B16	200	9.4	Metallography

Table 6 - DHC Incubation Times - N631B Material.

SPECIMEN	TEMP. (°C)	APPLIED K_I ($MPam^{1/2}$)	NUMBER OF TESTS	INCUBATION TIME, t_i (h)	
				RANGE	MEAN[1]
N631B-2	225	~9	6	0.13 - 0.32	0.19 ± 0.07
N631B-3	200	~10	10	0.02 - 0.12	0.07 ± 0.04

[1] Mean ± One Standard Deviation.

Table 7 - DHC Incubation Times - C148 Material.

SPECIMEN	TEMP. (°C)	APPLIED K_I ($MPam^{1/2}$)	NUMBER OF TESTS	INCUBATION TIME, t_i (h)	
				RANGE	MEAN[1]
C148-A15	200	~13	6	0.05 - 0.32	0.13 ± 0.10
C148-A16	200	~14	8	0.01 - 0.92	0.28 ± 0.23
C148-A17	200	~12	6	0.01 - 0.31	0.14 ± 0.14
		15 - 19	5	0.01 - 0.39	0.12 ± 0.16
C148-A18	200	13 - 14	7	0.15 - 2.35	1.5 ± 0.7
		15 - 16	4	0.30 - 1.55	0.7 ± 0.5
C148-A19	200	~10	6	0.03 - 1.17	0.57 ± 0.46
		~11	5	0.01 - 0.37	0.15 ± 0.19
C148-A20	200	11 - 13	12	0.03 - 12.0	0.28 ± 0.28
C148-A22	200	~18	1	0.03	-
C148-A24	250	15 - 20	6	0.06 - 0.95	0.48 ± 0.31
C148-A26	200	10 - 15	7	0.01 - 0.77	0.28 ± 0.34

[1] Mean ± One Standard Deviation.

Table 8 - DHC Incubation Times - H737 Material.

SPECIMEN	TEMP. (°C)	APPLIED K_I ($MPam^{1/2}$)	NUMBER OF TESTS	INCUBATION TIME, t_i (h)	
				RANGE	MEAN[1]
H737-B3	200	14[2]	1	0.05	
H737-B4	200	19	1	0.03	
H737-B6	200	14	1	0.12	
H737-B7	200	12	1	0.02	0.10 ± 0.14
H737-B8	200	13	1	0.08	
H737-B9	200	12	1	0.4	
H737-B11	200	13	1	0.02	
H737-B10	150	20	2	0.63 & 0.85	
H737-B12	150	19	2	0.02 & 0.93	
H737-B13	150	17	2	0.29 & 0.35	0.44 ± 0.34
H737-B14	150	18	2	0.24 & 0.71	
H737-B15	150	18	2	0.03 & 2.93[3]	
H737-B16	150	13	2	0.01 & 0.65	

[1] Mean ± One Standard Deviation.

[2] Applied K_I's are ± 1 $MPam^{1/2}$.

[3] Mean calculated without 2.93 h result.

Table 9 - Incubation Times for Specimens H737-B19 and H737-B20 at 15 $MPam^{1/2}$.

SPECIMEN	TEST NUMBER	TEMP. (°C)	INCUBATION TIME, t_i (hours)
H737-B19	1	150	0.829
	2	125	2.44
	3	125	4.43
	4	225	0.106
	5	250	0.015
	6	200	0.158
	7	275	>20
	8	100	15.7
H737-B20	1	150	0.078
	2	200	0.314
	3	100	11.7
	4	150	1.20
	5	225	0.098
	6	175	0.861
	7	250	0.062
	8	100	14.9

Table 10 - Projected Crack-tip Hydride Lengths (l_h).

SPECIMEN	TEMP. (°C)	NUMBER OF EXAMS[1]	HYDRIDE LENGTHS (μm)	APPLIED K_I ($MPam^{1/2}$)[2]
C148-A16	200	5	12 - 37	14.0 ± 1.2
C148-A20	200	11	10 - 70	13.4 ± 0.7
C148-A22	200	7	29 - 124	18.3 ± 0.9
C148-A26	200	5	0 - 76	15.4 ± 1.2
H737-B3	200	8	6 - 40	13.5 ± 1.0
H737-B4	200	10	0 - 55	18.7 ± 1.1
H737-B5	200	4	0 - 31	19.6 ± 1.2
H737-B6	200	8	3 - 22	14.0 ± 0.9
H737-B7	200	8	0 - 22	12.0 ± 0.5
H737-B8	200	9	10 - 38	13.0 ± 0.6
H737-B9	200	9	0 - 43	12.0 ± 0.6
H737-B11	200	8	3 - 20	13.0 ± 0.2
H737-B10	150	7	0 - 36	19.8 ± 0.6
H737-B12	150	7	0 - 44	19.1 ± 0.3
H737-B13	150	6	0 - 53	17.3 ± 0.5
H737-B14	150	6	0 - 29	17.6 ± 1.0
H737-B15	150	5	0 - 52	17.6 ± 0.5
H737-B16	150	5	2 - 33	12.9 ± 0.1

[1] The number of exams is the number of metallographic sections examined and thus the number of projected hydride lengths determined.

[2] Mean ± One Standard Deviation of the applied K_I's calculated using the crack depth from each metallographic section.

Table 11 - Incubation Time Data from Published Sources.

TEMPERATURE (°C)	K_I ($MPam^{1/2}$)	INCUBATION TIME, t_i (hours)	Ref.
100	10	2.73	[65]
	15	13.04	[40]
	15	13.3 ± 0.4	[44]
	20	0.96	[65]
	20	1.53	[65]
125	15	3.05	[40]
140	5	17.11	[65]
	8	10.43	[65]
	19	0.27	[65]
	19	0.80	[65]
	19	1.95	[65]
150	10	112 ± 4	[44]
	15	1.17 ± 0.08	[44]
	15	1.28	[40]
175	15	0.507	[40]
200	10	25 ± 4	[44]
	15	0.12 ± 0.04	[44]
	15	0.100	[40]
225	~7	> 26	[40]
	8.5 - 8.8	4.13	[40]
	8.6 - 10.2	2.12	[40]
	10.2 - 11.3	1.00	[40]
	12.7 - 14.1	0.41	[40]
	15	0.07 ± 0.02	[44]
	15.3 - 16.9	0.38	[40]
	15.5 - 16.9	0.81	[40]
	16.3 - 17.7	0.31	[40]
	17.7 - 19.3	0.17	[40]
250	15	0.017	[40]
	15	0.02 ± 0.01	[44]

Table 12 - Critical Hydride Lengths from Shalabi [71].

K_I ($MPam^{1/2}$)	TEMPERATURE (°C)	CRITICAL HYDRIDE LENGTH (μm)
10	150	6
	200	12
15	100	6
	150	10
	200	22
	225	36

Table 13 - Striation Spacings at 225°C (498 K) from Amouzouvi and Clegg [47].

K_I ($MPam^{1/2}$)	STRIATION SPACINGS (μm)
7.5	21.8 - 24.3
10.5	20.5 - 21.5
14.0	18.9 - 20.0
23.5	14.7 - 16.2
31.5	11.0 - 13.8

Table 14 - Summary of Projected Hydride Lengths (l_h).

l_h (μm)	APPLIED K_I RANGE (MPam$^{1/2}$)				
	≤ 12	12 - 14	14 - 16	16 - 18	> 18
150°C					
Maximum	-	33	-	53	52
Mean	-	17	-	35	27
Std. Dev.[1]	-	11	-	15	14
l_c[2]	-	28	-	50	41
200°C					
Maximum	43	70	76	77	124
Mean	22	23	25	50	47
Std. Dev.[1]	12	17	21	28	32
l_c[2]	34	39	46	77	78

[1] One Standard Deviation.

[2] l_c = Mean + One Standard Deviation.

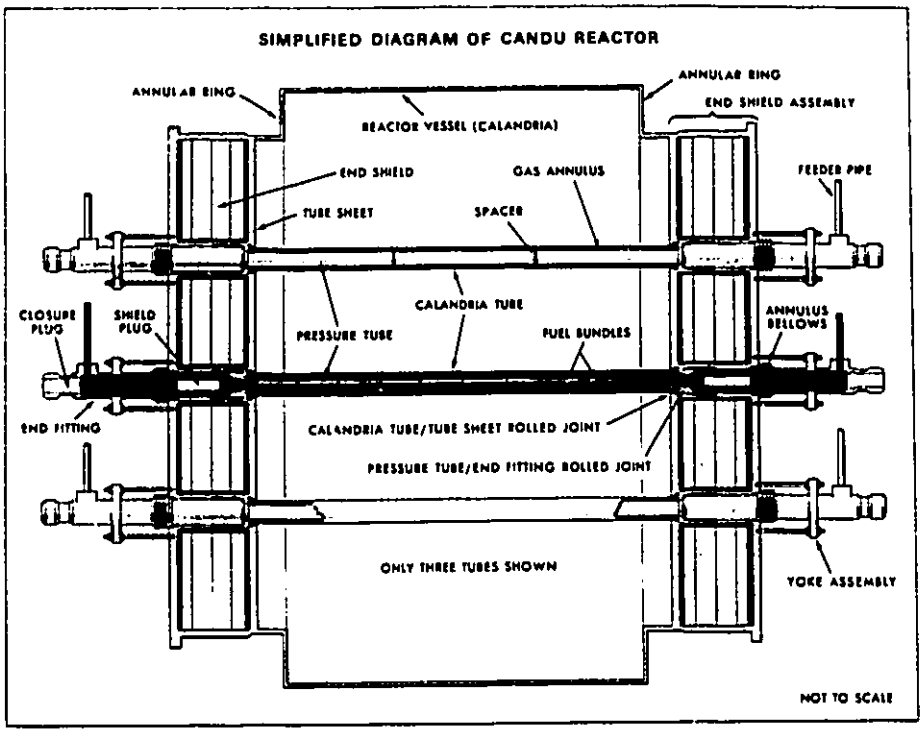

Figure 1 Simplified Diagram of a CANDU Reactor.

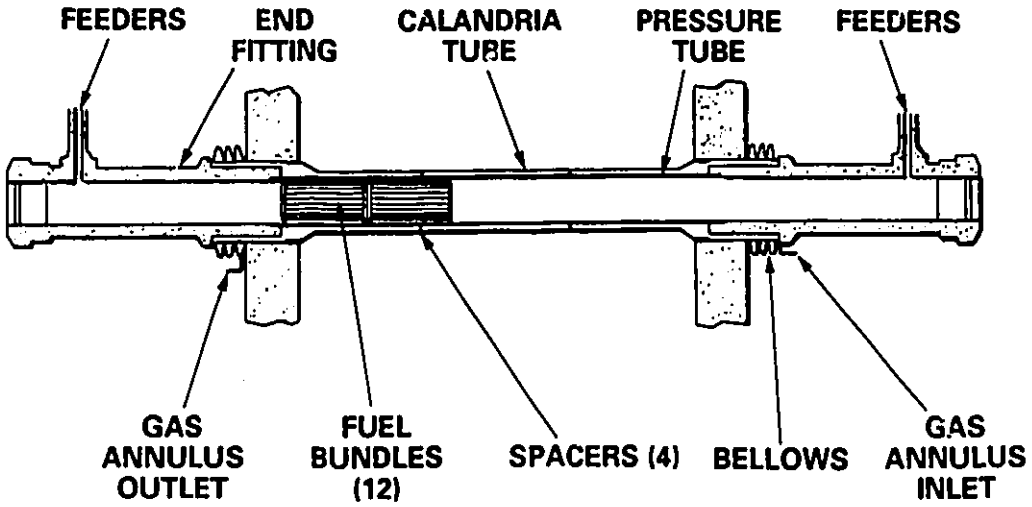

Figure 2 Simplified Diagram of a CANDU Reactor Fuel Channel.

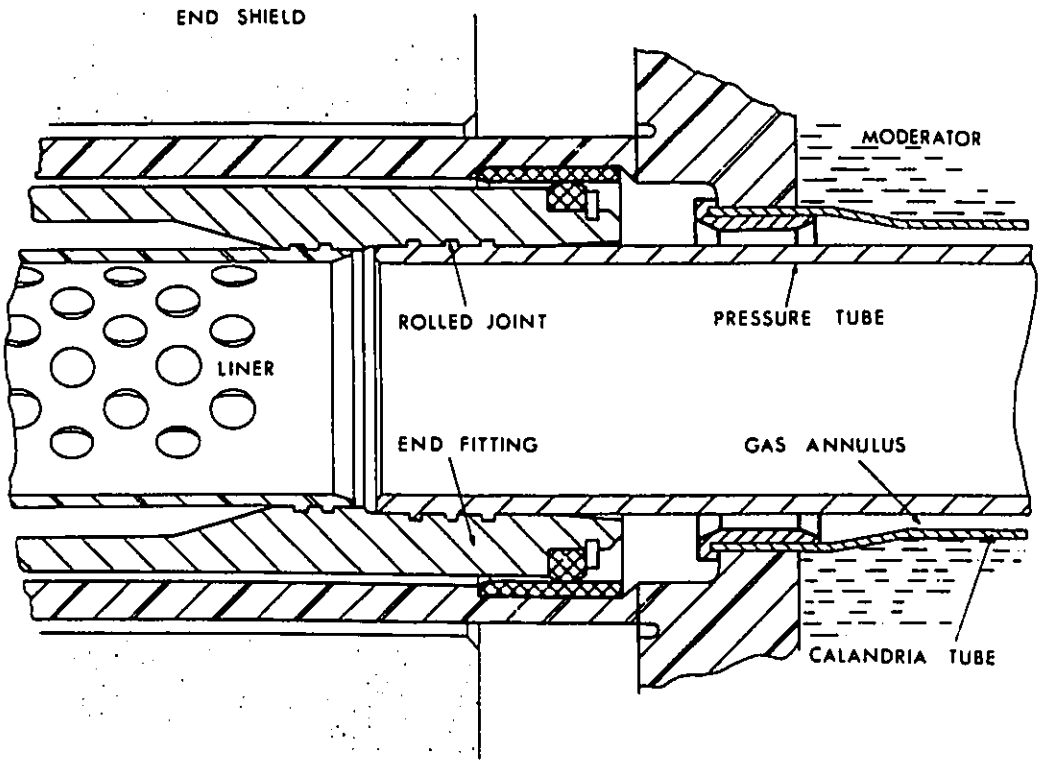

Figure 3 Rolled Joint between a Pressure Tube and an End Fitting.

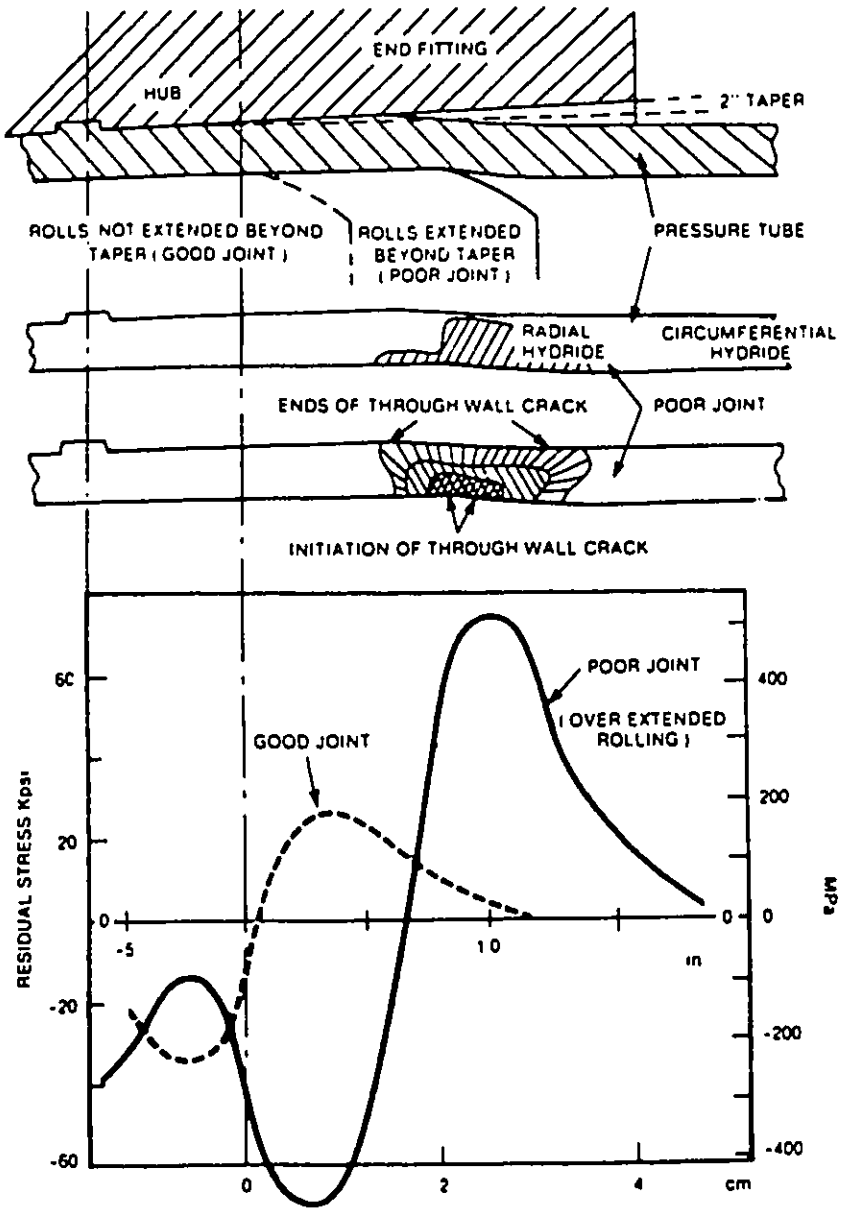

Figure 4 Effect of Roll Extension on the Residual Hoop Stresses in the Pressure Tube at a Rolled Joint [22].

Figure 5 DHC Crack in the Pressure Tube at a Rolled Joint of a Pickering NGS Unit 4 Pressure Tube.

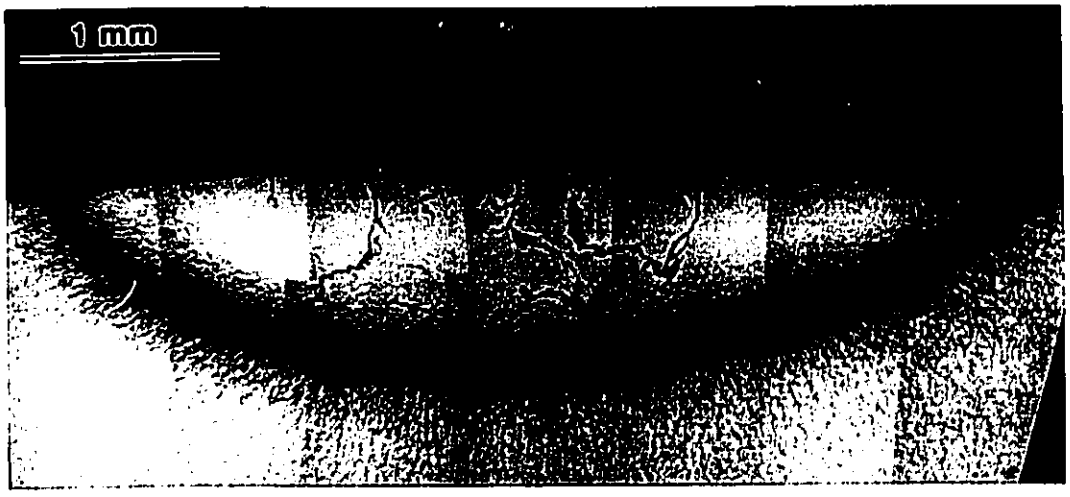

Figure 6 Zirconium Hydride Blister in a Zircaloy-2 Pressure Tube.

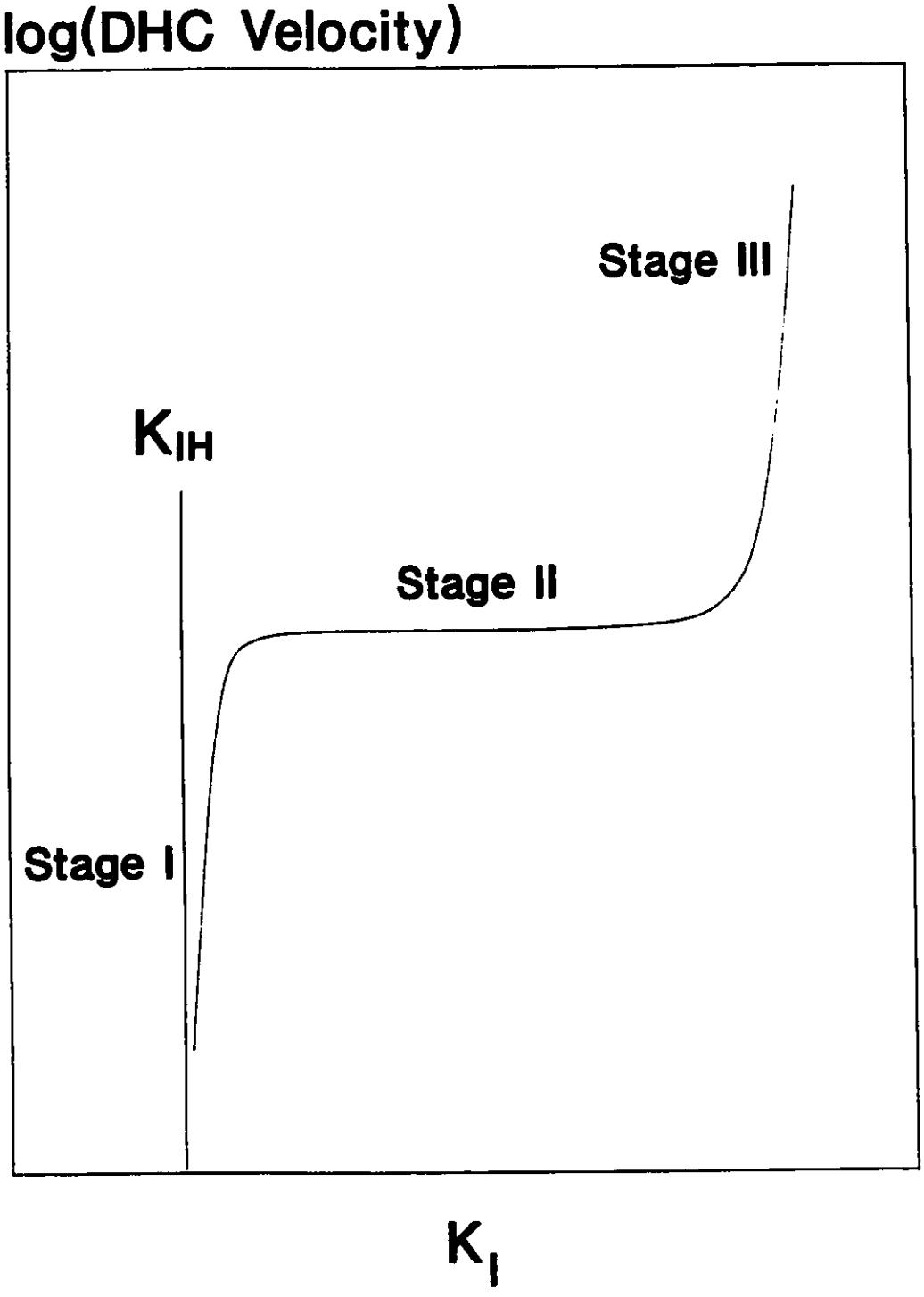

Figure 7 Dependence of DHC Crack Velocity on Stress-Intensity Factor.

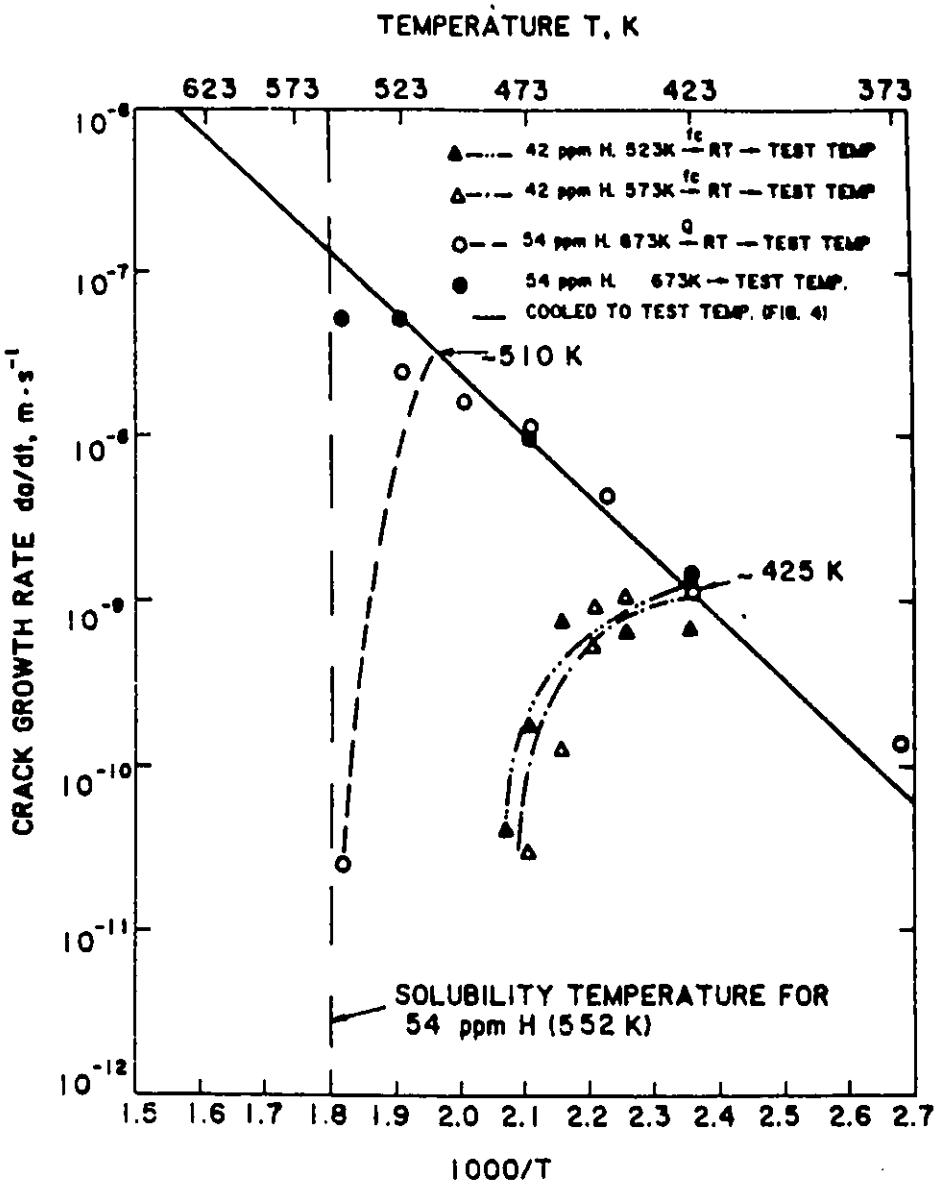

Figure 8 Dependence of DHC Crack Velocity on Heating or Cooling to the Test Temperature [38].

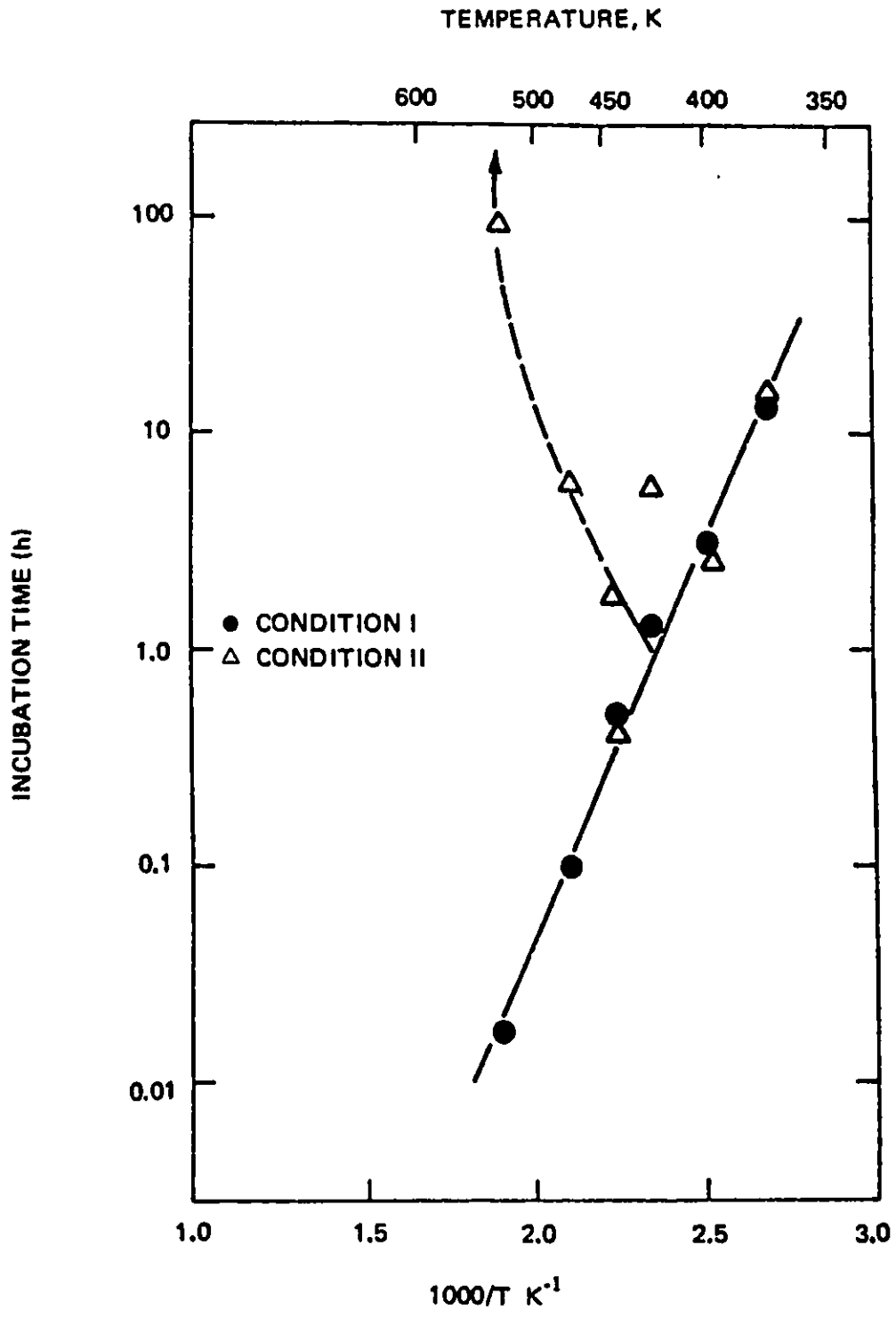

Figure 9 Dependence of Incubation Time on Test Temperature in a Cantilever Beam Specimen Containing 45 ppm Hydrogen at 15 $MPam^{1/2}$ [41].
Condition I: Specimen Cooled to Test Temperature.
Condition II: Specimen Heated to Test Temperature.

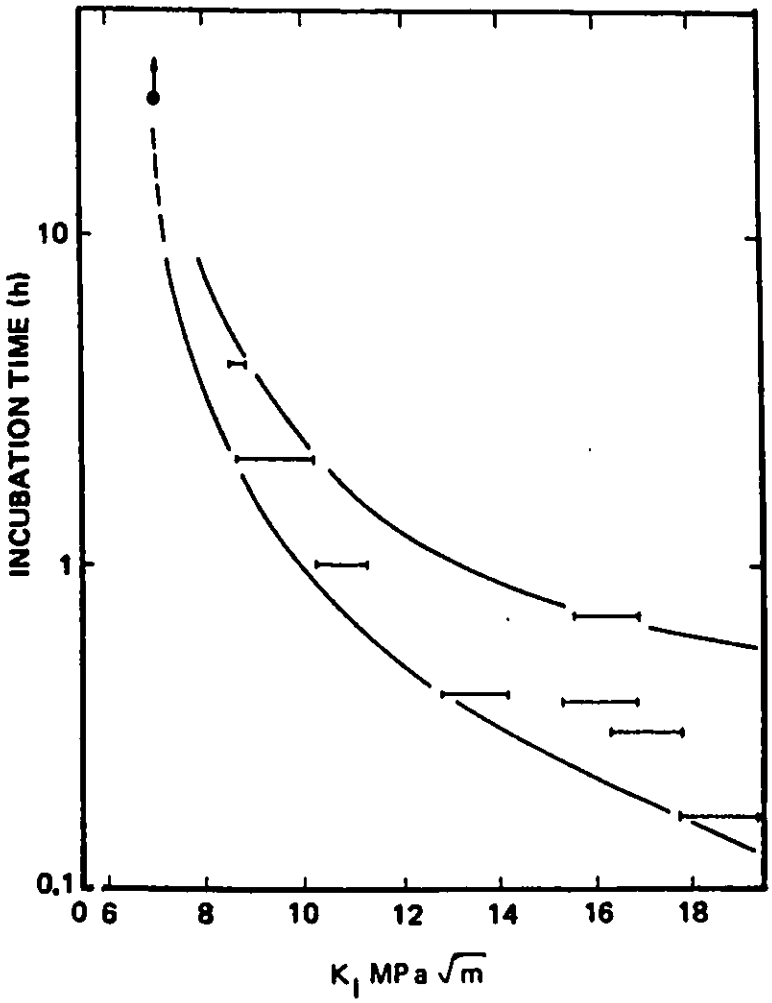

Figure 10 Dependence of Incubation Time on Stress-Intensity Factor at 225°C (500 K) in a Cantilever Beam Specimen Containing 45 ppm Hydrogen [41].

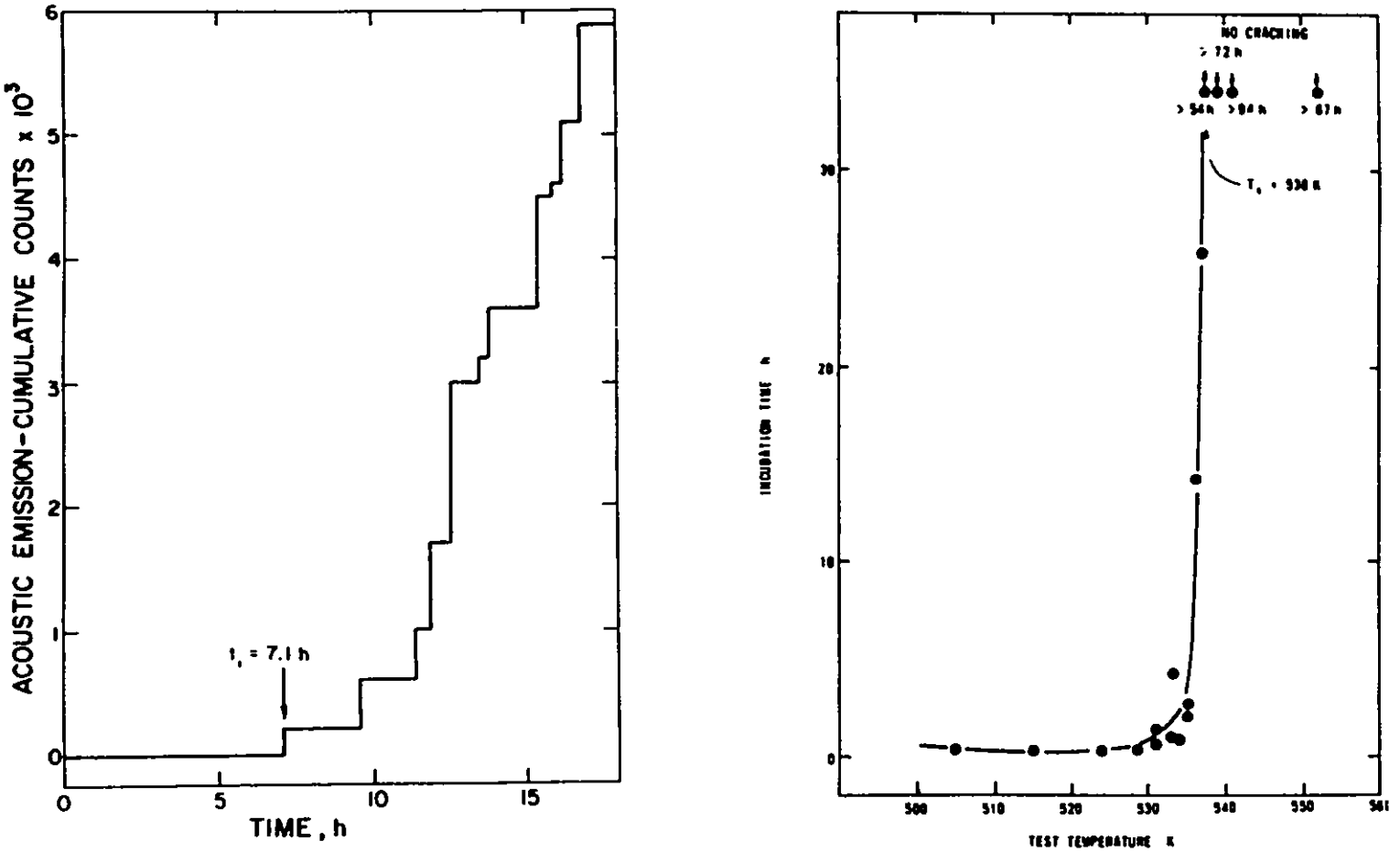

Figure 11 - Typical Incubation Time Data from Effective Solvus Temperature Determination Experiments [42].

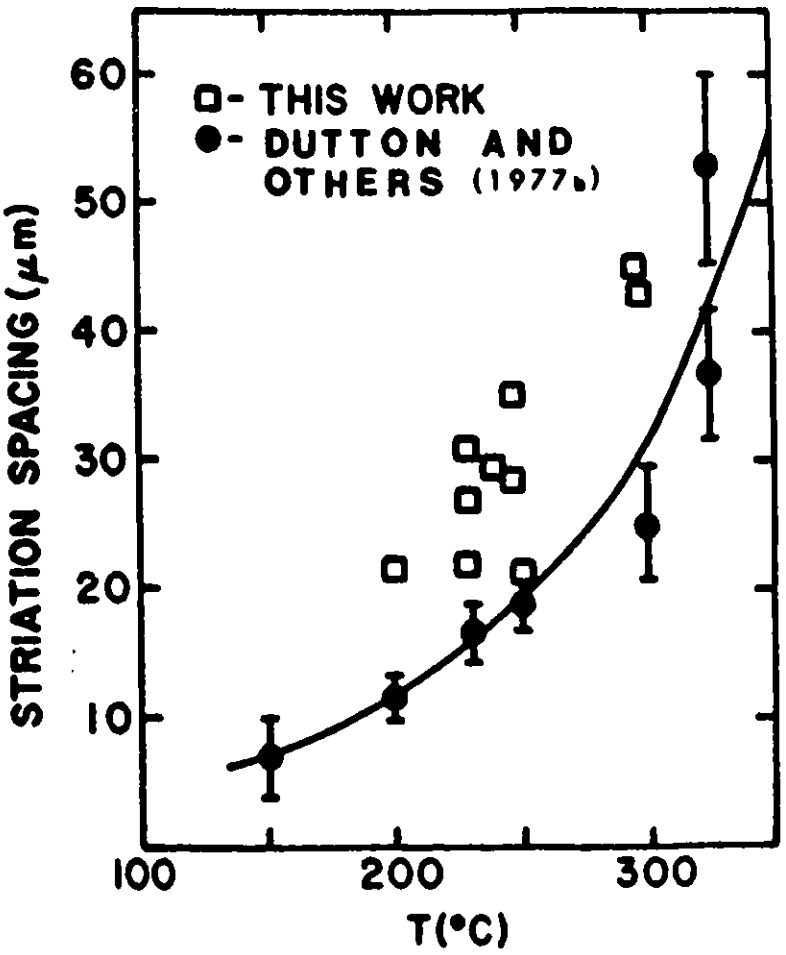

Figure 12 Dependence of DHC Fracture Surface Striation Spacing on Test Temperature [46].

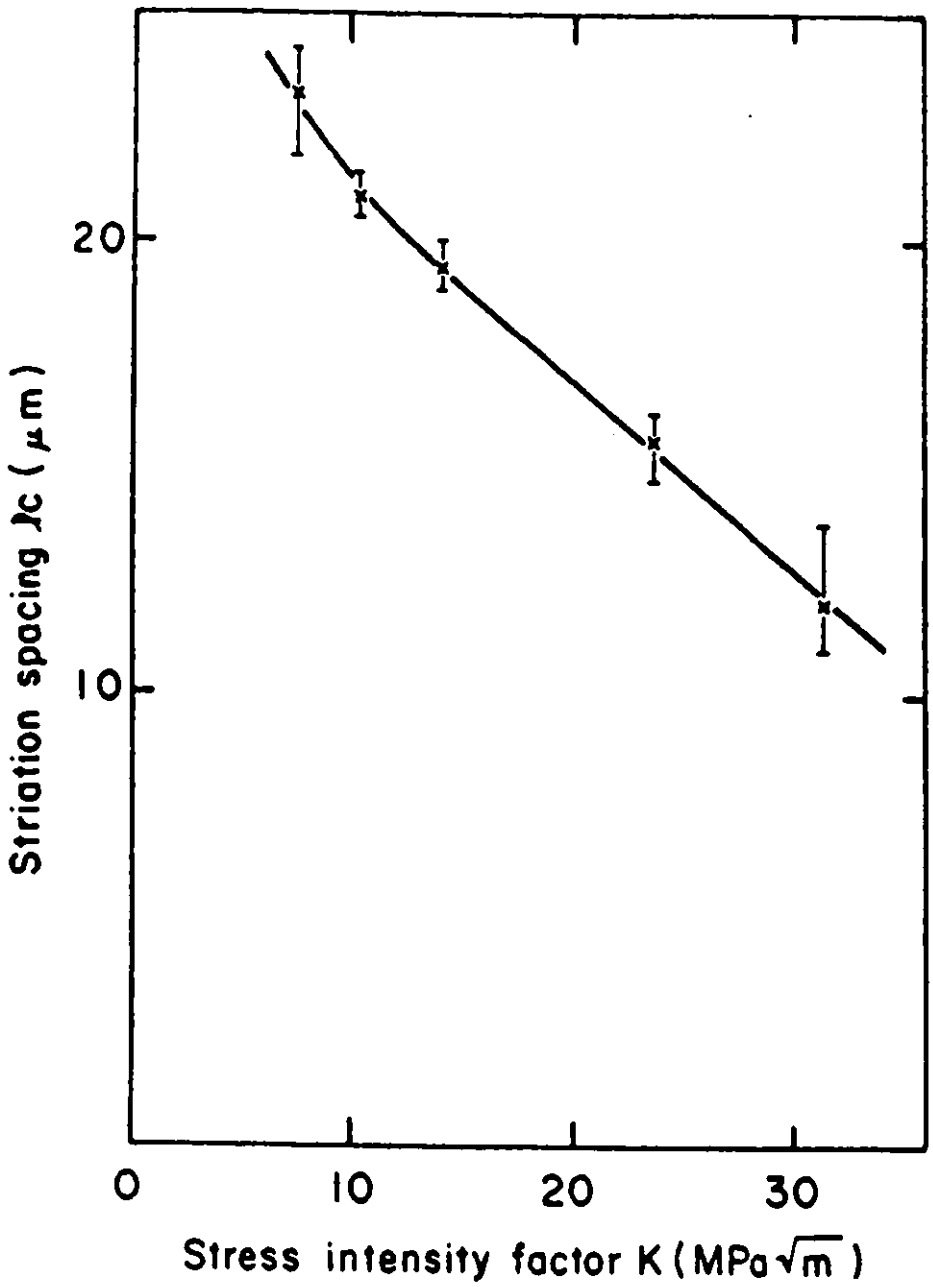

Figure 13 Dependence of DHC Fracture Surface Striation Spacing on Stress-Intensity Factor [47].

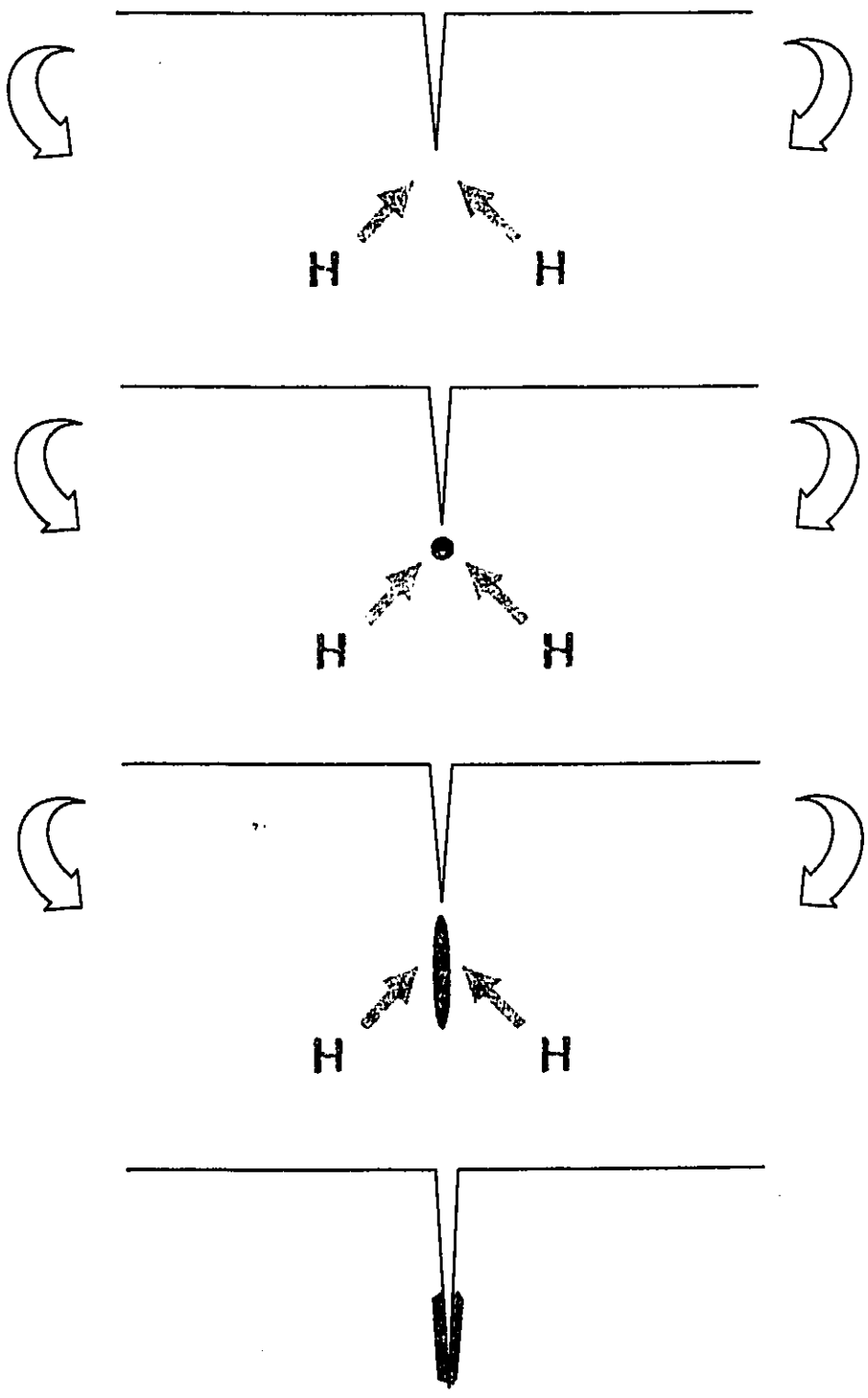

Figure 14 Simplified Model of Delayed Hydride Cracking.

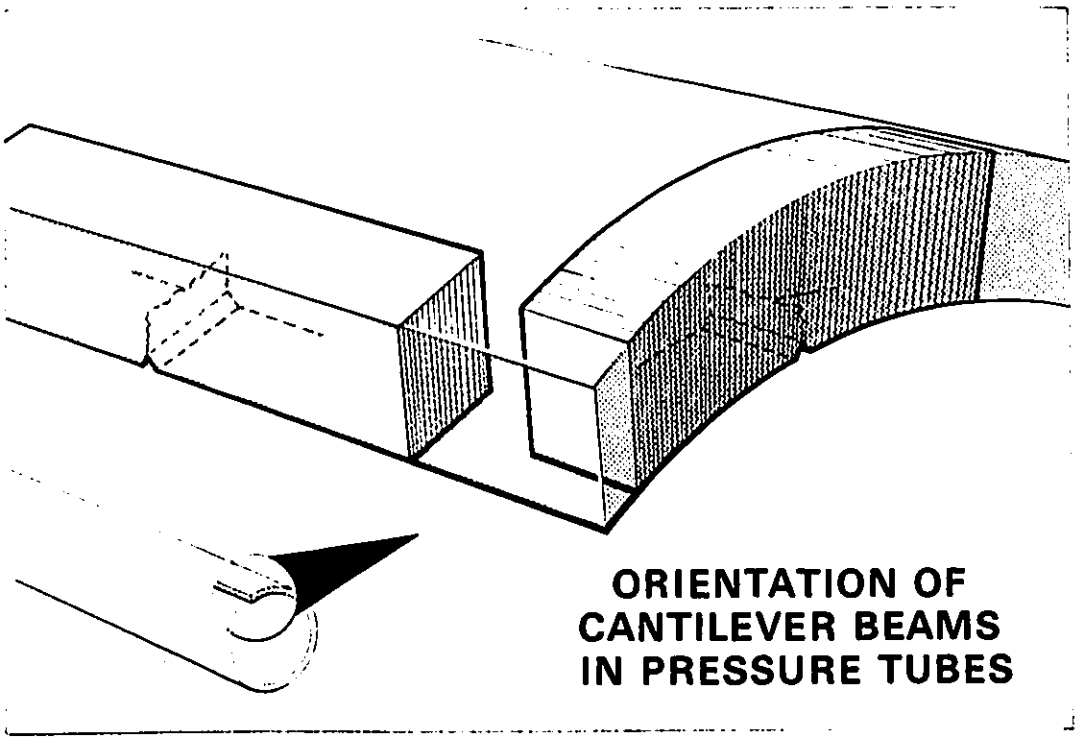

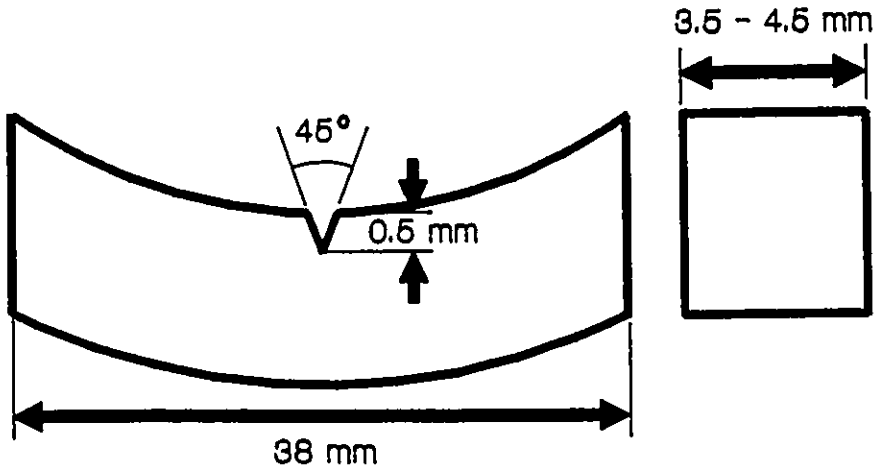

Figure 15 Cantilever Beam Specimen Configuration. Only the Curved Specimen Geometry was Used in this Study.

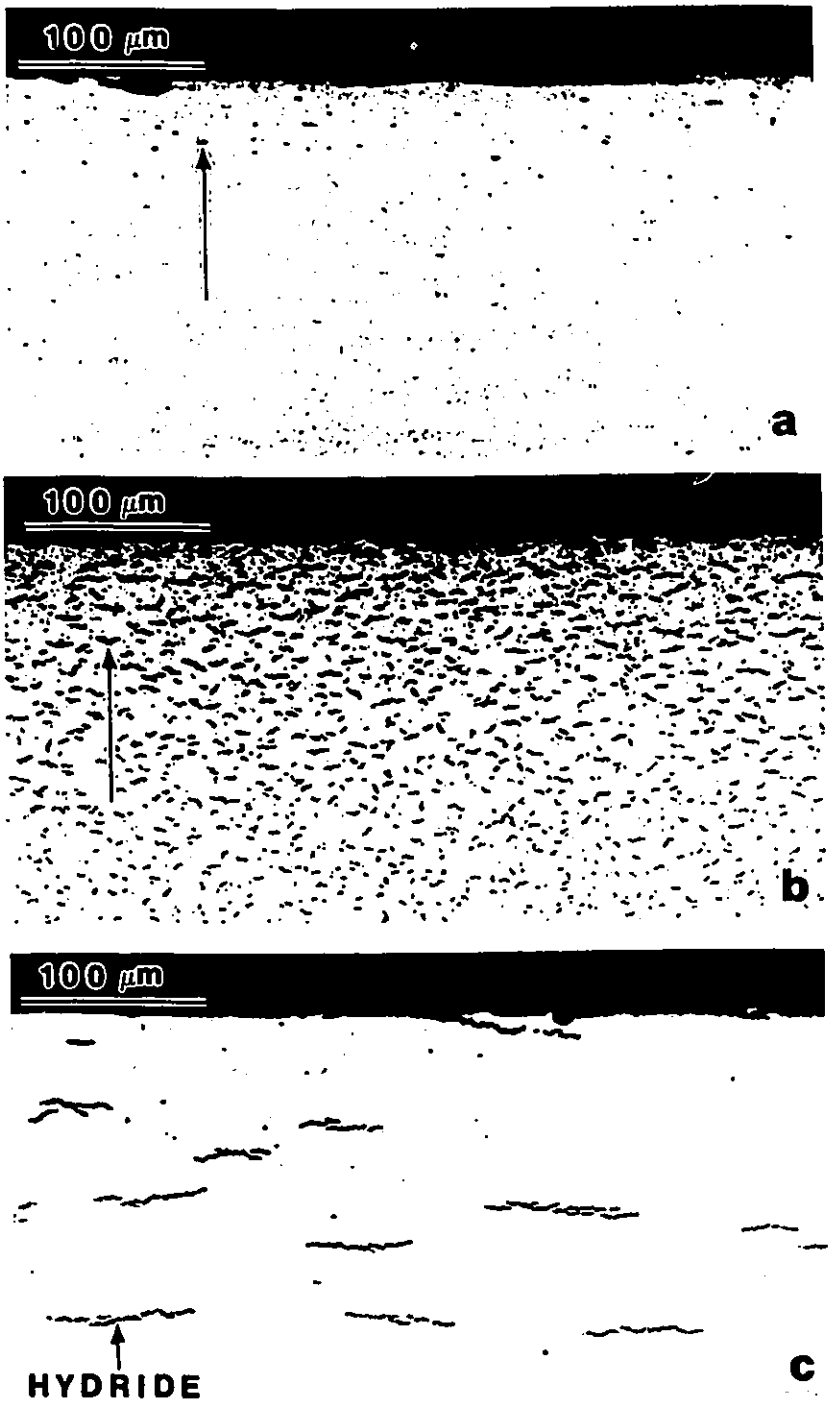

Figure 16 Zirconium Hydride Structures in Zr-2.5Nb Pressure Tube Material: (a) As-received (~10 ppm), (b) As-hydrided (note gradient of hydrides near specimen surface), and (c) After Homogenization (~58 ppm). [Radial-Circumferential plane of tube.]

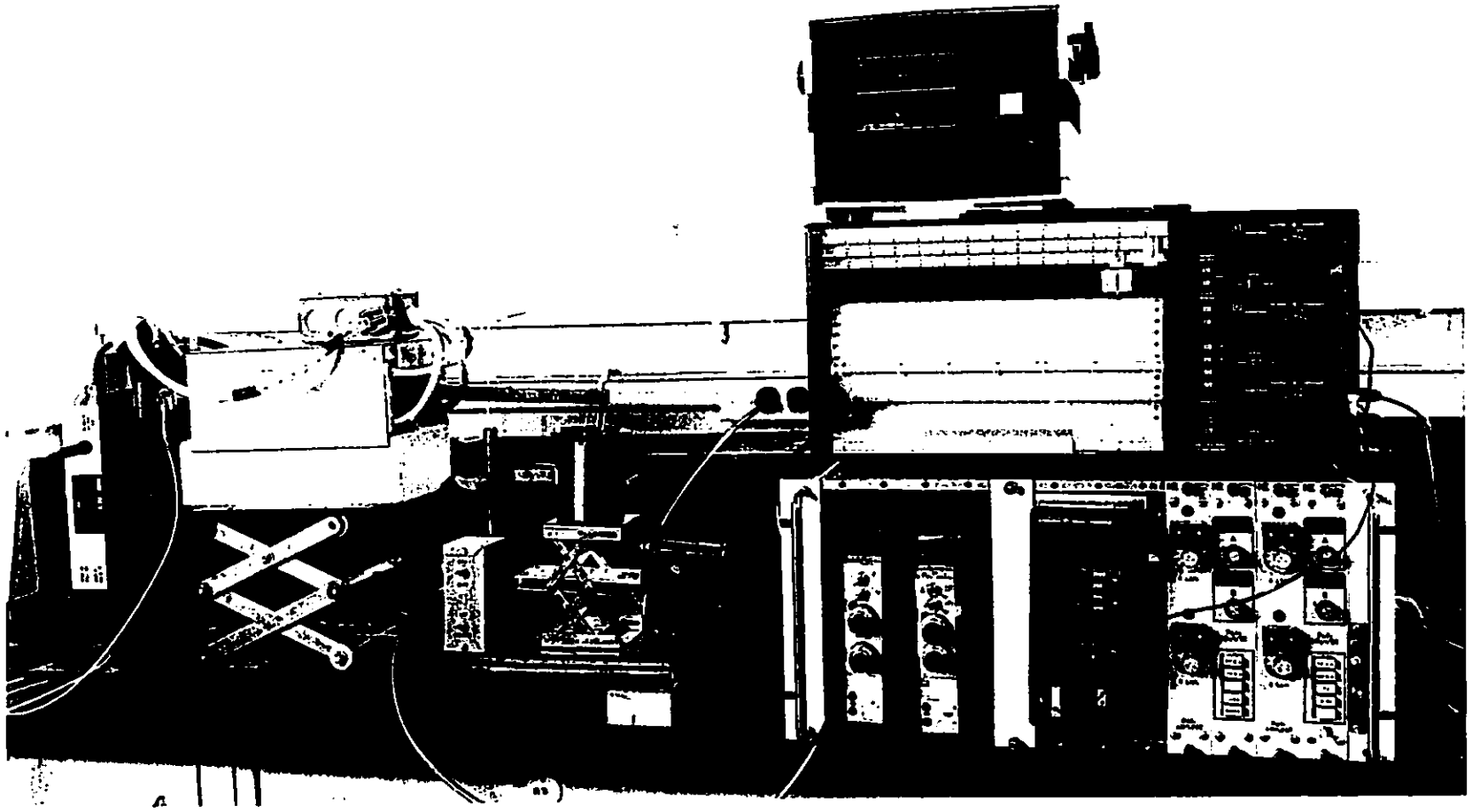

Figure 17 - Apparatus for DHC Initiation Tests Using Cantilever Beams.

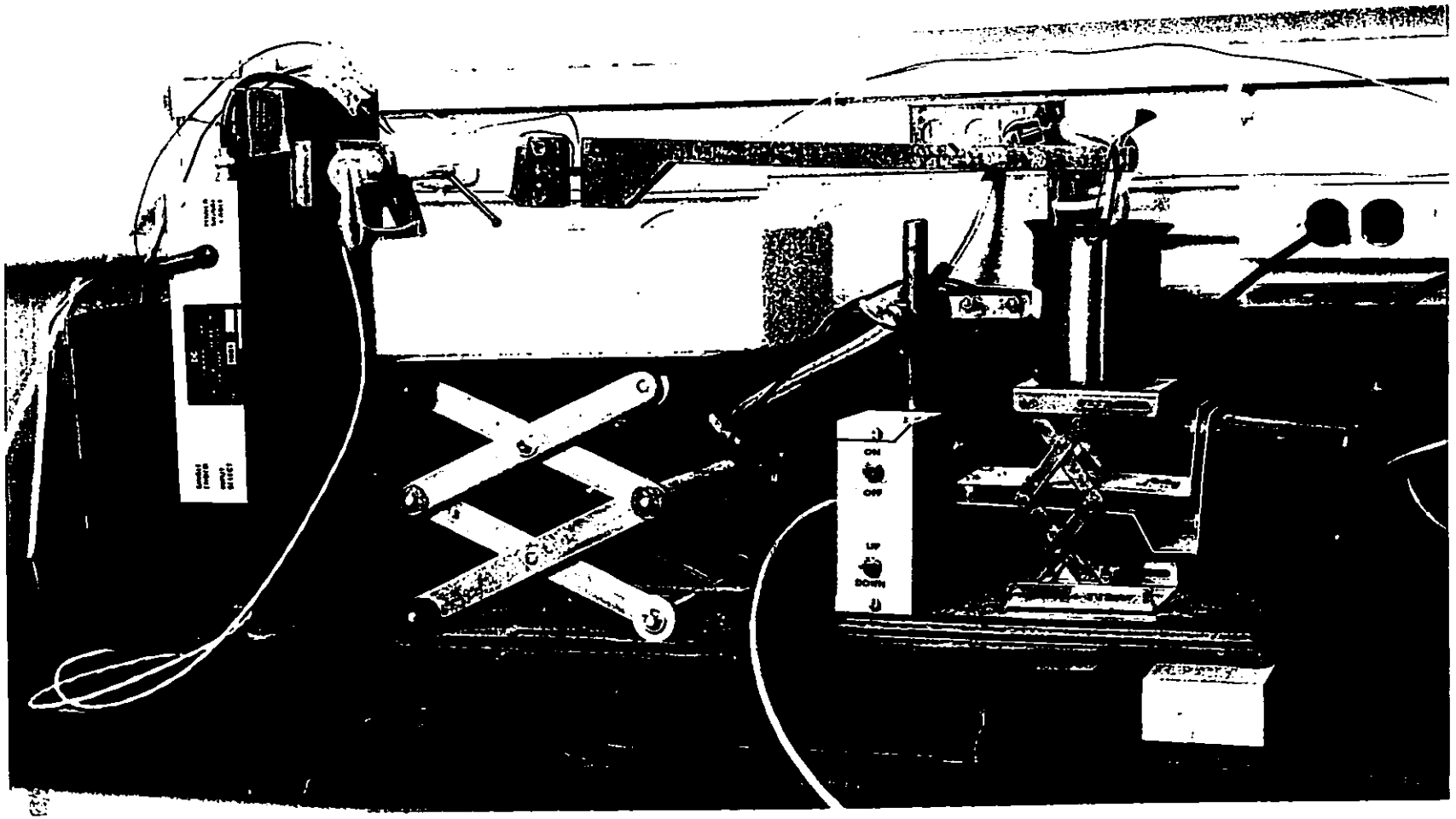

Figure 18 - Load-Frame for DHC Initiation Tests Using Cantilever Beams.

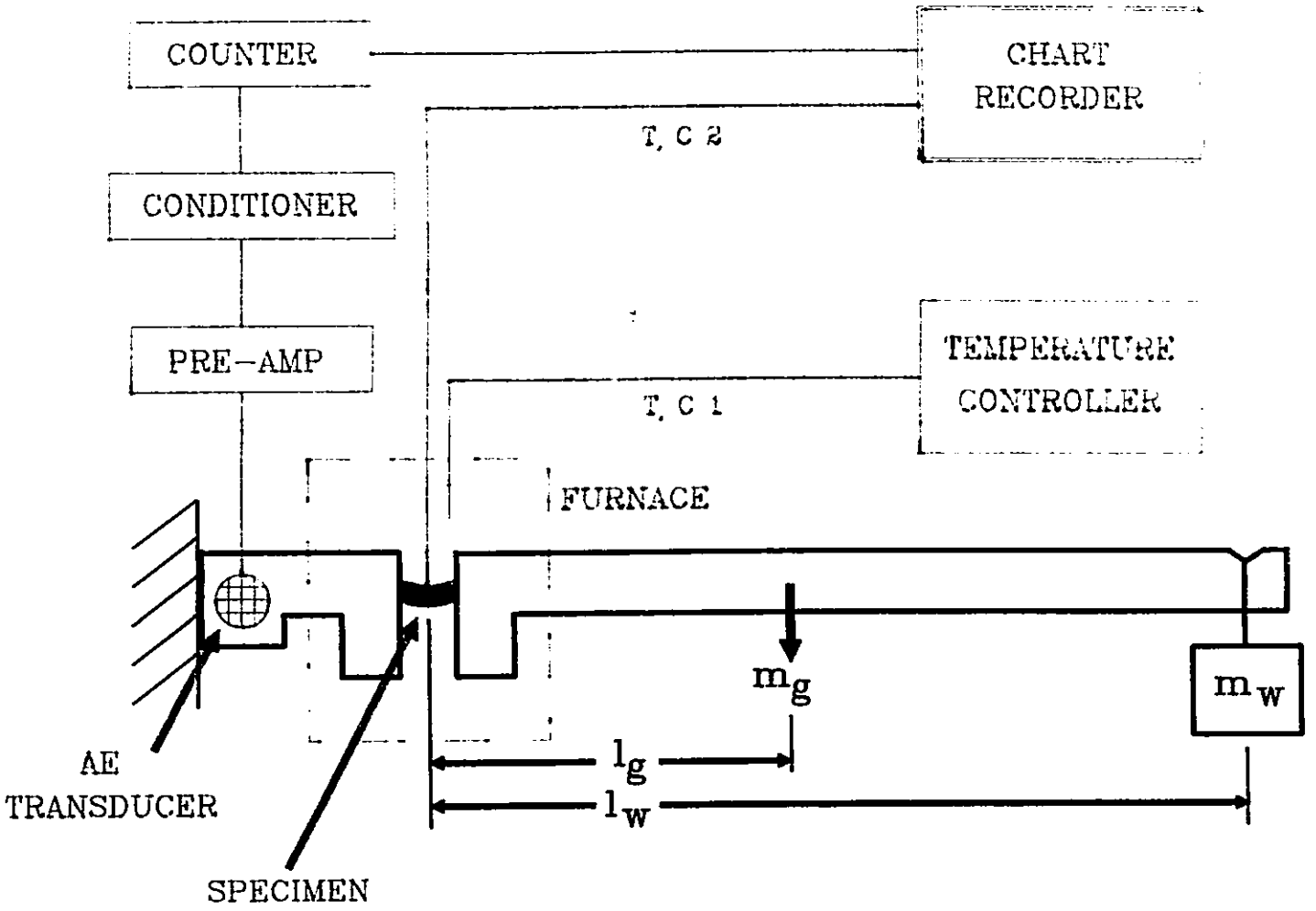

Figure 19 - Apparatus for DHC Initiation Tests Using Cantilever Beams - Schematic Diagram.

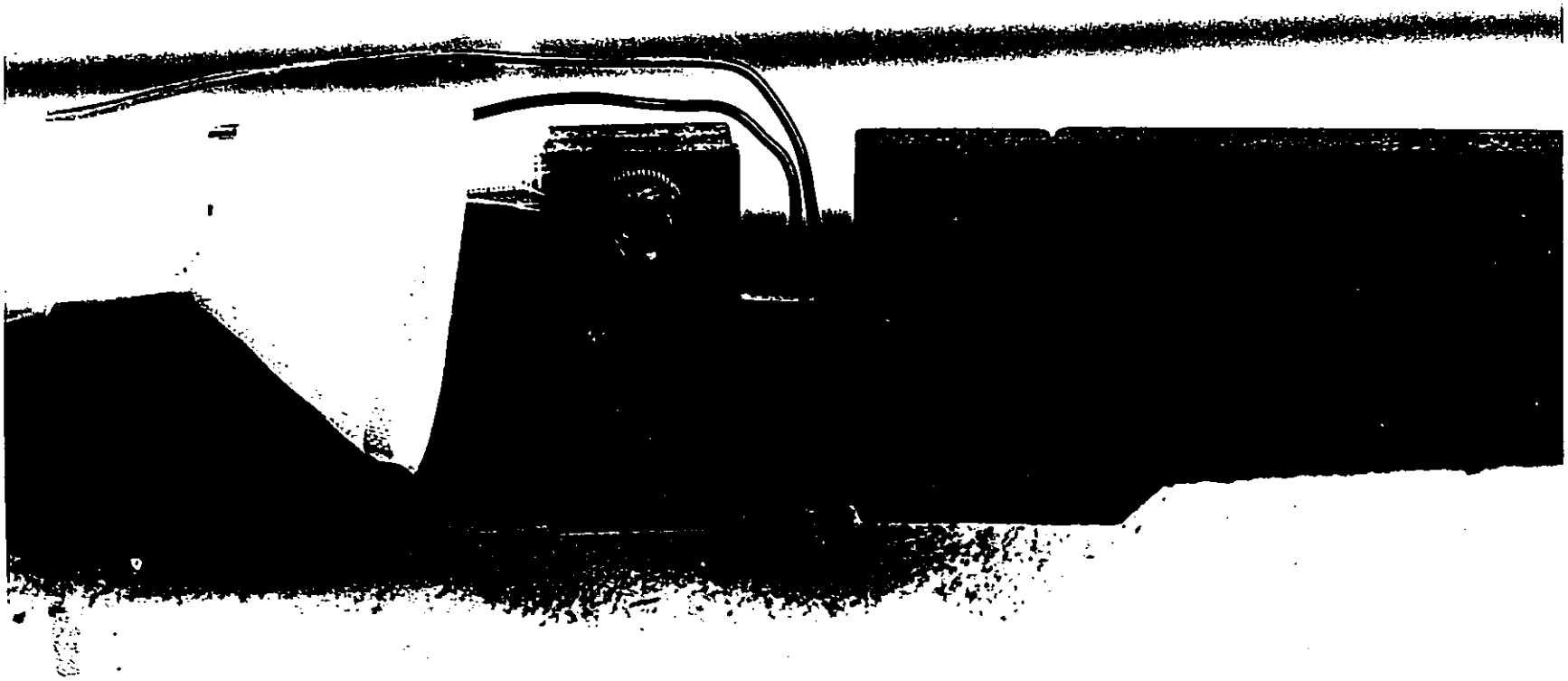

Figure 20 - Detail of Cantilever Beam Specimen Loaded Into the Test Rig.

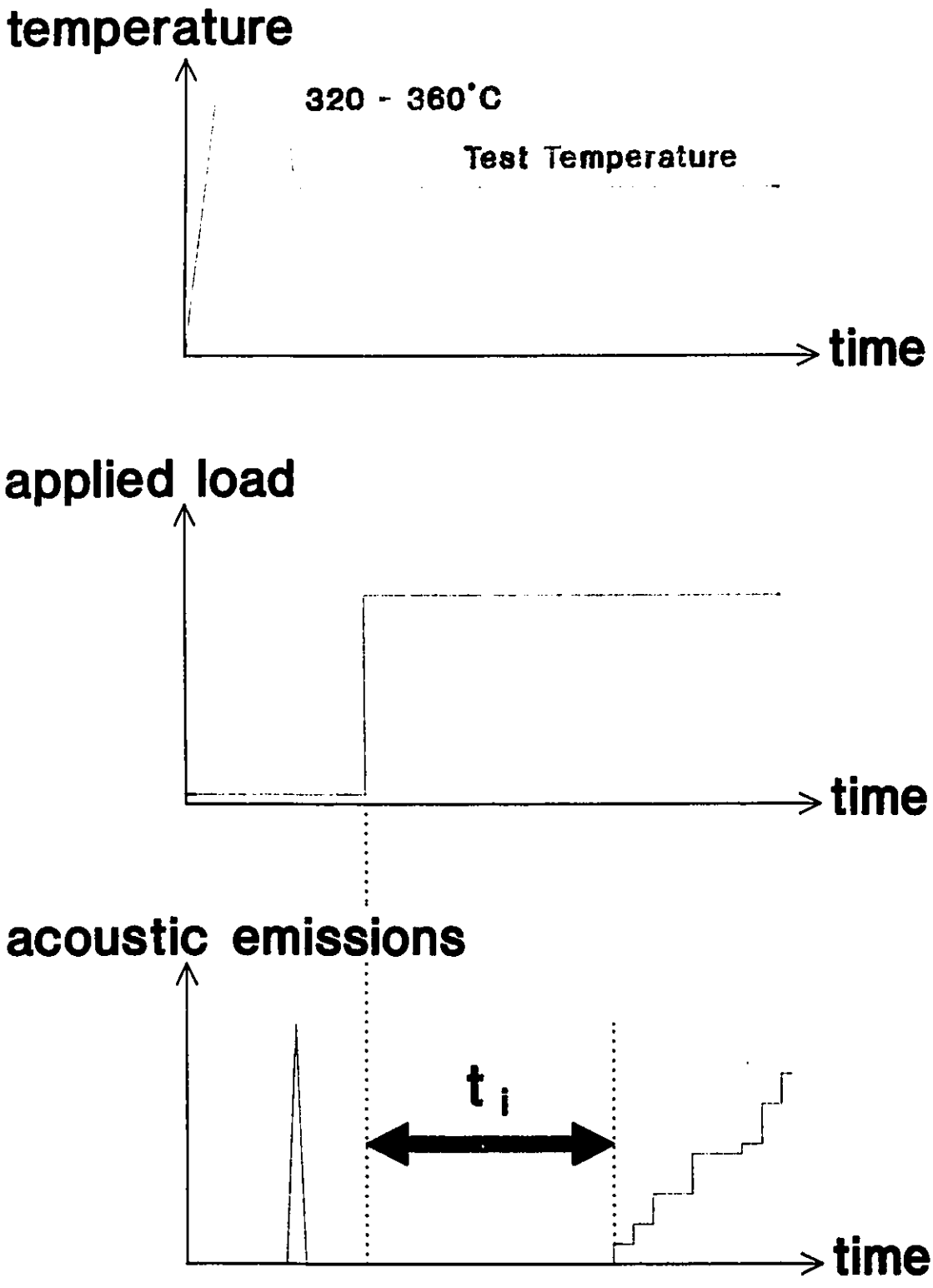

Figure 21 Testing Procedure - Schematic Diagram.

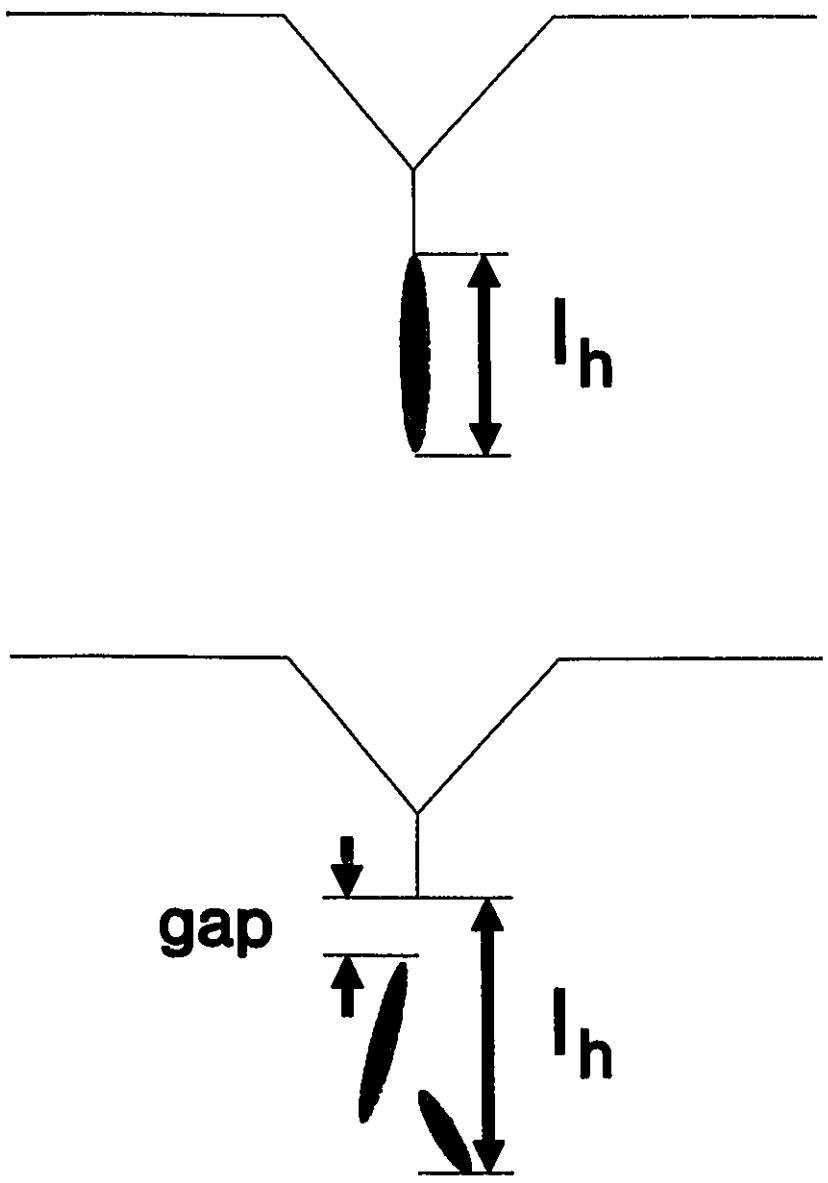

Figure 22 Schematic Diagram Illustrating the Method of Determining the Projected Crack-Tip Hydride Length.

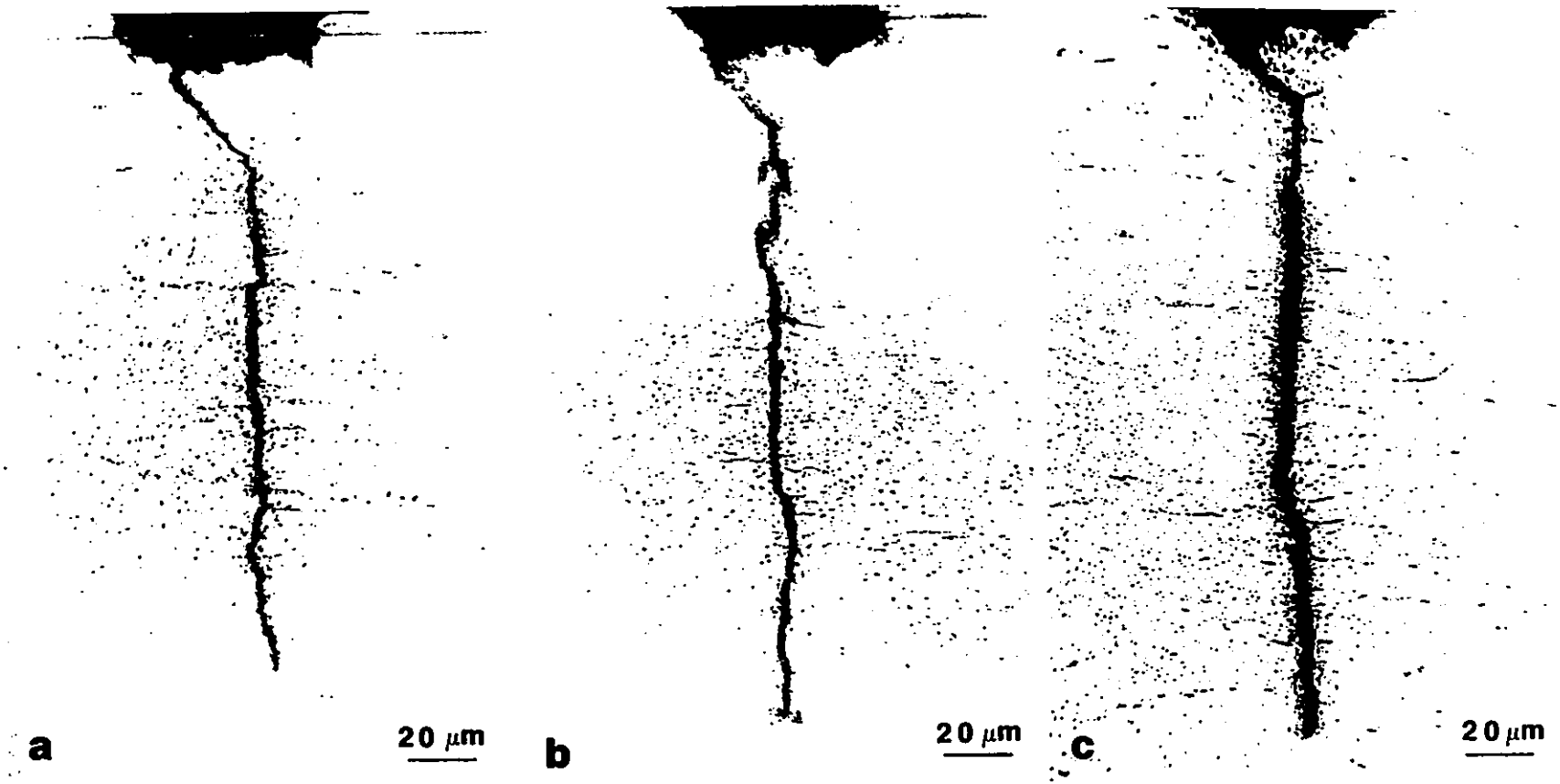

Figure 23 - Dependence of Hydride Structure on the Overnight Hold Temperature for Specimen N631B-1: (a) 320°C, (b) 340°C, and (c) 360°C.

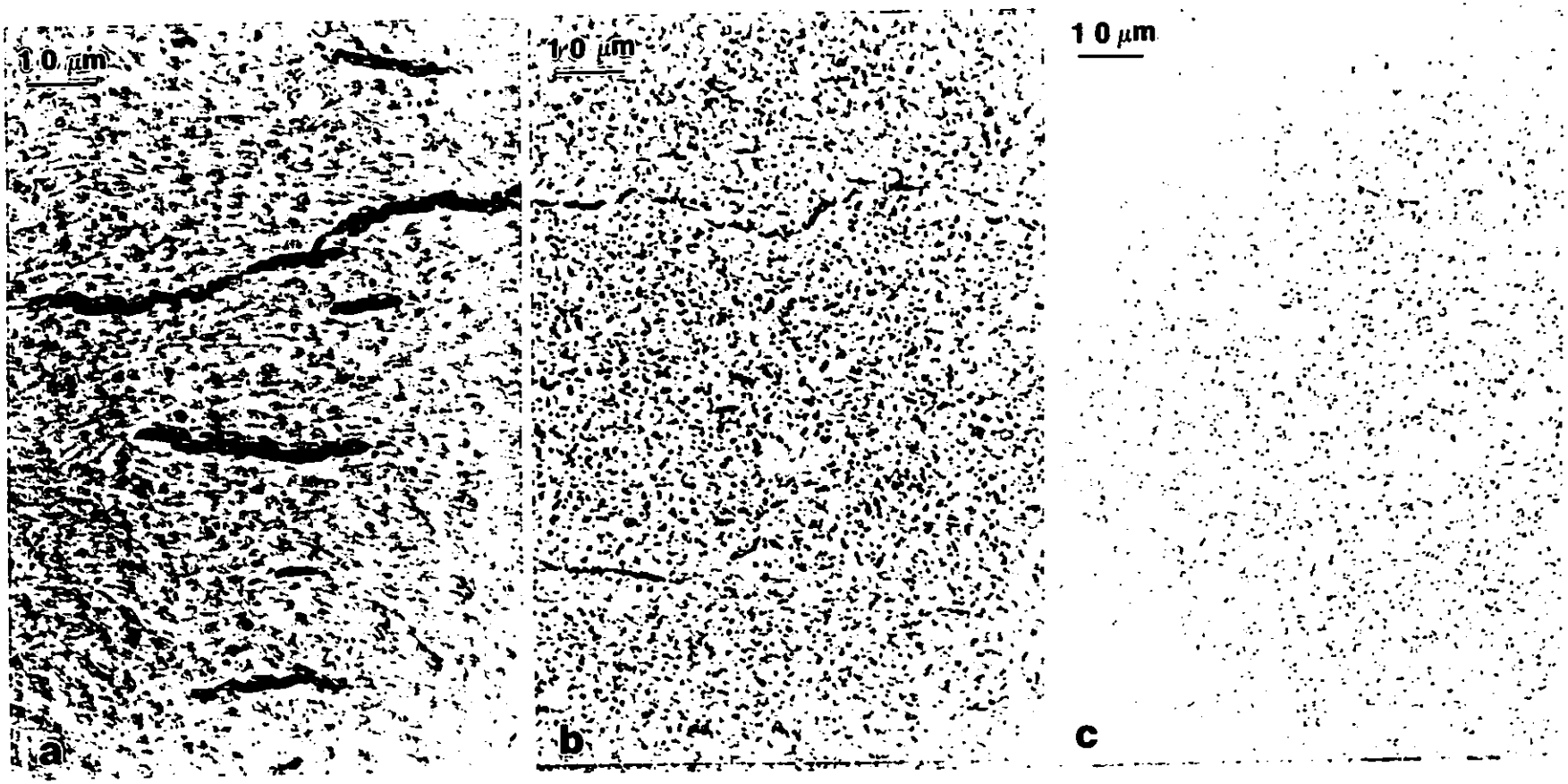

Figure 24 - Dependence of Hydride Structure on the Overnight Hold Temperature for Specimen C148-A1: (a) 320°C, (b) 350°C, and (c) 360°C.

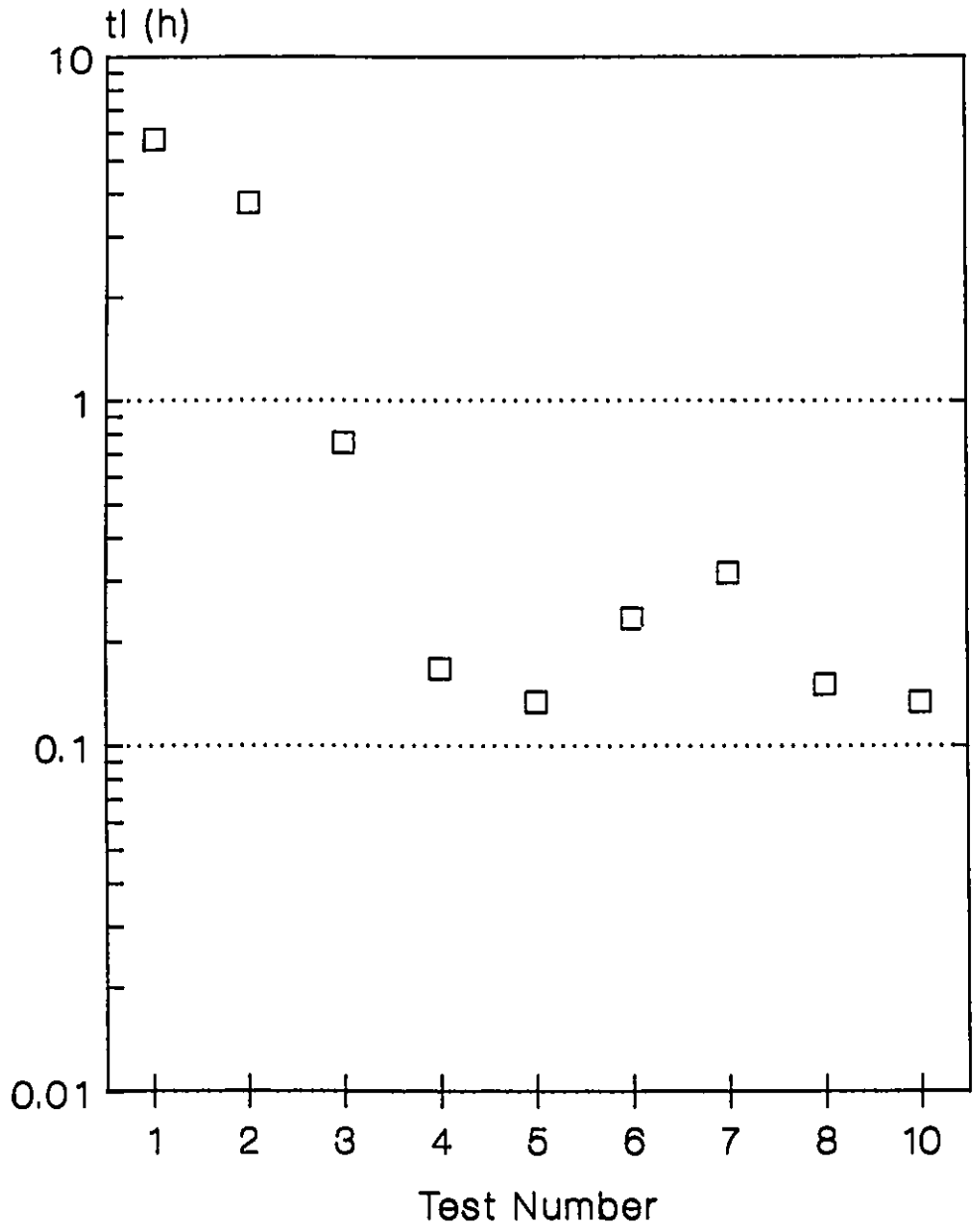

Figure 25 Incubation Times for Successive Tests of Specimen N631B-2.

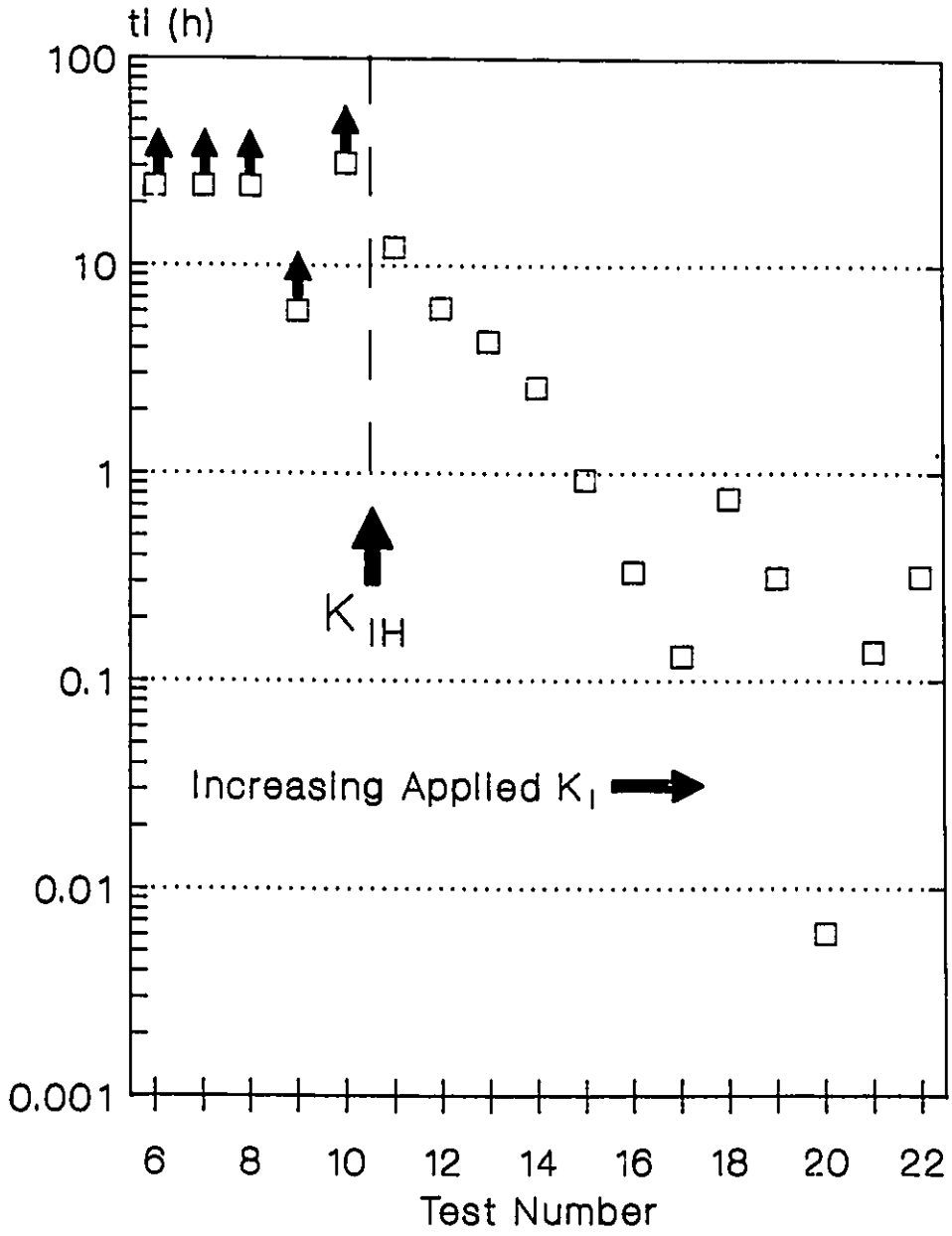

Figure 26 Incubation Times for Successive Tests of Specimen C148-A16.

Figure 27 Appearance of Crack-Tip Hydrides in Specimen C148-A22. Note that the crack-tip hydride is comprised of an aligned accumulation of smaller hydrides.

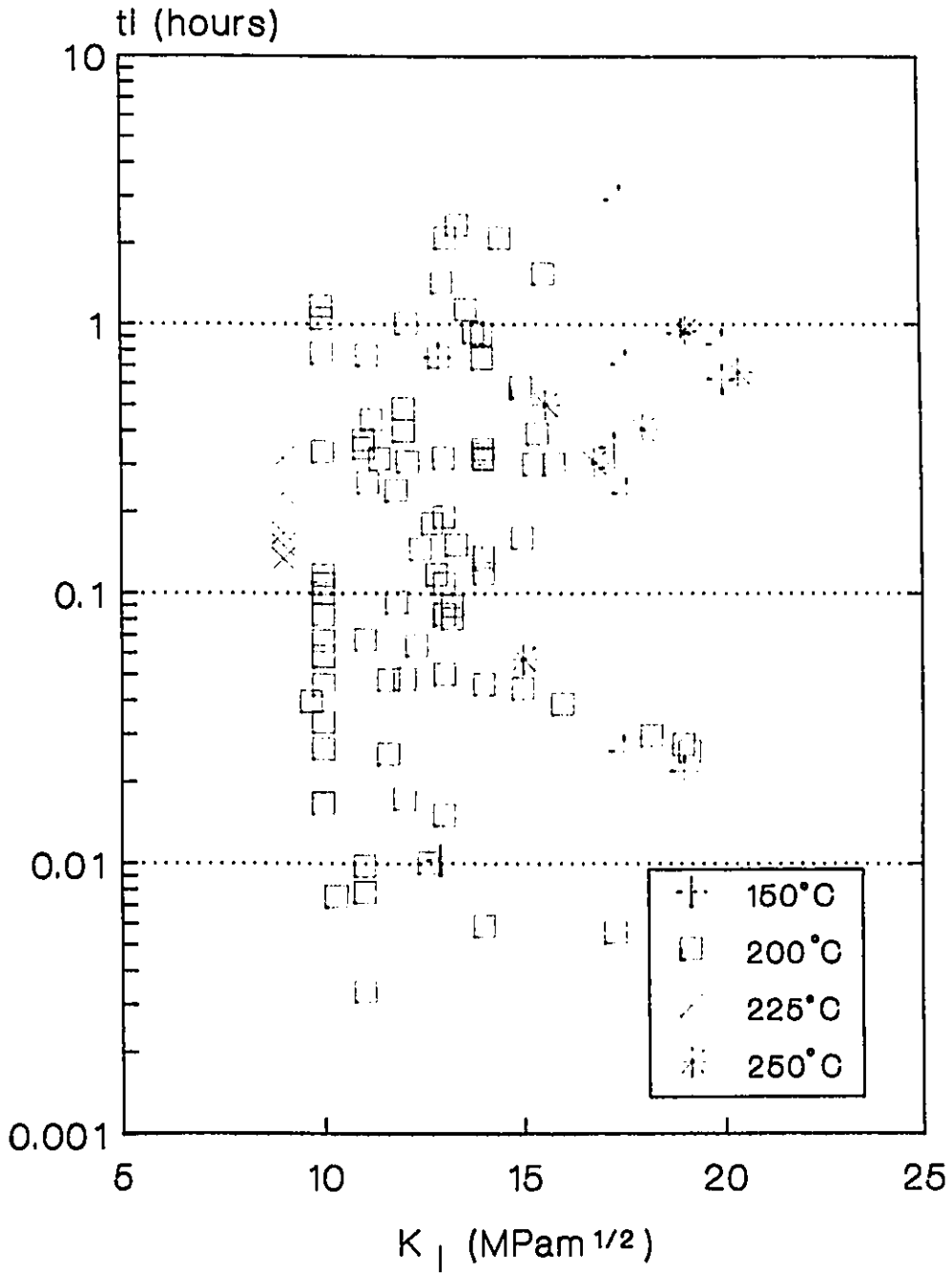

Figure 28 Dependence of Incubation Time on Stress-Intensity Factor.

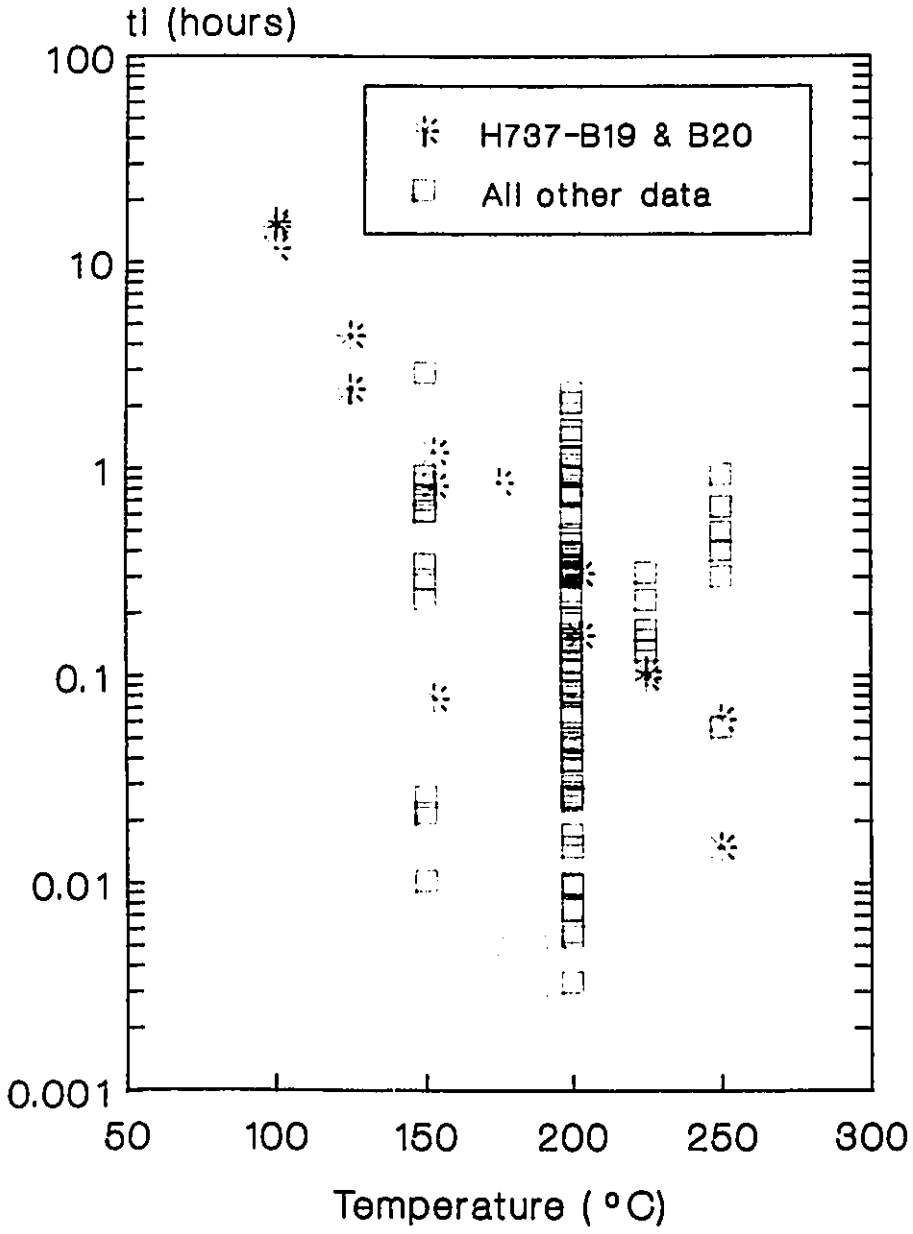

Figure 29 Dependence of Incubation Time on Temperature.

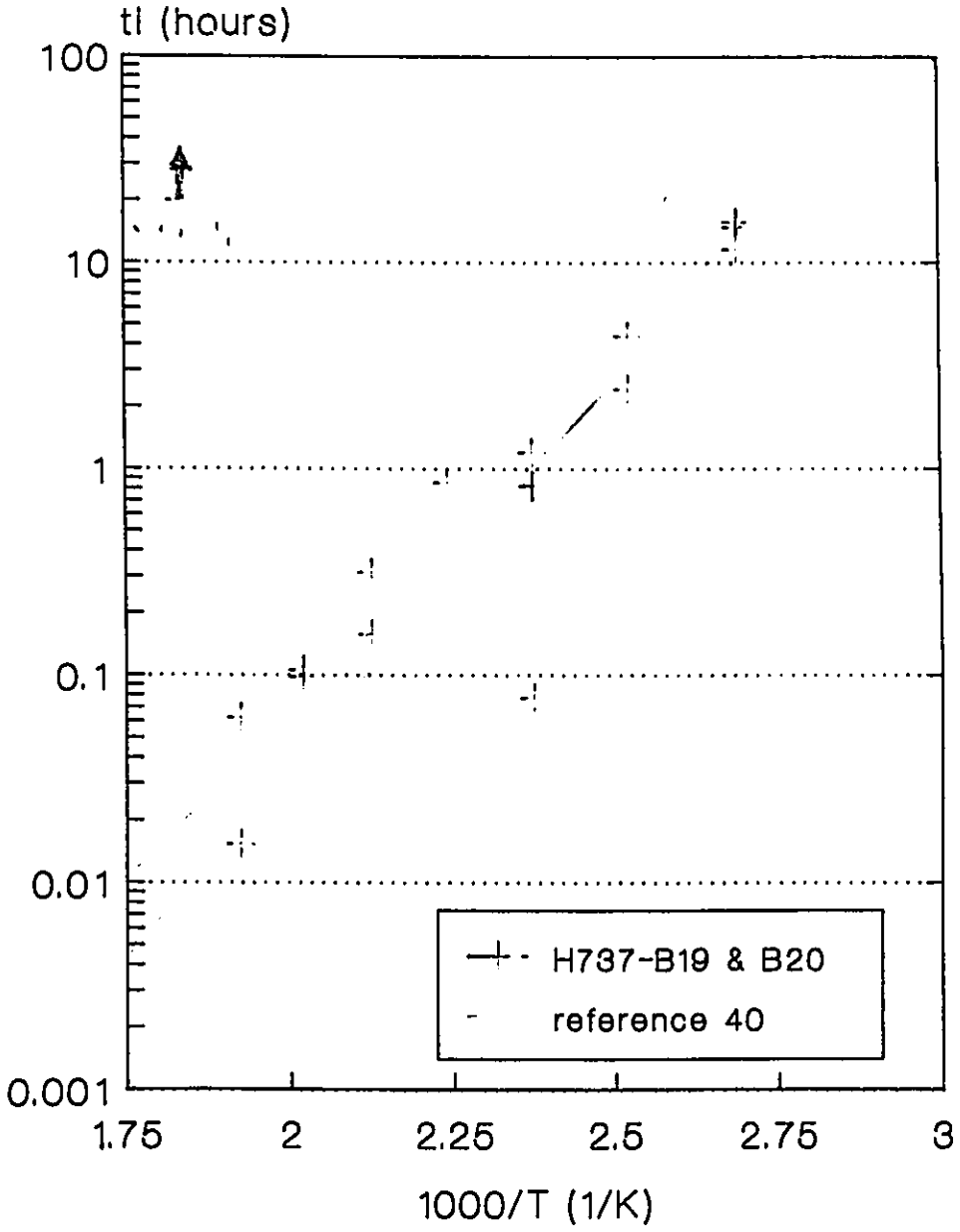

Figure 30 Dependence of Incubation Time on Temperature for Specimens H737-B19 and H737-B20.

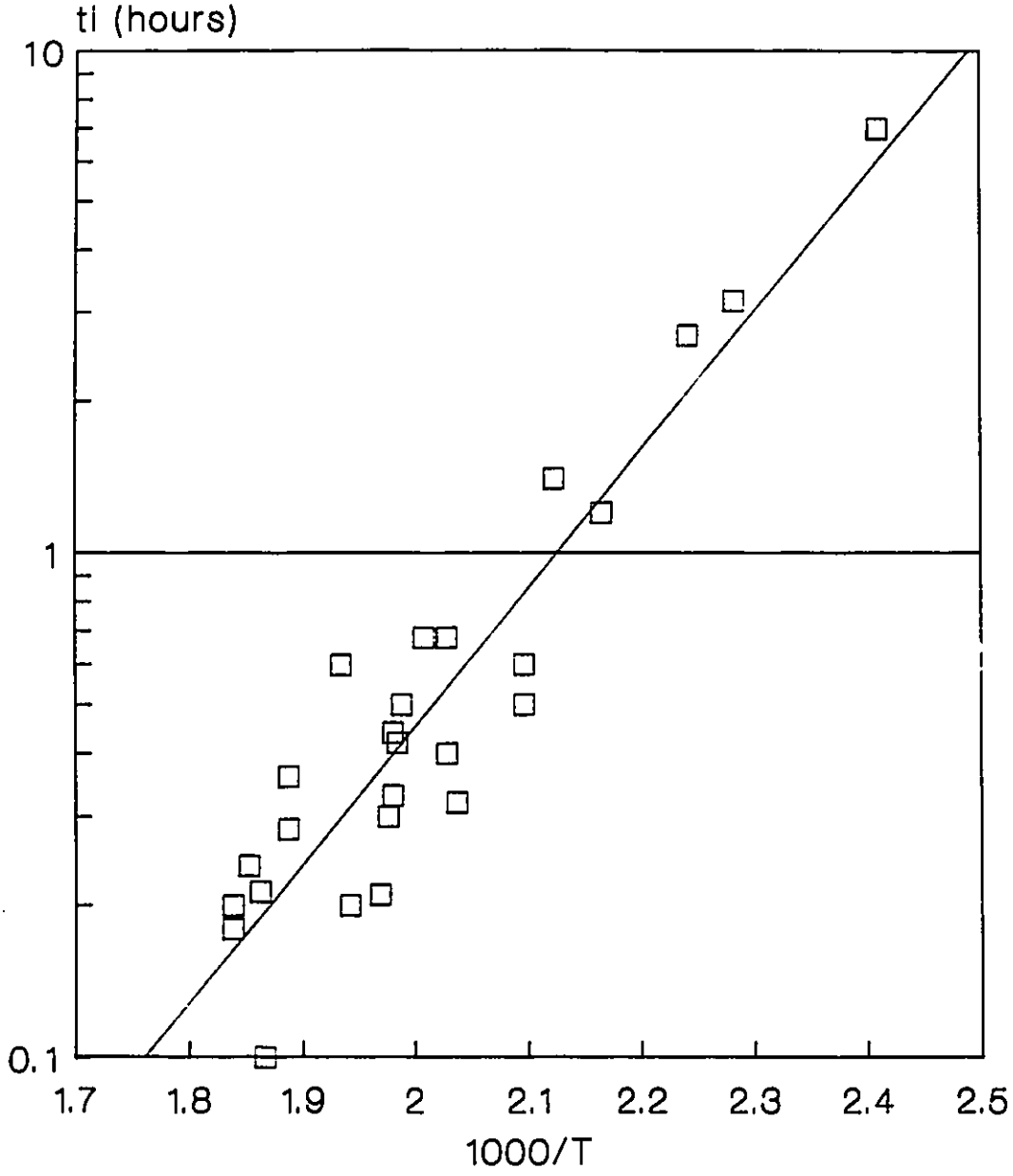

Figure 31 Dependence of Incubation Time on Temperature at 15 $MPam^{1/2}$ from Effective Solvus Temperature Determination Work by Coleman [66].

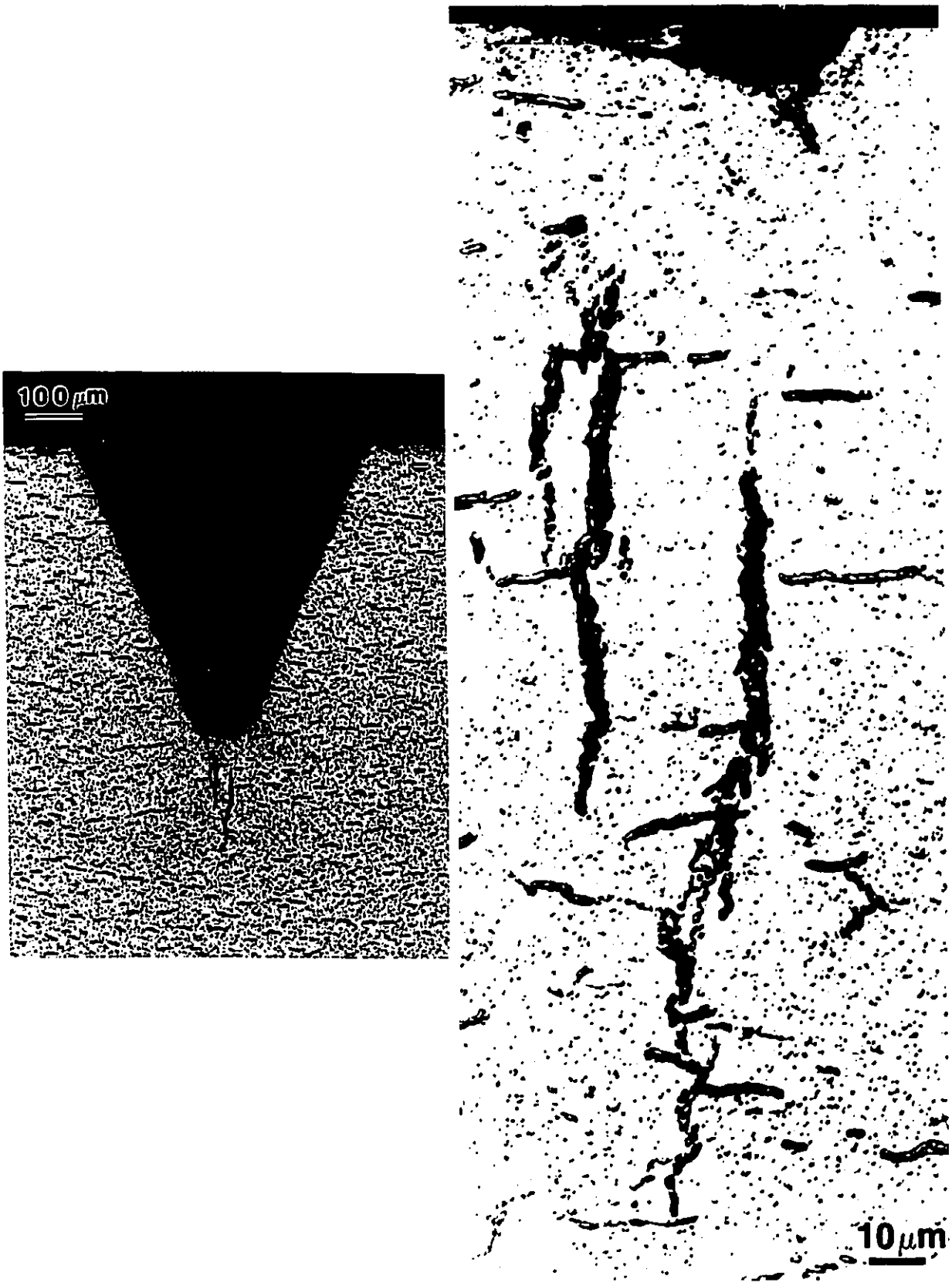

Figure 32 Hydrides Beneath the Notch Near the Edges of a Cantilever Beam Specimen.

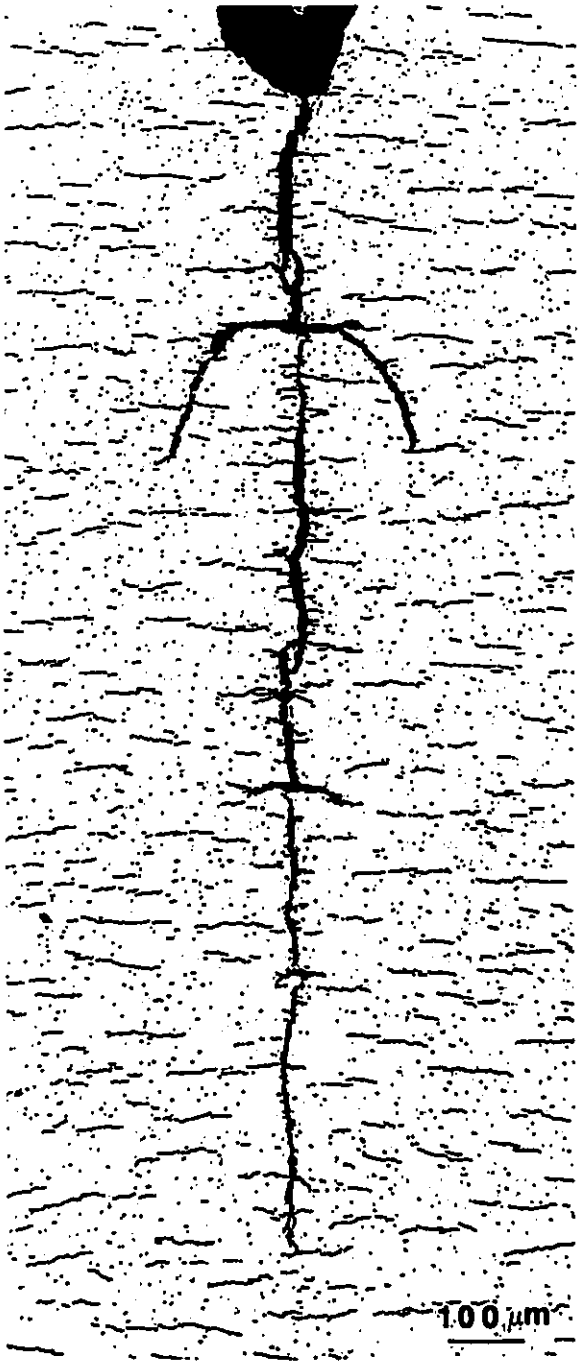

Figure 33 Irregular DHC Crack-Path Observed in Specimen H737-B4.

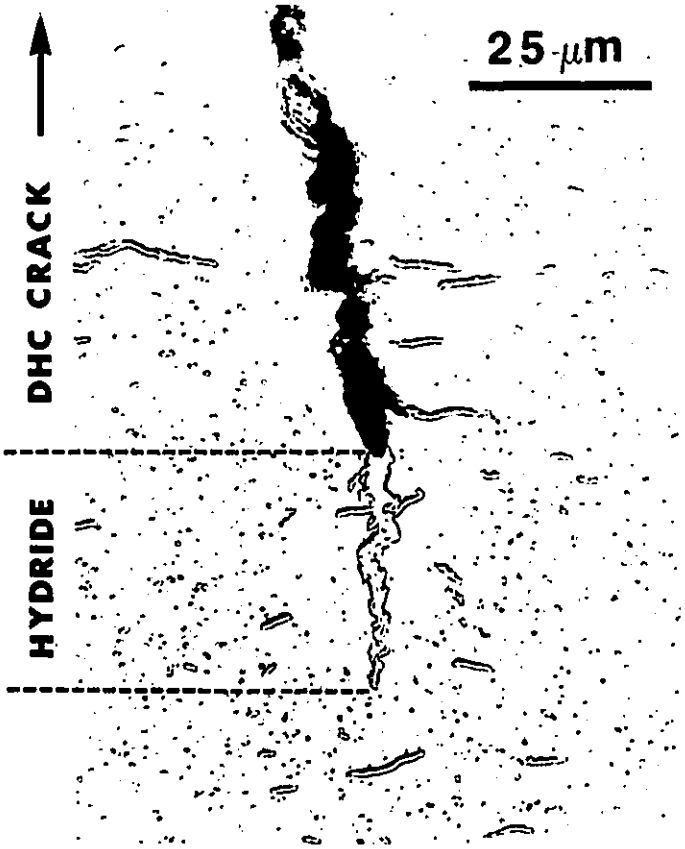

Figure 34 Single Crack-Tip Hydride Lying in the Crack Plane.

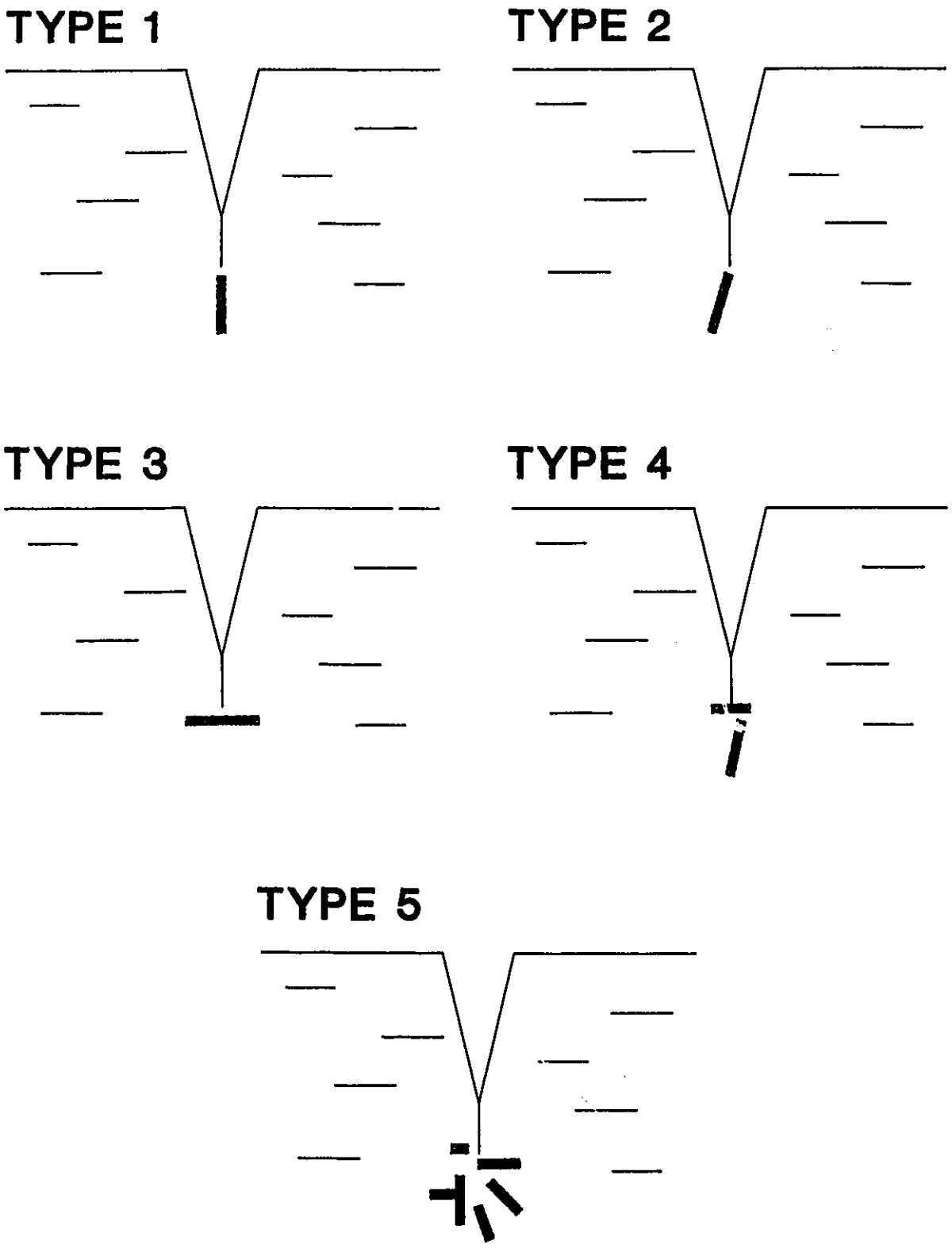

Figure 35 Classifications for Crack-Tip Hydride Morphologies.

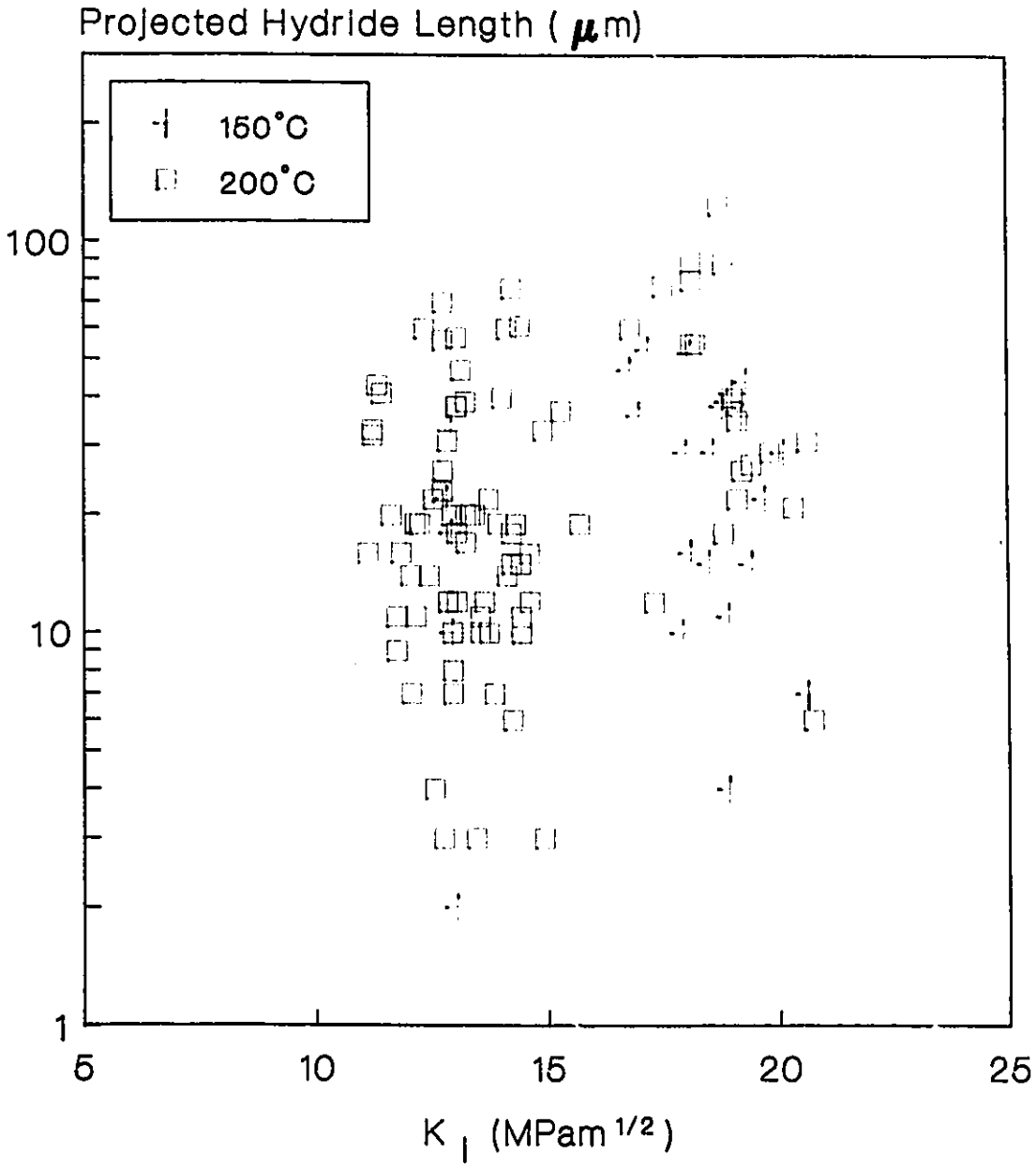

Figure 36 Dependence of Projected Crack-Tip Hydride Length on Stress-Intensity Factor.

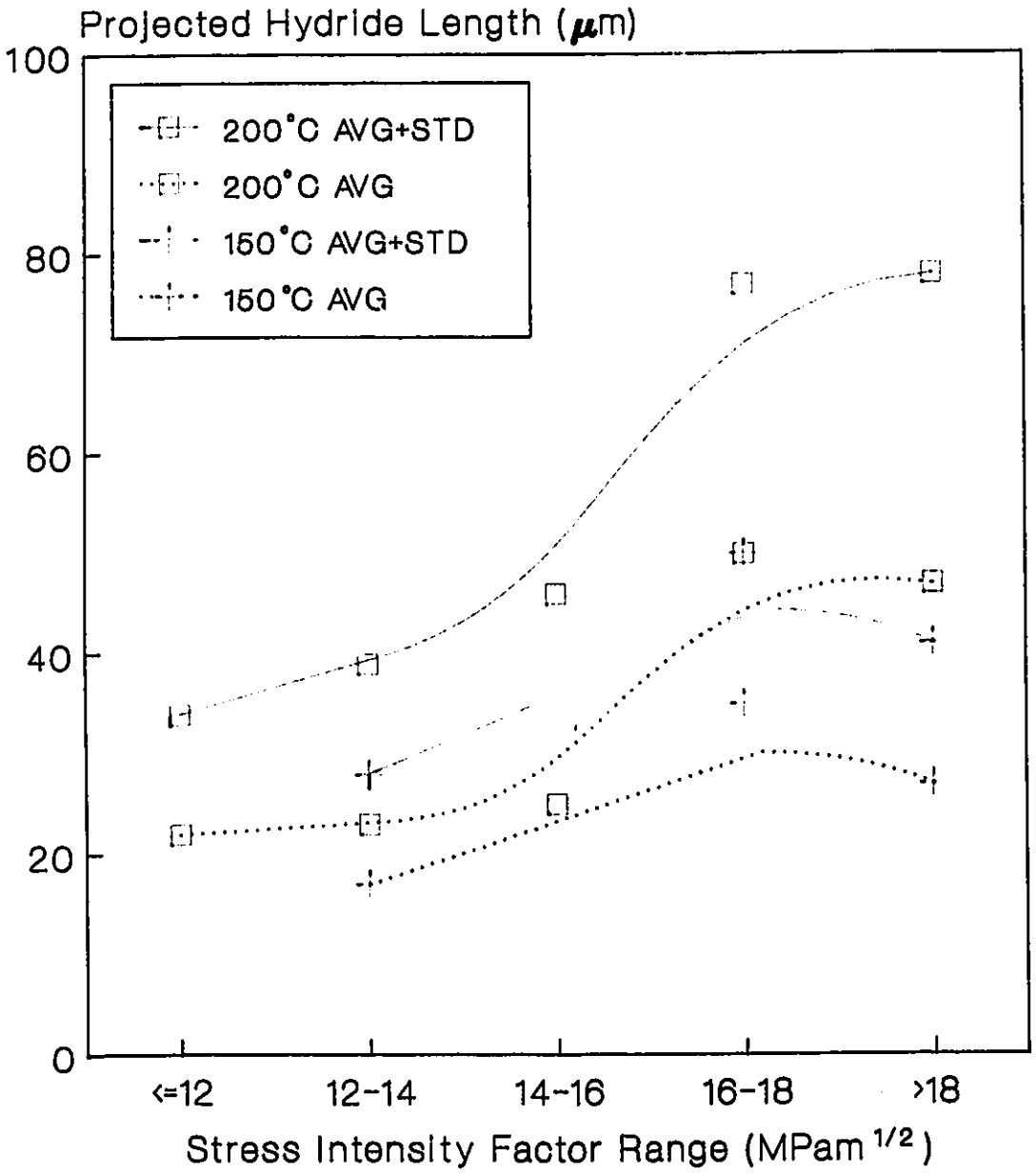

Figure 37 Dependence of Projected Crack-Tip Hydride Length on Stress-Intensity Factor Range at 150 and 200°C.